Abstract

Mechanisms of Protein Quality Control at the Nuclear Envelope and During Nuclear Pore Complex Biogenesis

Sarah M. Prophet

2022

Collapse of protein quality control (PQC) is a defining feature of numerous neurological diseases. Work described within this thesis argues that DYT1 dystonia, a neurological movement disorder of unclear etiology, arises due to a PQC defect. While it is clear that mutations in the AAA+ ATPase TorsinA cause this disease, it is not known why loss of this protein function causes DYT1 dystonia. In cells lacking Torsin function, nuclear pore complexes (NPCs) fail to be properly assembled. Instead, nuclear envelope (NE) herniations form that sequester abundant molecular chaperones. Ubiquitylated proteins, that in healthy cells are rapidly degraded, become sequestered with these chaperones. The protein MLF2, identified through proteomic approaches as enriched inside NE herniations, recruits DNAJB6 to these structures. Performing proteomic interrogations of bleb composition revealed that MLF2 possesses nucleoporin-directed chaperone activity. The characteristic ubiquitin accumulation in Torsin-deficient cells requires p97 activity, which is highly dependent on the adaptor UBXD1. p97 does not significantly depend on the Ufd1/Npl4 heterodimer to generate these ubiquitylated proteins, nor does inhibiting translation or depleting known retrotranslocons affect the ubiquitin sequestration. This work identifies a dual mechanism of proteotoxicity provoked

by loss of Torsin ATPase activity via the stabilization of otherwise rapidly degraded proteins and sequestration of abundant molecular chaperones. The Torsin-regulated PQC pathway utilizes p97 and its adaptor UBXD1, while operating independently from canonical ERAD machinery. With an ever-aging population comes more burden of neurological disease driven by defective PQC, and this work advances our knowledge of potentially druggable targets for developing life-saving therapies.

Mechanisms of Protein Quality Control at the Nuclear Envelope and During Nuclear Pore Complex Biogenesis

A Dissertation
Presented to the Faculty of the Graduate School
Of
Yale University
In Candidacy for the Degree of
Doctor of Philosophy

By
Sarah M. Prophet

Dissertation Director: Christian Schlieker

December 2022

Contents

Chapter 1: Introduction

Over billions of years, compartmentalization within cells enabled primitive lifeforms to evolve into creatures as complex as humans. Establishing distinct cellular compartments is achieved through multiple mechanisms, typically by enclosing regions of the cell within a phospholipid bilayer. Compartmentalization can also be accomplished via liquid-liquid phase separation. Perhaps the most recognizable compartment within a eukaryotic cell is the nucleus. Enclosed by the nuclear envelope (NE), a double membrane system, the nucleus enables spatial separation between transcription and translation [1]. While the NE was historically presumed to be a pair of relatively inert membranes, recent advances have revealed it as a highly active and metabolically critical region of the cell. From regulating vastly distinct signaling networks [2] to sensing mechanical forces [3], the NE serves as a central control hub within eukaryotic cells. The essential nature of NE-related processes is underscored by the many diseases associated with perturbations of this specialized region [4].

I: Overview of the nuclear envelope and nuclear pore complex

Metazoan nuclear envelope structure and function

The NE is composed of the inner (INM) and outer nuclear membranes (OMN), which are separated by the perinuclear space (PNS) and differ not only in relative position to the nucleoplasm but in protein composition (Fig. 1). These membranes are continuous with the endoplasmic reticulum (ER), and their distinct proteomes are achieved through a diffusion-retention mechanism: proteins freely diffuse within the ER, ONM, and INM but become retained at specific sites upon interacting with binding partners [5, 6]. Maintaining distinct proteomes across the INM/ONM is critical as many important processes depend on communication between the two membranes. For example, the linker of nucleoskeleton and cytoskeleton (LINC) complex is composed of KASH domain proteins in the ONM and

SUN domain proteins in the INM that interact within the PNS (Fig. 1) [7]. The LINC complex connects cytosolic microtubules, actin filaments, and intermediate filaments to the nucleoplasm, and without establishing non-identical proteomes across the INM/ONM, this mechanotransduction would fail [8].

One major feature of the NE that facilitates specificity of the INM/ONM proteomes is the nuclear lamina (Fig. 1). This meshwork of intermediate filaments associates with the INM on the nucleoplasmic face and, among other roles, provides an interaction matrix that retains over 50 different transmembrane lamin-binding proteins [9, 10]. The human genome harbors three genes that encode four major lamin proteins, which assemble into separate networks underlining the INM [11]. *LMNA* encodes lamins A and C while *LMNB1* and *LMNB2* encode the B-type lamins. Lamin expression is highly dependent on cellular differentiation and environment. For example, all mammalian cells express lamin B1 or B2 but only after differentiation do cells express lamin A/C [12, 13]. The posttranslational processing of B-type lamins is also distinct from lamin A/C. While B-type lamins are permanently farnesylated on the C-terminal end, lamin A has this modification cleaved off by the metallopeptidase Zmpste24 and lamin C is never farnesylated. Beyond farnesylation, lamins are heavily phosphorylated at certain stages of the cell cycle [14] and in response to stimuli such as changes in cytoskeletal tension [15].

These complex aspects of the nuclear lamina contribute to this region being a hotbed for disease-associated mutations. At least 15 diseases are attributed to mutations in lamins or lamin-binding proteins and are collectively referred to as laminopathies. Remarkably, over 600 mutations in *LMNA* have been identified in patients with laminopathies. Laminopathies affect a diverse array of tissues and manifest as muscular dystrophies, lipodystrophies, peripheral neuropathies, and multi-tissue disorders associated with rapid aging such as Hutchinson–Gilford progeria [16]. This broad set of affected tissue likely stems from a combination of compromised mechanosensing, mis-

regulation of gene expression, and accumulation of toxic lamin mutants. That such a range of diseases is caused by mutations within the lamina illustrates the crucial nature of a proper NE for cell function.

As the NE is contiguous with the ER, it has been technically challenging to determine whether these membranes have identical lipid compositions [17]. While it is undisputed that the majority of lipids are synthesized by the ER in yeast and animal cells [18], much of the work interrogating the INM for active lipid synthesis has been performed in *Saccharomyces cerevisiae*. In this system, studies have found that the INM is enriched for specific enzymes required for lipid droplet formation [19, 20] and triacylglycerol synthesis [21, 22]. INM enrichment of enzymes associated with lipid metabolism is a strategy also observed in *Caenorhabditis elegans*. In this model, the INM-associated phosphatase complex CTDNEP1/NEP1R1 regulates the amount of diacylglycerol (DAG) within the INM [23, 24]. Regulating the level of DAG, a lipid second messenger, is critically important in the timing of NE breakdown during open mitosis [25-27]. DAG also influences the INM association of the enzyme PCYT1A, which functions in one of two pathways to produce phosphatidylcholine (PC) [28]. Regulating PC at the INM appears to be evolutionarily conserved as the INM translocation of PCYT1A homologs in response to DAG levels is observed from yeast to mouse models [28].

The link between NE breakdown and lipid composition is not restricted to DAG. NE breakdown in metazoan cells requires that the lamina be disassembled, a task accomplished by cascades of phosphorylation [29]. As described above, B-type lamins are permanently farnesylated to facilitate their association with the INM. However, these lamins are also anchored within the INM by the polytopic protein lamin-B receptor (LBR) [30], an interaction that must be disrupted for efficient NE breakdown. LBR is a multifunctional protein that not only binds lamin B but contains a sterol reductase domain [31]. This domain renders LBR essential for cholesterol biosynthesis in mammalian cells

[32]. Although the ER/NE are cholesterol-poor membranes [18], at least two distinct laminopathies are caused by mutations that ablate the sterol reductase activity of LBR [32]. This observation highlights the importance of LBR-driven cholesterol synthesis and leaves open the question of why this process would be so closely associated with lamin B anchoring. While many aspects remain to be understood, especially in a mammalian context, the INM is clearly an active lipid biosynthesis hub required for normal cellular function.

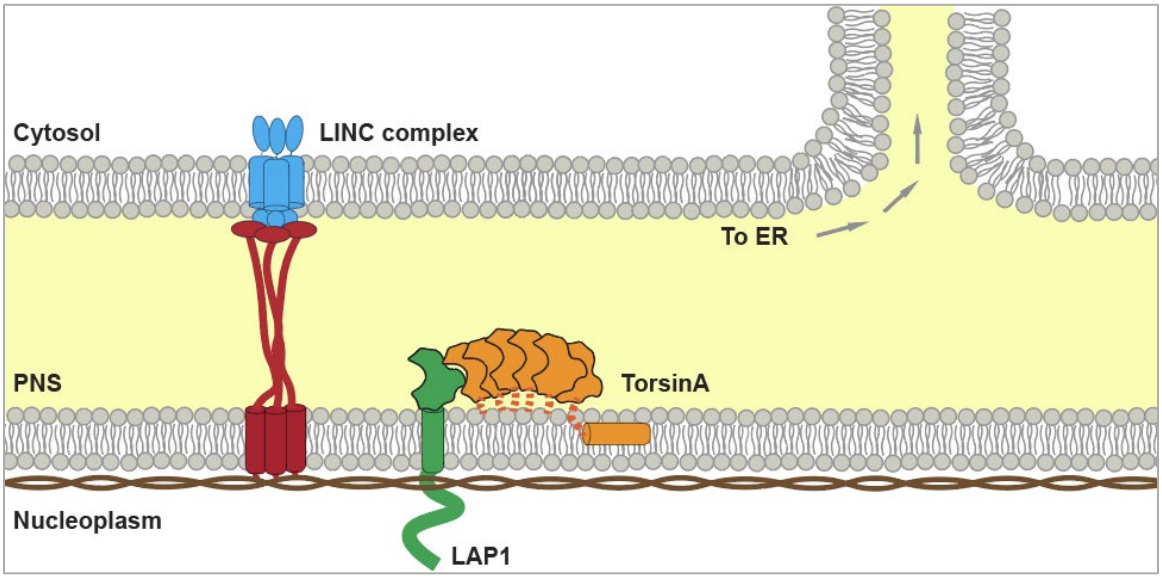

Figure 1. The NE is a double membrane system contiguous with the ER. The ONM (top membrane) and INM (bottom membrane) are separated by a ~45-50 nm perinuclear space (PNS). The spacing is imposed by protein complexes such as the LINC complex composed of SUN (red) and KASH (blue) domain proteins. Proteins such as LAP1 (green) are enriched at the INM via specific interactions with the lamina meshwork (brown). TorsinA (orange), which remains membrane-associated via a hydrophobic helix, forms oligomers that interact with monomeric LAP1.

Nuclear pore complex structure and function

The INM and ONM connect at the ubiquitous, many-megadalton nuclear pore complex (NPC), the function of which hardly needs to be spelled out; to allow for exchange between the cytosol and nucleoplasm (Fig. 2). In human cells, mature NPCs are approximately ~110 MDa in molecular mass and composed of roughly ~1,000 individual proteins called

nucleoporins (Nups). Upon reaching the G2 phase of the cell cycle, each mammalian cell contains about 4,000 pores that transport cargo at a rate of ~1,000 events per second [33]. Depending on the size of the cargo molecule, transport across the NPC happens either as a passive diffusion or a facilitated transport event. While recent advances suggest cast some uncertainty, it has historically been concluded that molecules with a mass less than ~40-60 kDa are able to diffuse freely through the pore but anything larger than this size limit requires help. Despite assistance from a family of proteins called nuclear transport receptors (NTRs), facilitated transport cargo still traverses the NPC at an exquisitely fast speed of ~10-20 MDa per second [33]. This quick and highly specific facilitated transport is achieved through multivalent, low-affinity interactions between NTRs and specialized Nups (see discussion below).

Approximately 30 distinct Nups exist in mammalian cells ranging in molecular mass from ~30-358 kDa and displaying highly diverse properties [34]. Nups assemble into distinct subcomplexes that when together, build mature NPCs [35, 36]. Roughly, these subcomplexes can be conceptualized as contributing to the symmetric core about the ONM/INM or the non-symmetric cytoplasmic/nucleoplasmic faces (Fig. 2). The symmetric core can be divided into the Nup107-160 complex (also referred to as the Y-complex) and the inner ring. The inner ring encloses a central channel in which a selective phase is formed by specialized Nups [37]. Each subcomplex is arranged within the NPC such that the mature complex exhibits an eight-fold rotational symmetry [38]. Emanating into the cytoplasm from the symmetric core are Nup filaments whereupon mRNA export factors and NTRs dock [39]. On the nucleoplasmic side, a basket of Nups extends and imposes directionality across the pore along with the cytoplasmic filaments.

While all Nups are amazing feats of evolution, about a third fall within a specialized class that forms the selective phase within the central channel. This phase prevents random or “inert” cargo from entering or exiting the nucleoplasm non-specifically. The

Nups that form the selective phase harbor long stretches of hydrophobic phenylalanine-glycine (FG) repeats and are aptly named FG-Nups [33]. FG-Nups confer the most important property of the NPC: they compose the selectively permeable barrier that fills the central channel [37]. Simply put, FG-Nups accomplish this incredible property by interacting with NTRs and allowing their passage across the NPC. But how can this explain the extraordinarily fast rate and specificity of NTR passage? The precise mechanism is, as nature tends to be, a little more complicated.

Low complexity FG repeats allow Nups to remain non-globular or intrinsically disordered [40]. This natively unfolded structure is critical for conferring selective properties to NPCs for two major reasons. First, the intrinsic disorder exposes up to 50 FG sites within a single Nup and allows for high valiancy, low affinity interactions with NTRs [33, 41]. Second, the exposed FG domains interact with each other to form a meshwork that physically excludes inert molecules exceeding the ~40 kDa size limit *in vitro* [42]. The local concentration of FG domains within the NPC central channel is in the millimolar range—high enough that when reconstituted *in vitro*, FG domains spontaneously form hydrogels that exhibit the permeability properties observed by bona fide NPCs [42-44]. While alternative models exist to explain NPC transport selectivity, these observations strongly support a selective phase model; NTRs can immerse into an otherwise impermeable hydrogel that provides many weak interactions between FG domains and NTR-cargo complexes, thus allowing their passage through the NPC.

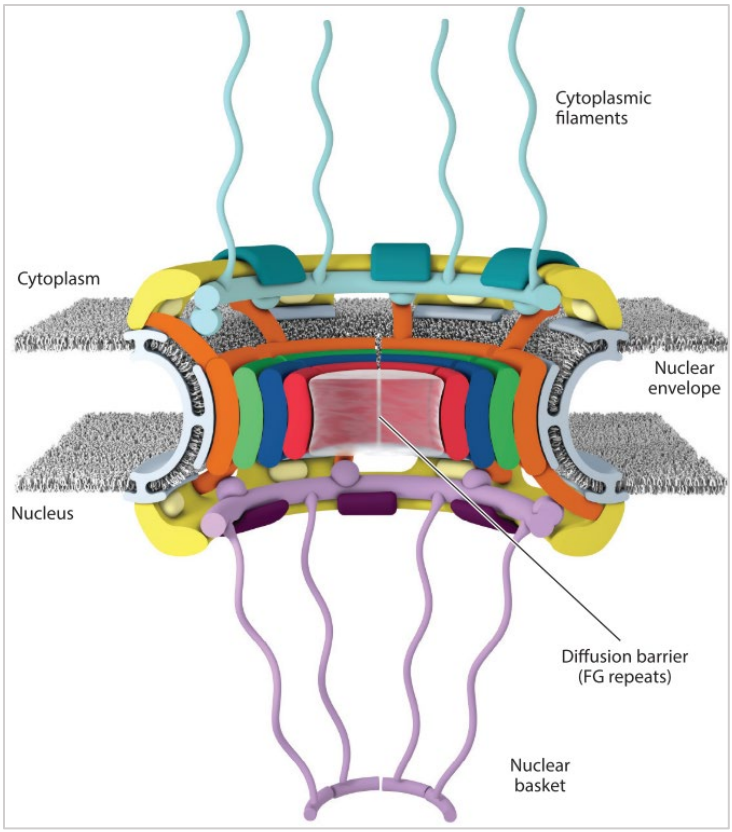

Figure 2. The NPC is a multi-megadalton complex that allows transport across the NE. The NPC has a symmetric core composed of transmembrane anchoring Nups (gray ring behind membrane), the Nup107-160 complex (yellow), the inner ring (orange), and the central channel (green, blue, and red rings). The symmetry is broken on both sides by the cytosolic filaments (light blue) and nucleoplasmic basket (purple). Adapted from [35].

Nuclear pore complex biogenesis

Weighing in at nearly 120 MDa in vertebrates, assembling NPCs poses a massive challenge to cells. Accurate de-mixing of the nucleoplasm and cytoplasm is essential after open mitosis and requires the rapid assembly of NPCs as the NE reforms. During interphase and in differentiated cells, nuclei grow and metabolic demands change. Therefore, to maintain homeostasis, the number of NPCs approximately doubles over the cell cycle [45]. Metazoan cells must thus be able to assemble NPCs with and without a fully formed NE. For this reason, two fundamentally distinct NPC assembly pathways have evolved and each form about half the pores in cells. During late anaphase, NPCs are

assembled though a so-called “postmitotic” pathway after which all pores are inserted into a sealed NE through an interphase insertion pathway [46].

As with many complicated processes, postmitotic NPC assembly occurs one step at a time [47]. After NE breakdown during early mitosis, NPCs are disassembled via phosphorylation cascades into “building blocks” of Nup complexes that persist in the mitotic cytosol [48-50]. Once mitosis has progressed to anaphase, phosphatases initiate NE reformation and NPCs begin to assemble. It would perhaps void the purpose of nuclei if this process did not capture the newly synthesized chromosomes; therefore, the first steps of NPC assembly occur on chromatin. This is coordinated by the Nup ELYS, which binds to chromatin and recruits the Nup107-160 complex [51]. To associate this chromatin-associated complex with the immerging NE membranes, the transmembrane Nups POM121 and NDC1 interact with the Nup107-160 complex and components of the inner ring [52, 53]. After this, the remaining components of the inner ring and central channel FG-Nups are recruited, eventually followed by the cytoplasmic filament and nuclear basket Nups [54]. Transport-competent pores are produced by this process within 10 minutes; however, it takes another two hours before NPCs are fully matured [55, 56]. Nonetheless, this rapid reestablishment of transport allows cells to exit mitosis and begin interphase.

After NE reformation during telophase, cells have a major problem to overcome. To keep up with metabolic requirements, new NPCs need to be inserted into a fully formed NE. This process involves not only bending a membrane, but also causing membrane fusion between the INM and ONM. These are no simple tasks and identifying the machinery responsible is an active area of research. Despite being less understood than the postmitotic pathway, interphase assembly also proceeds in a stepwise manner starting with the deformation of the INM. This membrane bending event depends on the transmembrane Nup POM121, which facilitates recruitment of the Nup107-160 complex

to sites of INM deformation [57, 58]. Once POM121 and the Nup107-160 complex are assembled at nascent pore sites, inner ring components and FG-Nups are recruited to begin establishing the permeability barrier [59]. Lastly, as is the case with postmitotic NPC biogenesis, the cytoplasmic filament and nuclear basket Nups are installed. In contrast to postmitotic assembly, many steps of interphase insertion are slow with the stepwise recruitment of Nups lasting hours before transport competence [60]. Future work will reveal whether this difference in kinetics is related to membrane bending or fusion as the machinery facilitating these processes has not been identified.

II: Pathologies affecting the NPC

Diseases can arise from mutations in nucleoporins

As important as nucleo/cytoplasmic transport is, it is no surprise that diseases arise when it is impaired. What may be surprising, however, is the diversity of pathologies perturbing the NPC can cause [4]. These diseases range from cancers to neurological movement disorders to extreme susceptibility to infection, and have been found to be caused by multiple mechanisms. For example, specific Nups interact with histone acetyltransferases and disrupting these important chromatin regulatory elements may be related to oncogenesis by changing gene expression [61]. A mechanistically distinct contribution to oncogenesis are the pathologic chimeras of Nups including Trp, Nup98, and Nup214, which have been reported to arise in blood cancers [62]. Nup214 is particularly associated with myeloid leukemia and can form multiple chimeric oncoproteins [63]. Mutations in Nups can cause disease beyond cancers including atrial fibrillation (Nup155) [64], infantile bilateral striatal necrosis (Nup62) [65], and susceptibility to necrotizing encephalitis (Nup358) [66]. Neurological diseases are also associated with defective NPCs; triple A syndrome, for example, is caused by a mutation in the protein Aladin, a mysterious component of the NPC with a poorly defined role.

DYT1 Dystonia: defective NPCs as the culprit

Dystonias are a group of neurological movement disorders that cause patients to experience involuntary muscle contractions and debilitating posturing. The most common congenital childhood-onset form is DYT1 dystonia, which is caused by an autosomal dominant mutation in the gene encoding TorsinA [67]. For over two decades, the mechanism by which mutant TorsinA causes DYT1 dystonia has been intensely investigated. Despite many advances, the precise molecular details have remained enigmatic, and treatment options for patients are currently limited to symptom management. However, recent research efforts have begun to reveal the details of DYT1 dystonia pathology with the potential to develop targeted therapies.

DYT1 dystonia is characterized, in part, by two intriguing features: a strictly early-in-life onset and a low genetic penetrance. If TorsinA mutation carriers do not develop DYT1 dystonia by the age of 30, they will never get the disease. This is in stark contrast to the onset pattern of other neurological diseases, the risks for which nearly always increase with age. Additionally, only approximately 30% of TorsinA mutation carriers will develop DYT1 dystonia. This low penetrance suggests a multifaceted and somewhat stochastic pathway of disease development. To understand how mutant TorsinA causes DYT1 dystonia, the mechanism must account for and explain these two features.

TorsinA is one of four human Torsin proteins. Torsins are highly unusual members of the AAA+ protein superfamily, which is composed of ATPases associated with diverse cellular activities [68]. These proteins represent the only members of the AAA+ superfamily to reside within the ER/NE membrane system [69]. Despite belonging to the AAA+ superfamily, Torsins are not inherently active ATPases as they lack a catalytic arginine within their active site [70, 71]. In order to hydrolyze ATP, Torsins must interact with a protein cofactor that complements the active site by donating a critical arginine residue [72, 73]. Two such cofactors have been identified as the ER/NE transmembrane

proteins lamina-associated polypeptide 1 (LAP1) and luminal domain like LAP1 (LULL1) [71, 72, 74] (Fig. 1). Mutations in TorsinA that cause DYT1 dystonia disrupt the interaction with LAP1 or LULL1, highlighting the importance of the Torsin-cofactor complex in neurological development [71, 75].

The most common TorsinA mutation that causes DYT1 dystonia results in an in-frame deletion of glutamic acid residue 302 or 303 and is therefore referred to as TorsinA ΔE. Cell culture and animal models of DYT1 dystonia that lack TorsinA or express TorsinA ΔE exhibit the same hallmark cellular phenotype: NE herniations or blebs [76-79] (Fig. 3). These blebs are protrusions of the INM into the PNS where it can physically contact the ONM but does not fuse with it. Recent studies have found that these blebs result from stalled interphase NPC insertion [80] (Fig. 3). Blebs harbor a specific subset of Nups that are added early during interphase NPC biogenesis and are devoid of those known to be incorporated later [80]. While blebs persist in cell culture models of DYT1 dystonia, mouse models have demonstrated that blebs are only observed during a developmental window [81, 82]. After this window, which is approximately from birth to day 20 of life, the blebs completely resolve. By extension from animal models, this resolution presumably correlates with the onset of TorsinB expression in neurons, a developmentally-regulated Torsin protein that exhibits low neural expression early in life but higher expression later in life [81].

Beyond harboring a specific subset of Nups, blebs are highly enriched for lysine 48-linked ubiquitin (K48-Ub) conjugates and abundant molecular chaperones [79, 83-85] (Fig. 3). K48-Ub is the canonical ubiquitin linkage associated with proteasome-mediated degradation and its presence inside blebs along with chaperones suggests a defect in protein quality control (PQC). Despite many technically distinct approaches, the K48-Ub proteins have not been identified and data presented in this thesis suggest these may simply be bulk metabolic degradation cargo that, for presently unknown reasons, fail to be

efficiently degraded. It is also unknown precisely how molecular chaperones are recruited to blebs. Future work that answers these questions will reveal many new concepts that relate PQC to NPC biogenesis.

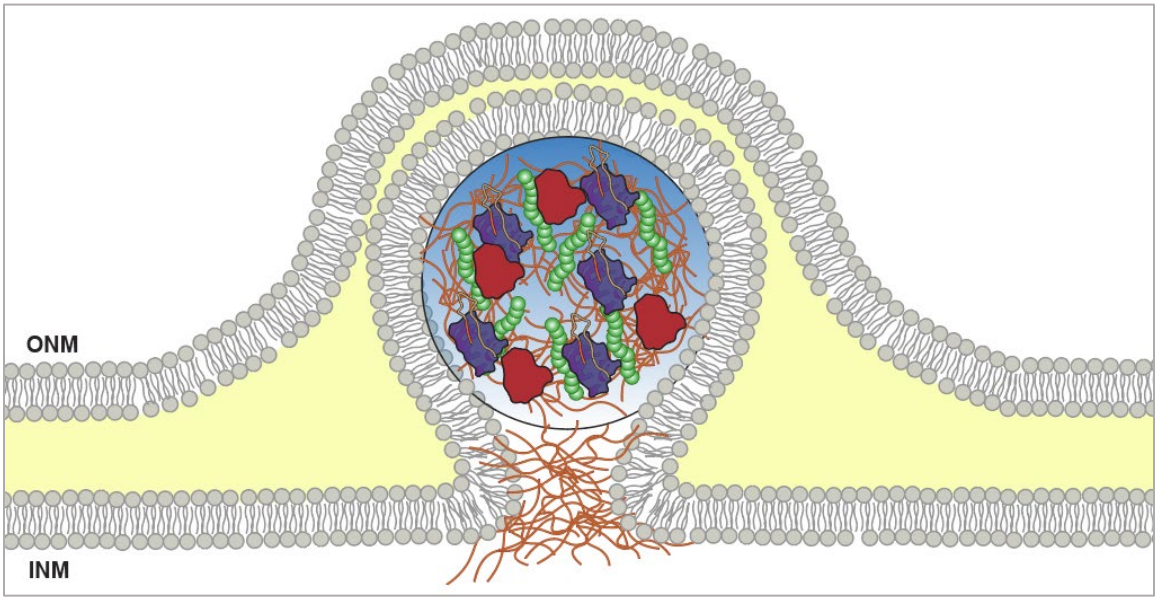

Figure 3. Loss of Torsin ATPase function causes defective NPC biogenesis and the formation of NE blebs. The narrow neck of blebs measures ~50 nm while the lumen can expand out to 200 nm. Blebs are filled with FG-Nups (orange fibrils) that form a phase separated condensate (blue sphere). This condensate sequesters K48-Ub chains (green), MLF2 (red), and chaperones (purple).

Many mechanisms have been proposed to explain how the TorsinA ΔE allele causes DYT1 dystonia [86]. However, many of these have insufficiently accounted for the exclusively childhood onset and reduced penetrance traits of the disease. Because blebs are transient structures, faulty nuclear transport cannot account for the entire pathogenesis. One recently developed model arising from data presented in this dissertation can address these two unique features. NE blebs arise in Torsin-deficient cells due to defective interphase NPC biogenesis and impose a window of vulnerability, which ends once TorsinB expression begins and blebs resolve (i.e., by the age of 30) [84] (Fig. 4). During this window, a metastable proteome is generated through the stabilization of aberrant, ubiquitylated protein and sequestration of chaperones. This model hypothesizes

that in ~30% of disease allele carriers, the metastable proteome is pushed to a proteotoxic level following some secondary insult such as a fever or exposure to environmental stress [84] (Fig. 4). Future studies are warranted to test this model and probe proteome stability in DYT1 dystonia models.

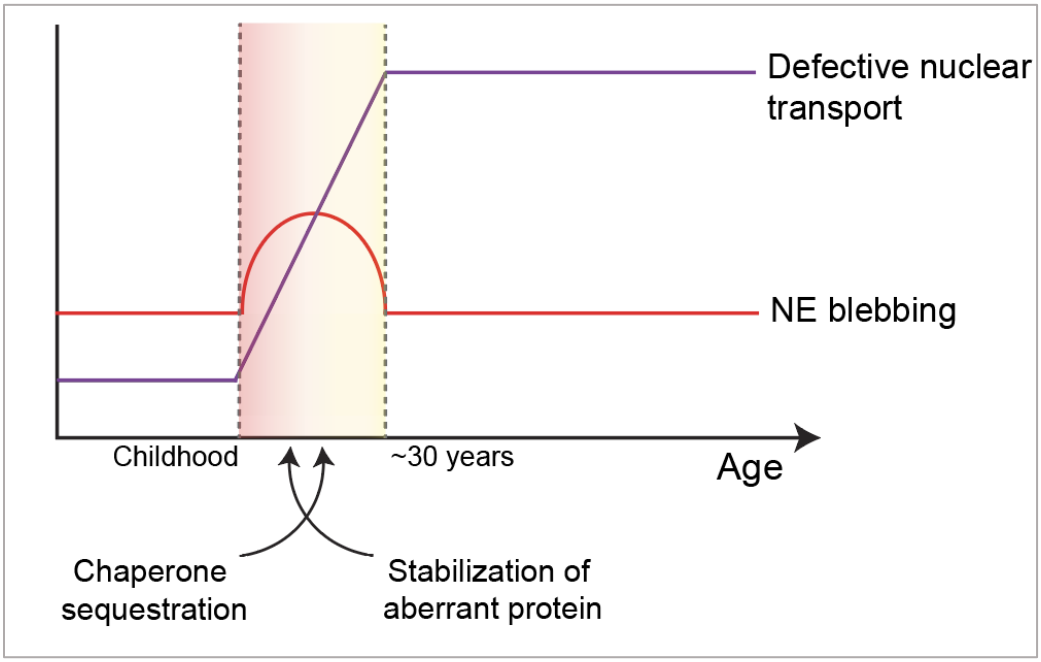

Figure 4. Transient blebbing in Torsin-deficient cells imposes a window of vulnerability for developing DYT1 dystonia. Before the age of 30, people harboring TorsinA mutations accumulate NE blebs in neurons. While this causes a lifetime of defective nuclear transport, blebs are resolved upon TorsinB expression. If the metastable proteome that arises due to chaperone sequestration and stabilization of aberrant protein is pushed into proteotoxicity, the person develops DYT1 dystonia. We hypothesize that this happens in ~30% of disease allele carriers.

III: Surveillance and protein quality control of NPCs

Processes during normal NPC biogenesis & maintenance

With such an essential role and as the largest protein complex, NPC integrity must be surveilled and maintained [87]. In postmitotic cells, NPCs cannot be disassembled (as there is no mitosis) and therefore, differentiated cells do not have an opportunity to do away with aberrantly assembled structures. Does this imply that NPC assembly must

always be perfect in somatic cells? In an ideal world, perhaps this would be the case. In reality, some NPCs fail during assembly and some deteriorate over time [88]. While Nups are rarely turned over and exhibit exceptionally long half-lives [89-91], two pathways of NPC maintenance have been reported in mammalian cells [92]. In myotubes, NPCs are replaced over time such that each pore is a “mosaic” of old and new Nups [92]. In quiescent cells, however, it appears that entire NPCs are replaced *en bloc* [92]. While the mechanistic details of this turnover strategy are still under investigation, the Nup POM121 and the ESCRT machinery likely contribute [92].

Replacing entire NPCs is a mechanism observed also in lower eukaryotes, however, the mechanism is vastly distinct. In these organisms, NPCs are selectively degraded by autophagy [93, 94]. Evidence also exists that yeast degrade Nups via the ubiquitin-proteasome system (UPS) [94]. While functional homologs of the required factors have not been identified in animal cells, Nups can be ubiquitylated and degraded via the mammalian UPS. In metazoan cells, Nups are heavily modified by *O*-linked N-acetylglucosamine (*O*-GlcNAc). Reducing the stoichiometry of *O*-GlcNAc modifications on Nups causes the ubiquitylation and subsequent proteasome-mediated degradation of Nups [95]. As depleting *O*-GlcNAc from Nups causes a collapse of the NPC permeability barrier, this modification could act as an indicator to accelerate the rejuvenation of compromised Nups. Additionally, proteasome clusters at the INM and potentially associated with the NPC have been observed, which could contribute to the UPS clearance of Nups [96].

Immerging aspects of NPC quality control

Painting a full picture of NPC surveillance has not been trivial due to the complexity of the pore. To facilitate studying mechanisms of NPC maintenance, disease models have proved to be invaluable. The neurological movement disorder DYT1 dystonia is associated

with a defect during interphase NPC insertion (see discussion above), and the stalled pore intermediates provide a model system for investigating relationships between Nups and PQC components [80, 84, 85]. From this model, it has become clear that one strategy cells use to respond to defects in NPC biogenesis is the HSP70 system. NE blebs in Torsin-deficient cells are highly enriched for the HSP70 family members HSPA1A and HSC70 [80, 84]. While the precise significance of HSP70s within stalled NPCs is not yet clear, HSP70s could function to relieve or prevent protein aggregation. While depleting HSP70s from blebs does not completely abrogate the sequestered K48-Ub, there are reasons to suggest at least some of the ubiquitylated cargo are HSP70 clients. When HSP70 is chemically trapped in a conformation with relatively high affinity for clients, significantly more K48-Ub is found inside NE blebs [84]. While this small molecule leads to an increase in HSP70 in both wild type (WT) and Torsin knockout (KO) HeLa cells, it normally leads to a depletion of K48-Ub as tightly-bound HSP70 accelerates the proteasome-mediated degradation of ubiquitylated clients. In TorsinKO cells, K48-Ub accumulates in NE blebs instead [84]. Thus, likely at least some K48-Ub protein inside blebs are HSP70 clients destined for degradation.

The permeability barrier established within the NPC by FG-Nups depends on a high concentration of extremely hydrophobic interactions that, importantly, do not aggregate *in vivo* [37]. In a properly assembled pore, this may be due to structural scaffolding and dynamic interactions with NTRs. In an arrested NPC intermediate that lacks much of the mature complex and is devoid of NTRs, how do FG-Nups avoid aggregation? Data suggest that FG-Nups remain soluble despite failing to incorporate into a mature pore [84]. Alone, HSP70 is of little utility to the cell in preventing FG-Nup aggregation as this protein does not possess inherent disaggregase activity. Instead, HSP70 requires interactions with a highly specific set of co-chaperones to build a disaggregase machine [97]. The metazoan disaggregase machinery involves three

players: HSP70 (namely HSPA1A), J-domain proteins (JDP), and a nucleotide exchange factor (NEF) of the HSP110 class (Fig. 5). All of these disaggregase components are detected inside the stalled NPC intermediates that arise in Torsin-deficient cells [80, 84]. These data propose a role for the HSP70 system in mitigating FG-Nup aggregation, and future work is warranted to understand the precise contribution of this chaperone network to NPC surveillance.

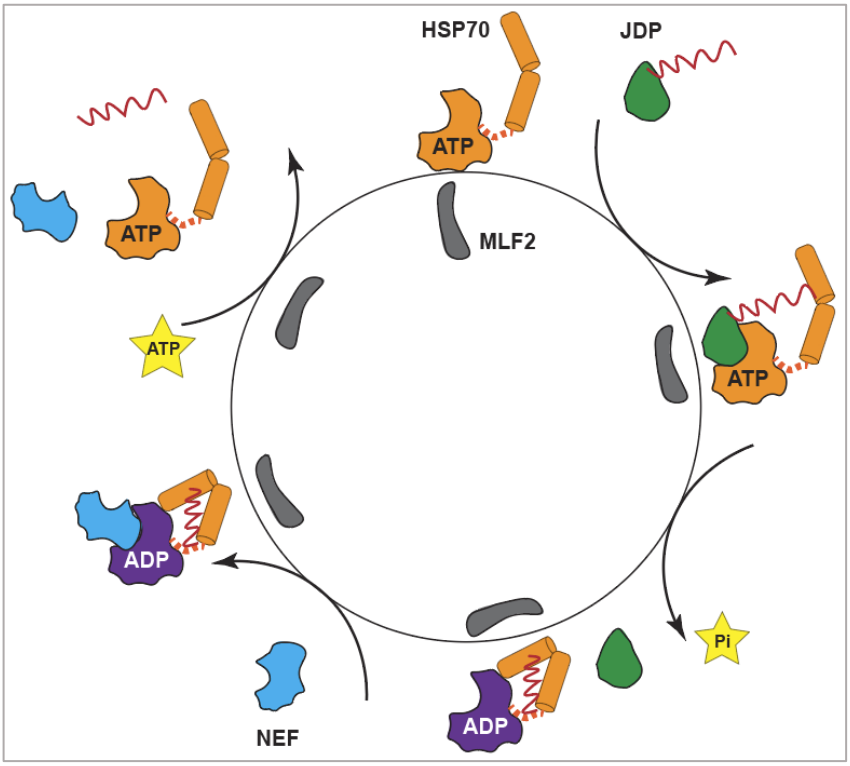

Figure 5. The HSP70 ATPase cycle requires protein cofactors. HSP70 requires J-domain proteins (JDP, green) to stimulate ATP hydrolysis and bring in substrates (red squiggle). Once bound to a JDP and substrate, HSP70 undergoes a conformational change and hydrolyzes ATP (purple). This traps substrate inside the HSP70 binding site. A nucleotide exchange factor (NEF, blue) is required to remove the ADP and release the substrate. MLF2 (gray) could function or interact at multiple points within this cycle.

HSP70s never function alone—they require JDPs and NEFs for all known activities [98] (Fig. 5). One JDP with a recently immerged relevance to NPC surveillance is DNAJB6. Long known as a potent inhibitor of protein aggregation, DNAJB6 prevents the seeding of new aggregates in an HSP70-independent manner [99, 100]. While this activity has been

extensively characterized using disease-relevant aggregates such as polyglutamine (polyQ) expansions [101], new data show that DNAJB6 also suppresses the aggregation of certain FG-Nups. *In vitro*, DNAJB6 prevents the aggregation of FG domains from many different Nups, while in cells, it can decrease the number of deposits formed by unincorporated Nup153 FG domains [85]. Loss of DNAJB6 causes mis-localization of Nups into the cytosol and a concomitant disruption to nucleo-cytoplasmic transport [85]. It is also found to be highly enriched in DYT1 dystonia-associated stalled NPC intermediates [84]. Taken together, DNAJB6 may reduce the aggregation potential of unincorporated FG-Nups and facilitate interphase NPC biogenesis by maintaining usable pools of building blocks.

Studies into NPC biogenesis and Torsin function have revealed myeloid leukemia factor 2 (MLF2) to be a major component of DYT1 dystonia-associated NE blebs [80]. MLF2 is a little-characterized protein with no obvious connection to NPCs. However, a combination of genetic manipulation, microscopy, and *in vitro* reconstitution have revealed that MLF2 may serve multiple purposes during NPC quality control. MLF2 recruits DNAJB6 to stalled NPC intermediates and its overexpression can even titrate DNAJB6 out of polyQ aggregates and into NE blebs [84]. Titrating DNAJB6 away from polyQ aggregates could significantly perturb proteostasis and along with the sequestration of HSP70s into blebs, contribute to DYT1 dystonia onset. While MLF2 strongly associates with HSP70s, its recruitment to blebs is not contingent on this interaction. Instead, MLF2 is likely recruited to stalled NPC intermediates by FG-Nups. *In vitro*, MLF2 can immerse into FG-Nup hydrogels due to its high methionine and arginine content, two amino acid residues that are associated with driving clients into FG hydrogels [102]. In solution with FG-Nups, MLF2 influences the formation and maintenance of FG phases: FG-Nup hydrogels formed in the presence of MLF2 produce larger spheres than those formed without MLF2 [84]. MLF2 also preserves FG hydrogel integrity over time and suppresses

FG amyloid formation *in vitro* [84]. In cells, overexpressing MLF2 reduces the amount of mis-assembled Nup plaques that arise when NPC biogenesis is perturbed, suggesting a chaperone-like activity for MLF2 exists *in vivo*. Thus, MLF2 may recapitulate the reported *in vitro* activities in cells and function as a chaperone to facilitate FG-Nup hydrogel formation and maintenance.

IV: It's not just a phase: biological condensates and PQC

Phase separation is often driven by protein-RNA interactions

The ability to respond quickly to stress and sequester potentially harmful species is an important requirement for successful cells. An illustrative example of such a system is stress granules (SGs), which form in the cytosol when translation is halted. SGs are composed of untranslated mRNA in complex with translation initiation factors and are therefore composed of both RNA and protein [103]. This property—the presence of RNA and protein—allows SGs to undergo a phase separation. SGs afford cells the ability to rapidly protect untranslated mRNA from damage during stress and resume active translation once conditions allow. Proteasomes have also been found to form phase separated proteolytic foci that degrade stress-induced unassembled ribosomal protein [104]. Other examples of membraneless organelles that accomplish similarly important roles are the nucleolus, Cajal body, and P-body. While these are all compositionally distinct, they share the same property that allows SGs to phase separate: they are composed of both RNA and protein.

Interactions between RNA and protein have proven to drive many (if not most) examples of phase separation in cells [105]. This makes the NPC an extremely distinct entity as the FG-Nup-driven phase separation occurs without significant contributions from RNA. Even in stalled NPC intermediates, which harbor only a subset of the FG-Nups found in mature pores, neither RNA nor RNA-binding proteins are enriched [79, 80]. Perhaps the

FG domains are enough to maintain phase separation in NE blebs, but it is also possible that a non-RNA component of NE blebs facilitates this process.

Beyond Nups, chaperones, and MLF2, NE blebs arising in Torsin-deficient cells are highly enriched for K48-Ub. K48-Ub chains have been shown to undergo phase separation when in solution with the UBA domain-containing protein RAD23B, an interaction that is strikingly multivalent [104]. The UBA domain has been shown to be required for phase separation of RAD23B and p62, another UBA domain-containing protein that forms condensates [104, 106]. This condensation is accomplished via multivalent interactions between ubiquitin chains and UBA domains within RAD23B and p62. Not only has RAD23B been detected in NE blebs using high throughput mass spectrometry, but other UBA domain-containing proteins may also be enriched within these stalled NPCs such as UBAC2 [80, 84]. These observations prompt the speculation that perhaps inside stalled NPC intermediates, both FG-Nups and ubiquitin chains contribute to phase separation. This RNA-free condensate may allow cells to sequester aberrant protein species while simultaneously maintaining soluble FG-Nups that could be assembled into mature NPCs upon bleb resolution.

While proteasomes have been found to act within condensates and localize within the nucleus, it would make sense if these degradation machines were to be enriched inside NE blebs. However, proteasome subunits have never been found within these structures. This could be an “intentional” strategy by the cell to concentrate ubiquitin chains inside blebs so that phase separation can be enhanced. Indeed, data show that the cargo inside blebs is highly specific and likely requires an active recruitment mechanism [80]. Thus, if cells can target ubiquitylated cargo to NE blebs, it may be beneficial to delay or prevent degradation of these species so that the ubiquitin chains can facilitate phase separation along with FG-Nups. Future work is required to understand the

role for these ubiquitin chains, the mechanism of their targeting to blebs, and the specific exclusion of proteasomes from stalled NPC intermediates.

V: Quality control through membrane blebbing

NE blebs are associated with neurological disease

While NE blebs are a widely reported phenotype observed in models of DYT1 dystonia, their contribution to disease onset has been mysterious. Critically, are NE blebs a protective or harmful phenomenon? From the outset, it may seem like NE blebs must be harmful as they arise from defective NPC biogenesis. These blebs also harbor ubiquitylated protein and chaperones, opening up the possibility that blebs pose a protective benefit to cells. Despite ubiquitin and chaperones representing major components of blebs, neither of these contribute to membrane herniation formation. When ubiquitin is depleted from NE blebs via the specific targeting of a deubiquitinase, blebs form with no change in size or abundance [80]. Likewise, when HSP70s or HSP40s are knocked down in cells, bleb formation is unperturbed [84]. Thus, the NE membrane deformation event is independent of these species and likely arises from a separate, albeit likely related, defect in DYT1 dystonia cells.

Ubiquitylated cargo that accumulates in Torsin-deficient cells is also generated independently of blebs. When the nucleoporins POM121 or Nup98 are depleted, the membrane herniations typically observed in Torsin-deficient cells do not form [80, 84]. However, particularly in the case of Nup98 depletion, ubiquitylated protein continue to accumulate under this condition; foci of ubiquitylated proteins, MLF2, chaperones, and FG-Nups condense within the cytoplasm [84]. This reflects the independent nature of the processes that produce NE membrane deformations and ubiquitylated cargo. Thus, one possible model for the role of NE blebs is they act as “parking spots” to an overwhelmed cell in which the UPS cannot efficiently process degradation cargo. This idea could be

experimentally addressed by interrogating the proteome stability of Torsin-deficient cells under conditions with Nup98 depleted or present.

NE blebs may serve as general PQC compartments

NE blebs are not exclusively observed in models of DYT1 dystonia. Genetically perturbing NPC biogenesis [107, 108] or subjecting yeast to heat shock or chemical stressors causes NE blebs to form [109]. These stress-related blebs contain ubiquitylated protein and the disaggregase chaperone Hsp104. Unlike the blebs in Torsin-deficient cells, these blebs are not associated with aberrant NPC biogenesis and do not contain nucleoporins. While these blebs are certainly distinct from those that form in models of DYT1 dystonia, there are indisputable similarities that support both structures serving protective roles. For example, heat shock causes a significant increase in the amount of ubiquitin sequestered in blebs formed in Torsin-depleted HeLa cells [110]. Heat shock can cause NE-associated ubiquitin foci to form even in WT HeLa cells. This illustrates that NE blebs can take up cargo destined for degradation when the PQC system becomes overwhelmed.

Beyond chemical stressors, heat shock, and disease, a natural stimulus for causing NE blebs is aging. As cells age, NE and NPC integrity is lost through multiple independent mechanisms including loss of lamin density [111]. While this can cause blebs that lead to NE rupture, cells can exploit blebs as sites to store potentially aberrant protein as we have seen for stressed or diseased cells. Thus, although blebbing can certainly contribute to the loss of NE integrity associated with aging, these structures may also provide protection from aggregate-prone species. This idea casts the NE as an active site of PQC and expands the mechanisms for compartmentalization particularly in metazoan cells.

Membrane fusion poses an experimental hurdle

To test the idea that NE blebs are an active mechanism of PQC requires knowledge of what is currently a missing piece of the puzzle: the membrane fusogenic machinery. In no model organisms or systems has this been identified despite all eukaryotic cells requiring such machinery for viability. As the NE is composed of two membranes (the INM and ONM), which are separated by the ~50 nm perinuclear space, a series of processes must exist to facilitate their fusion. The first step in the process involves a significant membrane bending event, which is no simple feat. Biophysical models predict that the bending stiffness of a double membrane system fused at pores is an order of magnitude higher than that for a single membrane [112]. While the lamina grants some stiffness to the nucleus, NE membranes have an estimated stiffness five times the lamina's value [112]. The major property of the NE contributing to this relatively extreme stiffness is the spacing between the INM and ONM, which may be imposed in part by the LINC complexes discussed above. Given that most biophysical studies do not account for LINC complexes in their modeling, the NE stiffness could be even higher than currently predicted. Thus, it is clear that the membrane bending event requires some sort of active facilitation.

Multiple mechanisms could explain how the INM and ONM approach each other. While differences in lipid composition between bilayers can drive membrane bending, it is presently unclear whether this contributes. While cholesterol influences membrane curvature and LBR, required for cholesterol synthesis, localizes within the INM, there is very little cholesterol within the ER/NE membranes [32, 113, 114]. Given the degree of bending, stiffness, and continuity with the ER, much of which is composed of tubulated membranes, a more likely scenario is that proteins facilitate the bending process by physically shaping them. In the ER, tubules are formed and maintained by two major classes of proteins—reticulons and REEPs [115]. Both of these families achieve membrane deformation by inserting an amphipathic helix into one membrane bilayer,

causing it to bend. An analogous role for these proteins at the NE has been proposed [116, 117], although it is unclear whether REEPs or reticulons are found at substantial concentrations within the NE system. Another mechanism of membrane bending has been proposed to involve Nups [118, 119]. While only three of the 30 identified Nups have transmembrane domains, the soluble Nup107-160 complex shows homology to vesicle coating complex proteins [120] and interacts with lipid bilayers via multiple membrane-binding ALPS motifs [121]. Furthermore, other Nups in distinct NPC subcomplexes, such as Nup53, have been found to interact directly with membranes [122]. Taken together, while it is possible that REEPs and/or reticulons facilitate NE membrane bending, Nups likely contribute to the process and may work in combination with other factors to accomplish such a difficult task.

Once the INM and ONM are apposed close to one another, the next difficult step can occur: membrane fusion. Little is known about the machinery responsible for mediating this process, but one protein family proposed to have fusogenic properties are Torsins [68, 123]. Torsins are attractive candidates to possess a functional role in this process for a few reasons. First, Torsins are the only AAA+ ATPases within the ER/NE system, and other members of this superfamily are involved in membrane fusion events. For example, the AAA+ protein NSF is required for vesicular transport as it disassembles and thereby recycles fusogenic machinery. The molecular target of Torsin ATPase activity has not been identified and it could relate to membrane fusion, an event that often requires energy. Second, two of the four Torsins interact with membranes via an N-terminal hydrophobic helix and have been shown to tubulate membranes *in vitro* [124]. While this is not the same as promoting membrane fusion, Torsins may remodel the membranes with which they interact. Third and perhaps most intuitive, loss of Torsin function stalls NPC biogenesis prior to fusion but after membrane bending [80]. It is thus very tempting

to speculate that Torsins contribute to this elusive step during NPC biogenesis, perhaps in disassembling fusogenic machinery or by mediating the fusion directly.

VI: New insights into PQC mechanisms at the vertebrate INM

Distant p97 activity affects quality control at the INM

Due to inherent differences in complexity, much of our understanding of PQC mechanisms is from yeast [125]. While this work has revealed foundational knowledge of conserved pathways and strategies, it is clear that metazoan cells evolved distinct mechanisms. As the Torsin ATPase system is not found in yeast, the PQC pathway that becomes dysregulated upon its depletion provides a unique opportunity to interrogate a metazoan quality control process.

It continues to remain elusive why ubiquitylated protein accumulate in DYT1 dystonia models or precisely what cellular process produces these. Work described within this thesis demonstrates that a highly specific p97 network is required to generate the K48-Ub cargo detected inside blebs [110]. p97 (VCP, or Cdc48 in yeast) is a AAA+ ATPase that contributes to highly diverse cellular processes ranging from membrane fusion to protein degradation to mitosis. When p97 ATPase activity is inhibited via a small molecule or RNAi-based knockdown, the K48-Ub normally observed within blebs is nearly completely depleted [110]. This reduction can occur in as little as four hours and strongly implicates p97 activity in the Torsin-regulated PQC pathway.

While p97 is an extraordinarily well conserved protein from yeast (Cdc48) to humans, it is functionalized by a host (>40) of adaptors/interactors that do not exhibit such a degree of conservation [126]. To determine which of the many p97-related processes may be related to the Torsin system, it is important to know which of these adaptors p97 requires. By far the best characterized role for p97 is extracting mis-folded or aberrant protein from the ER membrane into the cytosol where they become ubiquitylated and degraded by the proteasome [127]. This process, termed ER-associated degradation

(ERAD), is responsible for generating much of the K48-Ub-conjugated protein within cells. To participate in ERAD, p97 must interact with a conserved heterodimeric adaptor called Ufd1/Npl4, which directs it to retrotranslocon protein complexes embedded within the ER membrane.

Given its connection to the ER and producing ubiquitylated protein, ERAD would be a logical process to be regulated by Torsins. However, depleting cells of the Ufd1/Npl4 heterodimer or core retrotranslocon components only slightly decreases the amount of K48-Ub sequestered inside blebs and certainly not to the same degree as inhibiting p97 [110]. Depleting p47, the adaptor that functionalizes p97 during vesicular membrane fusion, also does not decrease the amount of K48-Ub in blebs. Knocking down the adaptor UBXD1, however, causes a significant reduction of bleb-associated ubiquitylated protein comparable to the inhibition of p97 [110]. Taken together, while ERAD may contribute a small fraction of the K48-Ub cargo, the p97-UBXD1 complex appears to participate in a Torsin-regulated PQC pathway.

UBXD1 is a relatively obscure, metazoan-specific p97 adaptor that has been implicated in ERAD [128], mitophagy [129], autophagy [130], and intracellular trafficking [131]. While UBXD1 is enriched in brain tissue and localizes to the cytoplasm and nucleus, it does not appear to be sequestered inside blebs [110]. The involvement of UBXD1 in multiple processes and lack of enrichment within blebs suggests that the sequestered K48-Ub does not stem from a single process and that a more general PQC defect may exist in cells without functional Torsin. This furthermore suggests that although Torsins localize within the ER, processes outside of this compartment likely contribute to DYT1 dystonia onset. One speculative model for how this could manifest would be that Torsins are required for the biogenesis of a proteasome adaptor for K48-Ub protein generated via processes involving UBXD1/p97. Without Torsins, these K48-Ub proteins fail to be degraded and instead, they are targeted to NE blebs via an unknown mechanism. While

UBXD1 could represent a therapeutic, future work is required to understand how this multifunctional p97 adaptor connects to a Torsin-regulated PQC pathway.

Protein turnover at the mammalian INM

While the ER and NE membranes are contiguous, degradation processes within this membrane system are primarily associated with the ER. However, recent advances in yeast have revealed a protein turnover process unique to the INM that depends on the Asi complex [132]. The Asi complex is a poorly conserved group of proteins that do not have homologs in higher eukaryotes. Does this imply that protein is not degraded at the INM in metazoan cells? While it may not be as active as the ER, it is becoming clear that the mammalian INM does indeed possess mechanisms of protein turnover. One model for studying such mechanisms employs the INM-resident protein LBR. Like many INM proteins, LBR is associated with disease-causing mutations. Normally long-lived, mutations within LBR cause it to undergo rapid degradation in the nucleoplasm after extraction from the INM [32].

Studying this model of INM degradation has revealed a novel mechanism for protein turnover in mammalian cells. This pathway requires the E2 ubiquitin-conjugating enzymes Ube2G2 and Ube2D3, along with the E3 ubiquitin ligase RNF5 [133]. An added level of regulation exists within this pathway via the poorly understood transmembrane protein TMEM33, which is required for efficient biosynthesis of RNF5. RNF5 is also a transmembrane protein and one of the only examples of an E3 ligase than is found not only in the ER but also at the NE. Thus, misfolded proteins that escape ERAD or become damaged at the INM can be ubiquitylated and degraded directly out of the INM in mammalian cells [133]. Identifying RNF5 as an INM-resident ubiquitin ligase will likely prompt the discovery of similar proteins contributing to degradation at the NE. This pathway also illustrates the difficulties faced when studying such a system as layers of regulation can occlude relationships between proteins.

Concluding remarks

The eukaryotic NE has immerged as an active site of PQC. As it is strongly associated with myriad diseases, continuing to uncover such mechanisms will be imperative for therapeutic advances. Given its contributions to numerous cellular processes ranging from gene expression to mechanotransduction and cholesterol biosynthesis, understanding how the NE is maintained will expand our knowledge of basic cellular biology.

One major knowledge gap that remains to be filled not just in the nucleus field but in all of membrane biology is the fusogen that acts during NPC biogenesis. Discovering this mechanism will reveal biophysical properties perhaps never before observed as the NE lipid and protein composition, along with the perforation by NPCs, creates an exquisitely unique scenario for membrane fusion. Many data suggest this mechanism will be distinct from that observed in ER membrane tubulation, and its identification is sure to affect many corners of biology.

As our understanding of Torsin ATPases continues to grow, so does the list of questions to be addressed. How can the only AAA+ ATPase within the ER/NE system affect so many aspects of PQC and NPC biogenesis? Loss of this protein function clearly ricochets affects across all of cellular homeostasis, and pinpointing its exact function will further our understanding of metazoan NE dynamics along with proteostasis. With these advancements will come new therapeutic avenues not only for DYT1 dystonia, but for a host of laminopathies with currently no targeted strategies.

References

[1] Martin W, Koonin EV. Introns and the origin of nucleus-cytosol compartmentalization. Nature. 2006;440:41-5.

[2] Gerace L, Tapia O. Messages from the voices within: regulation of signaling by proteins of the nuclear lamina. Curr Opin Cell Biol. 2018;52:14-21.

[3] Kirby TJ, Lammerding J. Emerging views of the nucleus as a cellular mechanosensor. Nat Cell Biol. 2018;20:373-81.

[4] Dauer WT, Worman HJ. The nuclear envelope as a signaling node in development and disease. Dev Cell. 2009;17:626-38.

[5] Powell L, Burke B. Internuclear exchange of an inner nuclear membrane protein (p55) in heterokaryons: in vivo evidence for the interaction of p55 with the nuclear lamina. J Cell Biol. 1990;111:2225-34.

[6] Ungricht R, Klann M, Horvath P, Kutay U. Diffusion and retention are major determinants of protein targeting to the inner nuclear membrane. J Cell Biol. 2015;209:687-703.

[7] Sosa BA, Rothballer A, Kutay U, Schwartz TU. LINC Complexes Form by Binding of Three KASH Peptides to Domain Interfaces of Trimeric SUN Proteins. Cell. 2012;149:1035-47.

[8] Isermann P, Lammerding J. Nuclear mechanics and mechanotransduction in health and disease. Curr Biol. 2013;23:R1113-21.

[9] Wilson KL, Foisner R. Lamin-binding Proteins. Cold Spring Harbor perspectives in biology. 2010;2:a000554.

[10] Cheng LC, Baboo S, Lindsay C, Brusman L, Martinez-Bartolome S, Tapia O, et al. Identification of new transmembrane proteins concentrated at the nuclear envelope using organellar proteomics of mesenchymal cells. Nucleus. 2019;10:126-43.

[11] Shimi T, Kittisopikul M, Tran J, Goldman AE, Adam SA, Zheng Y, et al. Structural organization of nuclear lamins A, C, B1, and B2 revealed by superresolution microscopy. Mol Biol Cell. 2015;26:4075-86.

[12] Rober RA, Weber K, Osborn M. Differential timing of nuclear lamin A/C expression in the various organs of the mouse embryo and the young animal: a developmental study. Development. 1989;105:365-78.

[13] Swift J, Ivanovska IL, Buxboim A, Harada T, Dingal PC, Pinter J, et al. Nuclear lamin-A scales with tissue stiffness and enhances matrix-directed differentiation. Science. 2013;341:1240104.

[14] Murray-Nerger LA, Cristea IM. Lamin post-translational modifications: emerging toggles of nuclear organization and function. Trends Biochem Sci. 2021;46:832-47.

[15] Buxboim A, Swift J, Irianto J, Spinler KR, Dingal PC, Athirasala A, et al. Matrix elasticity regulates lamin-A,C phosphorylation and turnover with feedback to actomyosin. Curr Biol. 2014;24:1909-17.

[16] de Leeuw R, Gruenbaum Y, Medalia O. Nuclear Lamins: Thin Filaments with Major Functions. Trends Cell Biol. 2018;28:34-45.

[17] Bahmanyar S, Schlieker C. Lipid and protein dynamics that shape nuclear envelope identity. Mol Biol Cell. 2020;31:1315-23.

[18] van Meer G, Voelker DR, Feigenson GW. Membrane lipids: where they are and how they behave. Nat Rev Mol Cell Biol. 2008;9:112-24.

[19] Romanauska A, Kohler A. The Inner Nuclear Membrane Is a Metabolically Active Territory that Generates Nuclear Lipid Droplets. Cell. 2018;174:700-15 e18.

[20] Romanauska A, Kohler A. Reprogrammed lipid metabolism protects inner nuclear membrane against unsaturated fat. Dev Cell. 2021;56:2562-78 e3.

[21] Barbosa AD, Sembongi H, Su WM, Abreu S, Reggiori F, Carman GM, et al. Lipid partitioning at the nuclear envelope controls membrane biogenesis. Mol Biol Cell. 2015;26:3641-57.

[22] Barbosa AD, Lim K, Mari M, Edgar JR, Gal L, Sterk P, et al. Compartmentalized Synthesis of Triacylglycerol at the Inner Nuclear Membrane Regulates Nuclear Organization. Dev Cell. 2019;50:755-66 e6.

[23] Bahmanyar S, Biggs R, Schuh AL, Desai A, Muller-Reichert T, Audhya A, et al. Spatial control of phospholipid flux restricts endoplasmic reticulum sheet formation to allow nuclear envelope breakdown. Genes Dev. 2014;28:121-6.

[24] Penfield L, Shankar R, Szentgyorgyi E, Laffitte A, Mauro MS, Audhya A, et al. Regulated lipid synthesis and LEM2/CHMP7 jointly control nuclear envelope closure. J Cell Biol. 2020;219.

[25] Golden A, Liu J, Cohen-Fix O. Inactivation of the C. elegans lipin homolog leads to ER disorganization and to defects in the breakdown and reassembly of the nuclear envelope. J Cell Sci. 2009;122:1970-8.

[26] Gorjanacz M, Mattaj IW. Lipin is required for efficient breakdown of the nuclear envelope in Caenorhabditis elegans. J Cell Sci. 2009;122:1963-9.

[27] Mall M, Walter T, Gorjanacz M, Davidson IF, Nga Ly-Hartig TB, Ellenberg J, et al. Mitotic lamin disassembly is triggered by lipid-mediated signaling. J Cell Biol. 2012;198:981-90.

[28] Haider A, Wei YC, Lim K, Barbosa AD, Liu CH, Weber U, et al. PCYT1A Regulates Phosphatidylcholine Homeostasis from the Inner Nuclear Membrane in Response to Membrane Stored Curvature Elastic Stress. Dev Cell. 2018;45:481-95 e8.

[29] Ungricht R, Kutay U. Mechanisms and functions of nuclear envelope remodelling. Nat Rev Mol Cell Biol. 2017;18:229-45.

[30] Olins AL, Rhodes G, Welch DB, Zwerger M, Olins DE. Lamin B receptor: multi-tasking at the nuclear envelope. Nucleus. 2010;1:53-70.

[31] Li X, Roberti R, Blobel G. Structure of an integral membrane sterol reductase from Methylomicrobium alcaliphilum. Nature. 2015;517:104-7.

[32] Tsai PL, Zhao C, Turner E, Schlieker C. The Lamin B receptor is essential for cholesterol synthesis and perturbed by disease-causing mutations. Elife. 2016;5.

[33] Ribbeck K, Gorlich D. Kinetic analysis of translocation through nuclear pore complexes. EMBO J. 2001;20:1320-30.

[34] Cronshaw JM, Krutchinsky AN, Zhang W, Chait BT, Matunis MJ. Proteomic analysis of the mammalian nuclear pore complex. J Cell Biol. 2002;158:915-27.

[35] Lin DH, Hoelz A. The Structure of the Nuclear Pore Complex (An Update). Annual review of biochemistry. 2019;88:725-83.

[36] Schuller AP, Wojtynek M, Mankus D, Tatli M, Kronenberg-Tenga R, Regmi SG, et al. The cellular environment shapes the nuclear pore complex architecture. Nature. 2021;598:667-71.

[37] Schmidt HB, Gorlich D. Transport Selectivity of Nuclear Pores, Phase Separation, and Membraneless Organelles. Trends Biochem Sci. 2016;41:46-61.

[38] Gall JG. Octagonal nuclear pores. J Cell Biol. 1967;32:391-9.

[39] Hodge CA, Tran EJ, Noble KN, Alcazar-Roman AR, Ben-Yishay R, Scarcelli JJ, et al. The Dbp5 cycle at the nuclear pore complex during mRNA export I: dbp5 mutants with defects in RNA binding and ATP hydrolysis define key steps for Nup159 and Gle1. Genes Dev. 2011;25:1052-64.

[40] Denning DP, Patel SS, Uversky V, Fink AL, Rexach M. Disorder in the nuclear pore complex: the FG repeat regions of nucleoporins are natively unfolded. Proc Natl Acad Sci U S A. 2003;100:2450-5.

[41] Patel SS, Belmont BJ, Sante JM, Rexach MF. Natively unfolded nucleoporins gate protein diffusion across the nuclear pore complex. Cell. 2007;129:83-96.

[42] Frey S, Gorlich D. A saturated FG-repeat hydrogel can reproduce the permeability properties of nuclear pore complexes. Cell. 2007;130:512-23.

[43] Frey S, Richter RP, Gorlich D. FG-rich repeats of nuclear pore proteins form a three-dimensional meshwork with hydrogel-like properties. Science. 2006;314:815-7.

[44] Schmidt HB, Gorlich D. Nup98 FG domains from diverse species spontaneously phase-separate into particles with nuclear pore-like permselectivity. Elife. 2015;4.

[45] Maul GG, Maul HM, Scogna JE, Lieberman MW, Stein GS, Hsu BY, et al. Time sequence of nuclear pore formation in phytohemagglutinin-stimulated lymphocytes and in HeLa cells during the cell cycle. J Cell Biol. 1972;55:433-47.

[46] Otsuka S, Ellenberg J. Mechanisms of nuclear pore complex assembly - two different ways of building one molecular machine. FEBS Lett. 2018;592:475-88.

[47] Kutay U, Juhlen R, Antonin W. Mitotic disassembly and reassembly of nuclear pore complexes. Trends Cell Biol. 2021;31:1019-33.

[48] Laurell E, Beck K, Krupina K, Theerthagiri G, Bodenmiller B, Horvath P, et al. Phosphorylation of Nup98 by multiple kinases is crucial for NPC disassembly during mitotic entry. Cell. 2011;144:539-50.

[49] Linder MI, Kohler M, Boersema P, Weberruss M, Wandke C, Marino J, et al. Mitotic Disassembly of Nuclear Pore Complexes Involves CDK1- and PLK1-Mediated Phosphorylation of Key Interconnecting Nucleoporins. Dev Cell. 2017;43:141-56 e7.

[50] Heusel M, Frank M, Kohler M, Amon S, Frommelt F, Rosenberger G, et al. A Global Screen for Assembly State Changes of the Mitotic Proteome by SEC-SWATH-MS. Cell Syst. 2020;10:133-55 e6.

[51] Franz C, Walczak R, Yavuz S, Santarella R, Gentzel M, Askjaer P, et al. MEL-28/ELYS is required for the recruitment of nucleoporins to chromatin and postmitotic nuclear pore complex assembly. EMBO Rep. 2007;8:165-72.

[52] Rasala BA, Ramos C, Harel A, Forbes DJ. Capture of AT-rich chromatin by ELYS recruits POM121 and NDC1 to initiate nuclear pore assembly. Mol Biol Cell. 2008;19:3982-96.

[53] Mitchell JM, Mansfeld J, Capitanio J, Kutay U, Wozniak RW. Pom121 links two essential subcomplexes of the nuclear pore complex core to the membrane. J Cell Biol. 2010;191:505-21.

[54] Otsuka S, Steyer AM, Schorb M, Hériché JK, Hossain MJ, Sethi S, et al. Postmitotic nuclear pore assembly proceeds by radial dilation of small membrane openings. Nat Struct Mol Biol. 2018;25:21-8.

[55] Dultz E, Zanin E, Wurzenberger C, Braun M, Rabut G, Sironi L, et al. Systematic kinetic analysis of mitotic dis- and reassembly of the nuclear pore in living cells. J Cell Biol. 2008;180:857-65.

[56] Dultz E, Huet S, Ellenberg J. Formation of the nuclear envelope permeability barrier studied by sequential photoswitching and flux analysis. Biophys J. 2009;97:1891-7.

[57] Funakoshi T, Clever M, Watanabe A, Imamoto N. Localization of Pom121 to the inner nuclear membrane is required for an early step of interphase nuclear pore complex assembly. Mol Biol Cell. 2011;22:1058-69.

[58] Doucet CM, Talamas JA, Hetzer MW. Cell cycle-dependent differences in nuclear pore complex assembly in metazoa. Cell. 2010;141:1030-41.

[59] Rothballer A, Kutay U. Poring over pores: nuclear pore complex insertion into the nuclear envelope. Trends Biochem Sci. 2013;38:292-301.

[60] Dultz E, Ellenberg J. Live imaging of single nuclear pores reveals unique assembly kinetics and mechanism in interphase. J Cell Biol. 2010;191:15-22.

[61] Kohler A, Hurt E. Gene regulation by nucleoporins and links to cancer. Mol Cell. 2010;38:6-15.

[62] Xu S, Powers MA. Nuclear pore proteins and cancer. Semin Cell Dev Biol. 2009;20:620-30.

[63] Mendes A, Fahrenkrog B. NUP214 in Leukemia: It's More than Transport. Cells. 2019;8.

[64] Zhang X, Chen S, Yoo S, Chakrabarti S, Zhang T, Ke T, et al. Mutation in nuclear pore component NUP155 leads to atrial fibrillation and early sudden cardiac death. Cell. 2008;135:1017-27.

[65] Basel-Vanagaite L, Muncher L, Straussberg R, Pasmanik-Chor M, Yahav M, Rainshtein L, et al. Mutated nup62 causes autosomal recessive infantile bilateral striatal necrosis. Annals of neurology. 2006;60:214-22.

[66] Neilson DE, Adams MD, Orr CM, Schelling DK, Eiben RM, Kerr DS, et al. Infection-triggered familial or recurrent cases of acute necrotizing encephalopathy caused by mutations in a component of the nuclear pore, RANBP2. Am J Hum Genet. 2009;84:44-51.

[67] Gonzalez-Alegre P. Advances in molecular and cell biology of dystonia: Focus on torsinA. Neurobiol Dis. 2019;127:233-41.

[68] Rose AE, Brown RS, Schlieker C. Torsins: not your typical AAA+ ATPases. Critical reviews in biochemistry and molecular biology. 2015;50:532-49.

[69] Jungwirth M, Dear ML, Brown P, Holbrook K, Goodchild R. Relative tissue expression of homologous torsinB correlates with the neuronal specific importance of DYT1 dystonia-associated torsinA. Hum Mol Genet. 2010;19:888-900.

[70] Zhu L, Millen L, Mendoza JL, Thomas PJ. A unique redox-sensing sensor II motif in TorsinA plays a critical role in nucleotide and partner binding. J Biol Chem. 2010;285:37271-80.

[71] Zhao C, Brown RS, Chase AR, Eisele MR, Schlieker C. Regulation of Torsin ATPases by LAP1 and LULL1. Proc Natl Acad Sci U S A. 2013;110:E1545-54.

[72] Brown RS, Zhao C, Chase AR, Wang J, Schlieker C. The mechanism of Torsin ATPase activation. Proc Natl Acad Sci U S A. 2014;111:E4822-31.

[73] Sosa BA, Demircioglu FE, Chen JZ, Ingram J, Ploegh HL, Schwartz TU. How lamina-associated polypeptide 1 (LAP1) activates Torsin. Elife. 2014;3:e03239.

[74] Goodchild RE, Dauer WT. The AAA+ protein torsinA interacts with a conserved domain present in LAP1 and a novel ER protein. J Cell Biol. 2005;168:855-62.

[75] Demircioglu FE, Sosa BA, Ingram J, Ploegh HL, Schwartz TU. Structures of TorsinA and its disease-mutant complexed with an activator reveal the molecular basis for primary dystonia. Elife. 2016;5.

[76] Goodchild RE, Kim CE, Dauer WT. Loss of the dystonia-associated protein torsinA selectively disrupts the neuronal nuclear envelope. Neuron. 2005;48:923-32.

[77] Jokhi V, Ashley J, Nunnari J, Noma A, Ito N, Wakabayashi-Ito N, et al. Torsin mediates primary envelopment of large ribonucleoprotein granules at the nuclear envelope. Cell Rep. 2013;3:988-95.

[78] VanGompel MJ, Nguyen KC, Hall DH, Dauer WT, Rose LS. A novel function for the Caenorhabditis elegans torsin OOC-5 in nucleoporin localization and nuclear import. Mol Biol Cell. 2015;26:1752-63.

[79] Laudermilch E, Tsai PL, Graham M, Turner E, Zhao C, Schlieker C. Dissecting Torsin/cofactor function at the nuclear envelope: a genetic study. Mol Biol Cell. 2016;27:3964-71.

[80] Rampello AJ, Laudermilch E, Vishnoi N, Prophet SM, Shao L, Zhao C, et al. Torsin ATPase deficiency leads to defects in nuclear pore biogenesis and sequestration of MLF2. The Journal of Cell Biology. 2020;219.

[81] Tanabe LM, Liang CC, Dauer WT. Neuronal Nuclear Membrane Budding Occurs during a Developmental Window Modulated by Torsin Paralogs. Cell Rep. 2016;16:3322-33.

[82] Li J, Kim S, Pappas SS, Dauer WT. CNS critical periods: implications for dystonia and other neurodevelopmental disorders. JCI Insight. 2021;6(4):e142483.

[83] Liang CC, Tanabe LM, Jou S, Chi F, Dauer WT. TorsinA hypofunction causes abnormal twisting movements and sensorimotor circuit neurodegeneration. J Clin Invest. 2014;124:3080-92.

[84] Prophet SM, Rampello AJ, Niescier RF, Shaw JE, Mallick S, Koleske AJ, et al. Atypical nuclear envelope condensates linked to neurological disorders reveal nucleoporin-directed chaperone activities. Nat Cell Biol. 2022. In press.

[85] Kuiper EF, Gallardo P, Bergsma T, Mari M, Musskopf MK, Kuipers J, et al. The molecular chaperone DNAJB6 provides surveillance of FG-Nups and is required for interphase nuclear pore complex biogenesis. Nat Cell Biol. 2022. In press.

[86] Rampello AJ, Prophet SM, Schlieker C. The Role of Torsin AAA+ Proteins in Preserving Nuclear Envelope Integrity and Safeguarding Against Disease. Biomolecules. 2020;10.

[87] Liu J, Hetzer MW. Nuclear pore complex maintenance and implications for age-related diseases. Trends Cell Biol. 2022;32:216-27.

[88] D'Angelo MA, Raices M, Panowski SH, Hetzer MW. Age-dependent deterioration of nuclear pore complexes causes a loss of nuclear integrity in postmitotic cells. Cell. 2009;136:284-95.

[89] Savas JN, Toyama BH, Xu T, Yates JR, 3rd, Hetzer MW. Extremely long-lived nuclear pore proteins in the rat brain. Science. 2012;335:942.

[90] Toyama BH, Savas JN, Park SK, Harris MS, Ingolia NT, Yates JR, 3rd, et al. Identification of long-lived proteins reveals exceptional stability of essential cellular structures. Cell. 2013;154:971-82.

[91] Hakhverdyan Z, Molloy KR, Keegan S, Herricks T, Lepore DM, Munson M, et al. Dissecting the Structural Dynamics of the Nuclear Pore Complex. Mol Cell. 2021;81:153-65 e7.

[92] Toyama BH, Arrojo EDR, Lev-Ram V, Ramachandra R, Deerinck TJ, Lechene C, et al. Visualization of long-lived proteins reveals age mosaicism within nuclei of postmitotic cells. J Cell Biol. 2019;218:433-44.

[93] Allegretti M, Zimmerli CE, Rantos V, Wilfling F, Ronchi P, Fung HKH, et al. In-cell architecture of the nuclear pore and snapshots of its turnover. Nature. 2020;586:796-800.

[94] Lee CW, Wilfling F, Ronchi P, Allegretti M, Mosalaganti S, Jentsch S, et al. Selective autophagy degrades nuclear pore complexes. Nat Cell Biol. 2020;22:159-66.

[95] Zhu Y, Liu TW, Madden Z, Yuzwa SA, Murray K, Cecioni S, et al. Post-translational O-GlcNAcylation is essential for nuclear pore integrity and maintenance of the pore selectivity filter. J Mol Cell Biol. 2016;8:2-16.

[96] Albert S, Schaffer M, Beck F, Mosalaganti S, Asano S, Thomas HF, et al. Proteasomes tether to two distinct sites at the nuclear pore complex. Proc Natl Acad Sci U S A. 2017;114:13726-31.

[97] Nillegoda NB, Kirstein J, Szlachcic A, Berynskyy M, Stank A, Stengel F, et al. Crucial HSP70 co-chaperone complex unlocks metazoan protein disaggregation. Nature. 2015;524:247-51.

[98] Kampinga HH, Craig EA. The HSP70 chaperone machinery: J proteins as drivers of functional specificity. Nat Rev Mol Cell Biol. 2010;11:579-92.

[99] Hageman J, Rujano MA, van Waarde MA, Kakkar V, Dirks RP, Govorukhina N, et al. A DNAJB chaperone subfamily with HDAC-dependent activities suppresses toxic protein aggregation. Mol Cell. 2010;37:355-69.

[100] Thiruvalluvan A, de Mattos EP, Brunsting JF, Bakels R, Serlidaki D, Barazzuol L, et al. DNAJB6, a Key Factor in Neuronal Sensitivity to Amyloidogenesis. Mol Cell. 2020;78:346-58 e9.

[101] Mansson C, Kakkar V, Monsellier E, Sourigues Y, Harmark J, Kampinga HH, et al. DNAJB6 is a peptide-binding chaperone which can suppress amyloid fibrillation of

polyglutamine peptides at substoichiometric molar ratios. Cell Stress Chaperones. 2014;19:227-39.

[102] Frey S, Rees R, Schunemann J, Ng SC, Funfgeld K, Huyton T, et al. Surface Properties Determining Passage Rates of Proteins through Nuclear Pores. Cell. 2018;174:202-17 e9.

[103] Protter DSW, Parker R. Principles and Properties of Stress Granules. Trends Cell Biol. 2016;26:668-79.

[104] Yasuda S, Tsuchiya H, Kaiho A, Guo Q, Ikeuchi K, Endo A, et al. Stress- and ubiquitylation-dependent phase separation of the proteasome. Nature. 2020;578:296-300.

[105] Roden C, Gladfelter AS. RNA contributions to the form and function of biomolecular condensates. Nat Rev Mol Cell Biol. 2021;22:183-95.

[106] Fu A, Cohen-Kaplan V, Avni N, Livneh I, Ciechanover A. p62-containing, proteolytically active nuclear condensates, increase the efficiency of the ubiquitin-proteasome system. Proc Natl Acad Sci U S A. 2021;118.

[107] Wente SR, Blobel G. A temperature-sensitive NUP116 null mutant forms a nuclear envelope seal over the yeast nuclear pore complex thereby blocking nucleocytoplasmic traffic. J Cell Biol. 1993;123:275-84.

[108] Zhang W, Neuner A, Ruthnick D, Sachsenheimer T, Luchtenborg C, Brugger B, et al. Brr6 and Brl1 locate to nuclear pore complex assembly sites to promote their biogenesis. J Cell Biol. 2018;217:877-94.

[109] Panagaki D, Croft JT, Keuenhof K, Larsson Berglund L, Andersson S, Kohler V, et al. Nuclear envelope budding is a response to cellular stress. Proc Natl Acad Sci U S A. 2021;118.

[110] Prophet SM, Naughton BS, Schlieker C. p97/UBXD1 Generate Ubiquitylated Proteins That Are Sequestered into Nuclear Envelope Herniations in Torsin-Deficient Cells. Int J Mol Sci. 2022;23.

[111] Rempel IL, Crane MM, Thaller DJ, Mishra A, Jansen DP, Janssens G, et al. Age-dependent deterioration of nuclear pore assembly in mitotic cells decreases transport dynamics. Elife. 2019;8.

[112] Agrawal A, Lele TP. Geometry of the nuclear envelope determines its flexural stiffness. Mol Biol Cell. 2020;31:1815-21.

[113] Chernomordik LV, Kozlov MM. Protein-lipid interplay in fusion and fission of biological membranes. Annual review of biochemistry. 2003;72:175-207.

[114] Ridsdale A, Denis M, Gougeon PY, Ngsee JK, Presley JF, Zha X. Cholesterol is required for efficient endoplasmic reticulum-to-Golgi transport of secretory membrane proteins. Mol Biol Cell. 2006;17:1593-605.

[115] Voeltz GK, Prinz WA, Shibata Y, Rist JM, Rapoport TA. A class of membrane proteins shaping the tubular endoplasmic reticulum. Cell. 2006;124:573-86.

[116] Dawson TR, Lazarus MD, Hetzer MW, Wente SR. ER membrane-bending proteins are necessary for de novo nuclear pore formation. J Cell Biol. 2009;184:659-75.

[117] Golchoubian B, Brunner A, Bragulat-Teixidor H, Neuner A, Akarlar BA, Ozlu N, et al. Reticulon-like REEP4 at the inner nuclear membrane promotes nuclear pore complex formation. J Cell Biol. 2022;221.

[118] Talamas JA, Hetzer MW. POM121 and Sun1 play a role in early steps of interphase NPC assembly. J Cell Biol. 2011;194:27-37.

[119] Hamed M, Antonin W. Dunking into the Lipid Bilayer: How Direct Membrane Binding of Nucleoporins Can Contribute to Nuclear Pore Complex Structure and Assembly. Cells. 2021;10.

[120] Devos D, Dokudovskaya S, Alber F, Williams R, Chait BT, Sali A, et al. Components of coated vesicles and nuclear pore complexes share a common molecular architecture. PLoS biology. 2004;2:e380.

[121] Drin G, Casella JF, Gautier R, Boehmer T, Schwartz TU, Antonny B. A general amphipathic alpha-helical motif for sensing membrane curvature. Nat Struct Mol Biol. 2007;14:138-46.

[122] Vollmer B, Schooley A, Sachdev R, Eisenhardt N, Schneider AM, Sieverding C, et al. Dimerization and direct membrane interaction of Nup53 contribute to nuclear pore complex assembly. EMBO J. 2012;31:4072-84.

[123] Laudermilch E, Schlieker C. Torsin ATPases: structural insights and functional perspectives. Curr Opin Cell Biol. 2016;40:1-7.

[124] Demircioglu FE, Zheng W, McQuown AJ, Maier NK, Watson N, Cheeseman IM, et al. The AAA + ATPase TorsinA polymerizes into hollow helical tubes with 8.5 subunits per turn. Nat Commun. 2019;10:3262.

[125] Sontag EM, Samant RS, Frydman J. Mechanisms and Functions of Spatial Protein Quality Control. Annual review of biochemistry. 2017;86:97-122.

[126] Buchberger A, Schindelin H, Hanzelmann P. Control of p97 function by cofactor binding. FEBS Lett. 2015;589:2578-89.

[127] Wu X, Rapoport TA. Mechanistic insights into ER-associated protein degradation. Curr Opin Cell Biol. 2018;53:22-8.

[128] Madsen L, Andersen KM, Prag S, Moos T, Semple CA, Seeger M, et al. Ubxd1 is a novel co-factor of the human p97 ATPase. Int J Biochem Cell Biol. 2008;40:2927-42.

[129] Bento AC, Bippes CC, Kohler C, Hemion C, Frank S, Neutzner A. UBXD1 is a mitochondrial recruitment factor for p97/VCP and promotes mitophagy. Sci Rep. 2018;8:12415.

[130] Papadopoulos C, Kirchner P, Bug M, Grum D, Koerver L, Schulze N, et al. VCP/p97 cooperates with YOD1, UBXD1 and PLAA to drive clearance of ruptured lysosomes by autophagy. EMBO J. 2017;36:135-50.

[131] Ritz D, Vuk M, Kirchner P, Bug M, Schutz S, Hayer A, et al. Endolysosomal sorting of ubiquitylated caveolin-1 is regulated by VCP and UBXD1 and impaired by VCP disease mutations. Nat Cell Biol. 2011;13:1116-23.

[132] Natarajan N, Foresti O, Wendrich K, Stein A, Carvalho P. Quality Control of Protein Complex Assembly by a Transmembrane Recognition Factor. Mol Cell. 2020. Jan 2;77(1):108-119.e9.

[133] Tsai PL, Cameron CJF, Forni MF, Wasko R, Naughton BS, Horsley V, et al. A Genome-wide CRISPR Screen Identifies Quality Control Machinery of Mammalian Nuclear Membrane Proteins. Cell Rep. 2022. In revision.

Chapter 2: p97/UBXD1 generate ubiquitinated proteins that are sequestered into nuclear envelope herniations in Torsin-deficient cells

Sarah M. Prophet[1], Brigitte S. Naughton[1], and Christian Schlieker[1,2,3]

[1]Department of Molecular Biophysics & Biochemistry, Yale University, New Haven, CT 06520, [2]Department of Cell Biology, Yale School of Medicine, New Haven, CT 06520

The following work was published in the journal *International Journal of Molecular Sciences*.

Abstract: DYT1 dystonia is a debilitating neurological movement disorder that arises upon Torsin ATPase deficiency. Nuclear envelope (NE) blebs that contain FG-nucleoporins (FG-Nups) and K48-linked ubiquitin are the hallmark phenotype of Torsin manipulation across disease models of DYT1 dystonia. While the aberrant deposition of FG-Nups is caused by defective nuclear pore complex assembly, the source of K48-ubiquitinated proteins inside NE blebs is not known. Here, we demonstrate that the characteristic K48-ubiquitin accumulation inside blebs requires p97 activity. This activity is highly dependent on the p97 adaptor UBXD1. We show that p97 does not significantly depend on the Ufd1/Npl4 heterodimer to generate the K48-ubiquitinated proteins inside blebs, nor does inhibiting translation affect the ubiquitin sequestration in blebs. However, stimulating global ubiquitylation by heat shock greatly increases the amount of K48-ubiquitin sequestered inside blebs. These results suggest that blebs have an extraordinarily high capacity for sequestering ubiquitinated protein generated in a p97-dependent manner. The p97/UBXD1 axis is thus a major factor contributing to cellular DYT1 dystonia pathology and its modulation represents an unexplored potential for therapeutic development.

1. Introduction

Torsins are essential [1] AAA+ ATPases that localize within the endoplasmic reticulum (ER)/nuclear envelope (NE) membrane system [2, 3] where they carry out poorly understood functions. Torsins are unusual AAA+ ATPases as they strictly require interactions with one of two transmembrane activators to hydrolyze ATP [4-6]. The first of these activating proteins is lamina-associated polypeptide 1 (LAP1) and the second is luminal domain like LAP1 (LULL1) [7]. Mutations within the C-terminal domain of TorsinA [8], one of the four Torsins encoded by the human genome [9], cause the neurological movement disorder DYT1 dystonia [2, 10, 11]. These DYT1 dystonia-causing mutations disrupt interactions between TorsinA and LAP1 or LULL1 [4, 8, 12], demonstrating the importance of the Torsin/activator complex during neurological development.

While the precise biological role of Torsins remains unknown, herniations of the NE are observed across all Torsin loss-of-function models ranging from *Caenorhabditis elegans* [13] to mouse neurons [1] (see schematic illustration, Figure 1A). These herniations, referred to as blebs, represent aberrant nuclear pore complex (NPC) biogenesis intermediates that are arrested prior to inner and outer nuclear membrane fusion [14-16]. Although blebs do not harbor mature NPCs, specific nucleoporins (Nups) associated with building multiple subcomplexes of the NPC are found inside these herniations [14, 15, 17, 18]. In addition to Nups, the protein of unknown function myeloid leukemia factor 2 (MLF2) localizes to blebs [15, 18] by a yet-to-be identified mechanism.

Beyond Nups and MLF2 [15, 18], blebs are also highly enriched for components that suggest a protein quality control (PQC) defect exists in Torsin-deficient cells. First, blebs harbor Lys48-linked polyubiquitin (K48-Ub) chains [17, 19] conjugated to proteins of unknown identity or origin. As K48-Ub is canonically associated with proteasome-mediated degradation [20], its enrichment inside blebs indicates that Torsin-deficient cells may have a compromised PQC mechanism. Secondly, blebs sequester a specific

chaperone network composed of abundant HSP70 and HSP40 members [18]. The presence of HSP70s and HSP40s inside blebs along with K48-Ub suggests that a stress-related chaperone activity such as facilitating protein degradation [21] may also become dysregulated in Torsin loss-of-function models.

As neither the identity nor the origin of the K48-Ub protein inside blebs is known, the PQC pathway that becomes dysregulated upon Torsin deficiency remains poorly understood. Consequently, whether and how this PQC pathway contributes to DYT1 dystonia remains unknown. K48-Ub accumulation in blebs could indicate that proteins become ubiquitylated in response to Torsin dysfunction or that proteins fail to be degraded when Torsin function is compromised. While DYT1 dystonia is the most common congenital form of dystonia [10], no curative treatment has been reported and therapeutic options are only partially effective. Thus, a more accurate characterization of the PQC defect in Torsin-deficient cells may lead to the identification of yet unexplored pathways, and define molecular players that might represent new targets for therapeutic intervention.

In this report, we employ a Torsin-deficient cell line as a model system to scrutinize the poorly understood process of K48-Ub accumulation widely observed in disease models of DYT1 dystonia. We demonstrate that p97 activity is required to generate the K48-Ub accumulation inside blebs. We further show that K48-Ub conjugates inside blebs are unlikely to result from de novo synthesis or canonical ER–associated protein degradation (ERAD) as depleting components of the Hrd1-Ufd1/Npl4/p97-axis has little effect on K48-Ub deposition in blebs. A candidate approach aimed at the identification of alternative p97 cofactors revealed that the incompletely understood p97 adaptor UBXD1 and the deubiquitylating enzyme YOD1 are required for Ub accumulation. Stimulating an increase in global ubiquitylation by heat shock results in a stark increase of K48-Ub conjugates sequestered into blebs. This supports the idea that NE blebs have a

remarkable capacity for sequestering misfolded, ubiquitylated proteins and preventing their degradation.

Taken together, our observations reveal that the p97/UBXD1 axis is a central player for the cellular pathology caused by defects in Torsin function. As p97 is a druggable target for a diverse set of diseases [22], its potential involvement in DYT1 dystonia reveals unexplored therapeutic opportunities to improve the lives of patients suffering from this debilitating disease.

2. Results

2.1. *p97 activity is required for the K48-Ub accumulation inside NE blebs.*

The cellular processes that produce the K48-Ub conjugates found inside blebs (Figure 1A) has not been identified. One essential K48-Ub-directed enzyme in mammalian cells is the p97 ATPase (also called VCP in mammals and Cdc48 in budding yeast). While p97 activity functions in a number of diverse processes, its best characterized role is to mobilize ubiquitinated clients from membranes, interaction partners, or aggregates [23]. After extraction, these ubiquitinated proteins are often degraded by the proteasome. Because p97 is a major K48-Ub-directed enzyme, we investigated whether its activity was relevant for generating the K48-Ub conjugates inside blebs.

To inhibit p97, we treated TorsinKO cells with the p97 inhibitor CB-5083 [24, 25]. As MLF2-HA localizes to blebs in a ubiquitin-independent manner [15], this construct was expressed to distinguish TorsinKO cells with blebs from those without. After four hours of p97 inhibition, the K48-Ub signal inside blebs was significantly depleted (Figure 1B, C) despite MLF2-HA remaining efficiently sequestered inside blebs (Figure 1B). To determine whether p97 is functioning directly within the bleb, we assessed its localization. Consistent with our previous observations [15, 17], we found it was not stably enriched within blebs (Figure 1D) although we cannot exclude the formal possibility that p97 is present at levels below the detection limit of immunofluorescence (IF). While it is possible that p97 acts

directly within the bleb lumen to generate the K48-Ub proteins, p97 activity at locations distinct from the bleb may also be required for the K48-Ub accumulation in Torsin-deficient cells.

2.2. *Increased K48-Ub association with p97 in Torsin-deficient cells.*

Upon finding that p97 activity is important for accumulating K48-Ub conjugates inside blebs, we asked whether p97 is generally associated with more ubiquitin in TorsinKO cells compared to wild type (WT). To address this, we prepared soluble detergent extracts and performed an immunoprecipitation (IP) under native conditions with an anti-p97 antibody. Upon immunoblotting the IP with an anti-K48-Ub antibody, we observed that endogenous p97 was associated with significantly more K48-Ub in TorsinKO cells compared to WT (Figure 1E). This suggests that cells with deficient Torsin ATPase activity have more ubiquitylated p97 clients than cells with functional Torsins.

Taken together, we demonstrate that p97 associates with K48-Ub to a greater extent in TorsinKO cells compared to WT and that p97 activity is required for these ubiquitylated proteins to localize within blebs.

2.3. *p97 does not require the Ufd1/Npl4 heterodimer for the majority of the K48-Ub protein deposition to blebs.*

The increased association of p97 with K48-Ub in TorsinKO cells suggests that a process linked to p97 function becomes perturbed during Torsin deficiency. One major p97-dependent process is ERAD [26]. During ERAD, p97 interacts with the Ufd1/Npl4 heterodimer to extract ubiquitylated glycoproteins from the ER membrane [27]. To determine whether ERAD-directed adaptor proteins contribute to the K48-Ub accumulation within blebs, we depleted the heterodimer by treating cells with Ufd1/Npl4 targeting siRNA for 48 hours (Figure 2A, cf Figure 3D). Knocking down Ufd1/Npl4 caused

a minor decrease in the number of K48-Ub foci around the nuclear rim of TorsinKO cells (Figure 2A, B). However, this effect was far less pronounced compared to the K48-Ub depletion observed upon inhibiting p97 activity (Figure 1B, C). This suggests that a Ufd1/Npl4-independent p97 activity generates the majority of the K48-Ub protein inside blebs.

To validate that knocking down Ufd1/Npl4 resulted in measurable functional defects, i.e., stabilizing substrates destined for degradation, we expressed the short-lived protein LBR-1600* [28] (Figure 2C). LBR-1600* is a mutant of the ER- and inner nuclear membrane-localized lamin B receptor that is degraded in a p97- and proteasome-dependent manner [28, 29]. Upon knocking down Ufd1/Npl4, LBR-1600* was strongly stabilized to the same extent as co-overexpressing a dominant-negative p97 construct, p97-QQ (Figure 2C). We therefore conclude that depleting the Ufd1/Npl4 heterodimer substantially stabilizes ERAD substrates but does not deplete blebs of K48-Ub conjugates to a similar extent as inhibiting p97.

2.4. *Many canonical ERAD-associated E3 ligases do not significantly contribute to the K48-Ub protein inside blebs.*

Prior to cytosolic degradation, ERAD substrates must be ubiquitinated and (in some cases) translocated across the lipid bilayer of the ER [26]. Ubiquitylation occurs on the cytosolic face of the ER and can be achieved by several E3 ligases embedded within the ER membrane. These E3 ligases not only ubiquitinate ERAD substrates but can also serve as dislocon channels within the ER membrane [30-32]. ERAD substrates are primed with ubiquitin by these E3 ligases so that the p97 machinery can recognize and extract these clients [27, 33]. Depending on the nature of the ERAD substrate [34-36], the dislocon that enables passage out of the ER is canonically formed by either of the two highly conserved complexes composed of Hrd1 [30, 37] or Doa10 [32] (MARCH6 in

mammalian cells). While lower eukaryotic ERAD relies mostly on these two complexes, metazoans have alternative E3 ligases and mechanisms such as, for example, gp78 [26, 36].

To investigate the involvement of the canonical E3 ligases in K48-Ub bleb accumulation, we depleted Hrd1, MARCH6, or gp78 from TorsinKO cells for 48 hours (Figure S2A, B). None of these conditions significantly affected the K48-Ub accumulation inside blebs to the extent achieved by p97 inhibition (compare Figure S2 and 1B). Taken together with the minimal to modest effect of Ufd1/Npl4 depletion described above (Figure 2A-C), these data suggest that p97 does not require canonical ERAD machinery to generate the K48-Ub proteins sequestered inside blebs. These results further suggest that if ERAD substrates contribute to the K48-Ub inside blebs, they are likely retrotranslocated and ubiquitinated by a noncanonical mechanism largely independent of Hrd1, MARCH6, and gp78.

2.5. *Newly synthesized, misfolded proteins do not account for the majority of the K48-Ub protein inside blebs.*

An estimated 30% of all newly synthesized proteins are defective and degraded by the proteosome [38]. Newly synthesized misfolded proteins thus represent a constant threat to cellular proteostasis [39]. For this reason, cells have evolved multiple mechanisms to prevent translational errors and degrade aberrant proteins [40]. As the process of translation produces a significant number of ubiquitylated polypeptides, we determined whether newly synthesized ubiquitylated proteins contribute to the K48-Ub signal inside blebs. To this end, we monitored the K48-Ub accumulation in blebs when translation was inhibited via cycloheximide (CHX) treatment. To confirm the efficacy of inhibiting translation, we performed a CHX chase in WT HeLa cells expressing the short-lived protein HA-LBR 1600* [28]. As expected, CHX treatment resulted in a steady decline

of HA-LBR 1600* over time, consistent with a blockage of *de novo* synthesis and concomitant proteasomal turnover (Figure 2D). When translation was inhibited in TorsinKO cells by CHX treatment for up to seven hours, we observed no change in the accumulation of K48-Ub protein within the bleb (Figure 2E). As a four-hour treatment with the p97 inhibitor CB-5083 results in a near-complete depletion of K48-Ub inside blebs (Fig. 1B, C), this suggests that newly synthesized misfolded proteins are unlikely to significantly contribute to the K48-Ub cargo sequestered into blebs.

2.6. *The relevant p97 activity for accumulating K48-Ub inside blebs depends on the cofactors YOD1 and UBXD1.*

p97 acts with at least 40 different interaction partners in mammalian cells [41] that direct its ATPase activity to distinct processes including ERAD, membrane fusion, and lysosome clearance [41, 42]. To better understand what cellular process(es) requires p97 activity to produce the K48-Ub conjugates inside blebs, we determined the effect of depleting specific p97-interacting proteins.

While p97 interacts with many cofactors/adaptors, at least three major p97 complexes exist. These are the Ufd1/Npl4 heterodimer, p47, and UBXD1 [41]. The Ufd1/Npl4 dimer is canonically associated with recruiting p97 to the ER membrane during ERAD [43] whereas p47 functionalizes p97 during homotypic membrane fusion [44]. UBXD1, however, has been reported to contribute to a number of processes including trafficking events [45, 46], autophagy of lysosomes [47], mitophagy [48], and ERAD [49]. Beyond these three complexes, p97 requires the deubiquitinase (DUB) YOD1 to participate in a number of processes including ERAD [50] and lysosome clearance [47].

To interrogate the diverse processes to which p97 contributes, we depleted p47 and UBXD1 by RNAi in TorsinKO cells (Figure 3A-C). To monitor bleb formation, these cells expressed MLF2-HA (Figure 3A). To perturb YOD1 activity, we expressed WT or a

dominant-negative YOD1 construct YOD1-CS-FLAG [50] in TorsinKO cells co-expressing MLF2-HA (Figure 3A, B).

Upon depleting UBXD1 or perturbing YOD1 activity, the number of K48-Ub foci around the nuclear rim was significantly decreased (Figure 3A, B). This was not the case when p47 was depleted (Figure 3A, B). As WT YOD1 is an active DUB, expressing the WT construct also resulted in a significant decrease in the number of K48-Ub foci in TorsinKO cells (Figure 3A, B). This finding suggests that ubiquitylated proteins targeted by YOD1 localize to blebs as removing the ubiquitin modification by overexpressed WT YOD1 also depletes blebs of K48-Ub (Figure 3A, B). Taken together, these results suggest that the p97 interactors UBXD1 and YOD1, but not p47, participate in the process(es) that generate the K48-Ub proteins inside blebs.

MLF2, a protein of unknown function, is highly enriched inside the lumen of blebs [15, 18]. While UBXD1, WT YOD1, and YOD1-CS are not enriched inside blebs (Figure S1), MLF2 may contribute to bleb formation by interacting with these p97 adaptors elsewhere within the cell. To test this possibility, we conducted an IP with an anti-FLAG antibody from TorsinKO cells expressing FLAG-tagged WT YOD1, YOD1-CS, UBXD1, or AIFM1 (Figure 3D). AIFM1 is a known MLF2-interacting protein [51, 52] and therefore served as a positive co-IP control (Figure 3D). We found that MLF2-HA specifically co-immunoprecipitated with UBXD1 and WT but not dominant-negative YOD1 in TorsinKO cells (Figure 3D). While these interactions may be direct or indirect, MLF2 may function with specific p97 complexes during the generation of ubiquitylated protein and rely on active YOD1 for recruitment to these sites.

2.7. *Provoking an increase in global ubiquitylation causes more K48-Ub conjugates to become sequestered inside blebs.*

Whether blebs are enriched for specific K48-ubiquitylated proteins or sequester general ubiquitin cargo is not known. While we have performed multiple mass spectrometry-based analyses in an attempt to identify the K48-Ub conjugates inside blebs [15, 18], we have not observed the enrichment of a specific set of ubiquitylated proteins. This suggests that blebs may possess an extraordinarily high capacity for sequestering a wide variety of ubiquitylated species, and the enrichment of specific proteins may therefore be difficult to capture by mass spectrometry. Thus, to probe the capacity of blebs to sequester ubiquitylated protein, we subjected WT and TorsinKO cells to heat shock, a condition that is known to greatly increase the amount of ubiquitylated protein inside cells [53-55].

Upon incubating TorsinKO cells at 42ºC for 16 hours, the amount of K48-Ub inside blebs increased significantly (Figure 4A-D). This effect was observed by IF (Figure 4A, B) and by biochemical fractionation wherein cells were enriched for ER/NE fractions (Figure 4C, D). This enrichment involved isolating nuclei and membrane fractions by centrifugation through a sucrose gradient. ER/NE fractions were further enriched by centrifugation following DNase/heparin treatment. Successful fractionation was confirmed by immunoblot using antibodies against emerin (enriched in the ER/NE) and hnRNPA1 (enriched in the nucleoplasmic fraction) (Figure 4C). After validating successful fractionation, the ER/NE samples were subjected to immunoblot with an anti-K48-Ub antibody (Figure 4D). While WT HeLa cells had approximately the same amount of ER/NE-associated K48-Ub during unstressed (37ºC) and stressed (42ºC) conditions (Figure 4D), TorsinKO cells had significantly more ER/NE-associated K48-Ub upon heat shock (Figure 4D). Thus, when a global increase in ubiquitin is provoked, TorsinKO cells sequester more K48-Ub inside blebs.

Heat shock results in the ubiquitylation and degradation of many proteins that are otherwise relatively stable [55, 56]. One possibility is that blebs stabilize proteins that are targeted for degradation, as we have demonstrated for the model substrate Δ133-ORF10 [18]. While MLF2 is not directly ubiquitylated inside blebs [15], we found that MLF2-HA undergoes degradation in WT cells exposed to heat shock (Figure 4E). Note that p97 is included in the immunoblot as a loading control (Figure 4E). In contrast to WT HeLa cells under stress, MLF2-HA is stabilized in TorsinKO cells under heat shock conditions with a steady state abundance that is relatively unchanged from unstressed to stressed conditions (Figure 4E).

To determine whether the K48-Ub accumulation inside blebs upon heat shock also depends on YOD1 activity, we expressed the dominant-negative YOD1-CS-FLAG construct and exposed cells to heat shock (Figure 4F, G). In untransfected heat shocked TorsinKO cells, an intense K48-Ub signal was detected within NE foci by IF (Figure 4F, yellow arrowhead). However, upon expression of YOD1-CS-FLAG, this NE accumulation was reduced (Figure 4F, blue arrow). We quantified this effect by determining the percent of K48-Ub foci that localize to the nuclear rim upon heat shock with or without YOD1-CS-FLAG overexpression (Figure 4G). This analysis demonstrated that upon heat shock, TorsinKO cells overexpressing YOD1-CS developed significantly fewer NE-associated K48-Ub foci (Figure 4G).

As WT YOD1 overexpression also significantly reduced the amount of K48-Ub inside blebs (Figure 3A, B), we expressed WT YOD1-FLAG in WT and TorsinKO undergoing heat shock stress (Figure 4H). These cells were fractionated into ER/NE enrichments and analyzed by immunoblot with antibodies against K48-Ub, calnexin as a loading control, and FLAG (Figure 4H). As described above, untransfected TorsinKO cells accumulated a significant amount of ER/NE-associated K48-Ub upon heat shock (Figure 4H). However, when WT YOD1-FLAG was expressed, this heat shock-specific increase

in K48-Ub was significantly reduced (Figure 4H). These results are consistent with a model wherein Torsin-deficient cells sequester ubiquitylated proteins that are–to a large extent–clients of the p97 machinery and heat-labile.

3. Discussion

NE blebs are the conserved cellular phenotype observed in Torsin ATPase loss-of-function models, which result from defective nuclear pore complex biogenesis (Figure 1A). These blebs are enriched for specific components including FG-nucleoporins [15, 17], chaperones [18, 57], MLF2 [15], and K48-Ub [14, 17]. We report that cells devoid of Torsin function sequester K48-Ub protein in a p97-dependent manner (Figure 1B, C). The accumulation of ubiquitylated proteins inside blebs is only slightly decreased upon knockdown of the Ufd1/Npl4 heterodimer (Figure 2A, B), a major adaptor that recruits p97 to ubiquitylated substrates during ERAD. This suggests that the relevant p97 activity is not critically dependent on Ufd1/Npl4. Similarly, neither depletion of canonical Ub ligases implicated in ERAD (Figure S2A) nor a block of *de novo* protein synthesis (Figure 2E) significantly affect Ub deposition in NE blebs to the extent of p97 inhibition (Figure 1B, C). Unexpectedly, depletion of the p97 adaptor UBXD1, which has to our knowledge not been tied to nuclear processes, leads to a drastic reduction of Ub accumulation in NE blebs (Figure 3A, B).

We demonstrated that globally increasing the number of ubiquitylated proteins by heat shock causes significantly more K48-Ub to be trapped inside blebs (Figure 4). This finding may argue against a specific enrichment of K48-Ub proteins and suggest that a more general degradation defect exists in Torsin-deficient cells. Another interpretation consistent with this result is that blebs harbor specific heat-labile proteins that become defective and ubiquitylated under heat shock conditions. Future studies are warranted to distinguish between these two possibilities.

Our findings are consistent with a model wherein Torsin deficient cells fail to efficiently degrade ubiquitylated proteins and instead sequester this cargo into NE herniations. We have previously demonstrated that Δ133-ORF10, a short-lived virally-derived model substrate, is rapidly degraded in WT cells but is stabilized in TorsinKO cells where it is sequestered into blebs [18]. In the present study, we generalize this finding in the physiological context of heat shock. We demonstrate that endogenous, ubiquitylated cargo provoked by heat shock is sequestered into blebs. In further support of the concept that cargo is stabilized within blebs, we find that while MLF2 is turned over in WT cells exposed to heat shock, it is strongly stabilized in TorsinKO cells following heat shock (Figure 4E). As MLF2 and Δ133-ORF10 are tightly sequestered inside blebs in TorsinKO cells, these data are consistent with the idea that proteins normally efficiently degraded in WT cells are sequestered and consequently stabilized inside blebs in Torsin-deficient cells.

Given that DYT1 dystonia is a neurological disease, a general defect in the ability to turn over potentially aberrant proteins would disproportionally affect postmitotic neurons as this cell type is unable to dilute harmful species though cell division. As this cell type is particularly vulnerable to TorsinA mutation [19, 58, 59], this defect may at least partially explain why TorsinA mutation exclusively causes a neurological disease. Therefore, we propose that the p97/UBXD1 axis represents a potential therapeutic target for DYT1 dystonia as its inhibition reduces the K48-Ub accumulation inside blebs.

As Torsin ATPases localize within the ER/NE system [3, 60, 61], the protein quality control defect arising upon Torsin loss-of-function may be related to ERAD. While the involvement of Torsin activity in ERAD has been investigated [14, 62], it has not been found to play a critical role in processing many canonical ERAD model substrates. Furthermore, Torsin depletion is not consistently associated with causing general ER stress [14, 17, 63]. As we found, inhibiting translation (Figure 2E), depleting the Ufd1/Npl4

heterodimer (Figure 2A, B) or canonical Ub ligases required for ERAD (Figure S2A) fail to significantly reduce the amount of K48-Ub sequestered into blebs. Thus, if Torsin loss-of-function results in a PQC defect related to ERAD, it would likely affect clients of a distinct pathway that are retrotranslocated and ubiquitinated by a non-canonical mechanism. It is unlikely that these clients would be newly synthesized proteins given that CHX treatment has little impact on the K48-Ub cargo inside blebs (Figure 2E).

Our data suggest that the p97 interaction partners UBXD1 and YOD1 function in the PQC pathway that becomes dysregulated upon Torsin deficiency. While YOD1 is best characterized as participating in ERAD-related processes [50, 64], it has also been reported to facilitate autophagy of damaged lysosomes [47]. Notably, this latter function is in conjunction with UBXD1 and the p97 adaptor PLAA [47]. While we did not find that knockdown of PLAA effected K48-Ub levels inside blebs (data not shown), UBXD1 has been reported to function in a wide range of processes including mitophagy [48] and trafficking [46]. Thus, it will be interesting to determine whether UBXD1 and YOD1 contribute to the same p97-dependent process in Torsin-deficient cells or if these two adaptors function with p97 in distinct, albeit perturbed, processes.

The small molecule p97 inhibitor CB-5083 depletes the K48-Ub cargo inside blebs within four hours of treatment (Figure 1B). This relatively short treatment time reveals a previously unappreciated feature of blebs: K48-Ub cargo must undergo some dynamic exchange with the nucleoplasm. This dynamic feature of blebs has not been detected by previous workflows monitoring steady-state levels of K48-Ub sequestration [14, 15, 17, 58]. It will be important to determine the fate of the K48-Ub protein once they are released from blebs under p97 depletion conditions. For example, this cargo could be degraded once inside the nucleoplasm or it could persist within the cell and pose an even greater proteotoxic threat, depending on the resident times in NE blebs versus the nucleoplasm. Efforts to uncover how p97 inhibition affects blebs may also reveal whether proteasome

flux is impaired in models of DYT1 dystonia and the identity of K48-Ub conjugates. Answering these questions will not only advance therapeutic options but further our understanding of Torsin ATPases.

4. Materials and methods

Antibodies

The following antibodies were used in this study (WB, Western blot. IF, immunofluorescence): K48 linkage-specific polyubiquitin (WB, 1:4000. IF, 1:500. MilliporeSigma, Apu2), HA-peptide (WB, 1:2000. IF, 1:500. Roche, 3F10), p97 (WB, 1:7000. Abcam, ab109240), α-tubulin (WB, 1:5000. MilliporeSigma, T5168), α-GAPDH (WB, 1:10,000. Proteintech, 60004-1-Ig), α-Ufd1 (WB, 1:1,000. Cell Signaling, 13789), α-Npl4 (WB, 1:1,000. Cell Signaling, 13489), α-UBXD1 (WB, 1:500. Bethyl Laboratories, A302-931A), α-hnRNPA1 (WB, 1:2,000. Abcam, ab5832), α-emerin (WB, 1:4000. Cell Signaling, 30853S), α-calnexin (WB, 1:2,000. Abcam, 75801), FLAG peptide (WB, 1:4000. IF, 1:500. MilliporeSigma, F3165), rabbit IgG HRP conjugate (WB, 1:10,000. SouthernBiotech, 4030-05), mouse IgG HRP conjugate (WB, 1:20,000. SouthernBiotech, 1030-05), rabbit & mouse IgG Alexa488 conjugates (IF, 1:700. Invitrogen, A11008 & A28175), rabbit & mouse IgG Alexa568 (IF, 1:700. Invitrogen, A-11011& A-11004).

Cell culture and cell lines

Torsin-deficient [17] and WT HeLa cells were maintained in Dulbecco's Modified Eagle's Medium (DMEM) supplemented with 10% fetal bovine serum (Thermo Fischer Scientific) and 100 units mL^{-1} of penicillin-streptomycin (Thermo Fischer Scientific). Cells were verified to be free of mycoplasma contamination through the absence of extranuclear

Hoechst 33342 (Life Technologies) staining. Heat shock was achieved by incubating cells for 16 hours at 42ºC.

Small molecule treatment, plasmids, and transient transfections

Inhibition of p97 was achieved using the small molecule CB-5083 [24, 25] (Apexbio Technology, 1542705-92-9). The compound was dissolved in DMSO to a stock concentration of 10 mM. The stock solution was diluted 1:2000 in DMEM for a final concentration of 5 μM. Cells were exposed to medium containing CB-5083 for four hours prior to harvesting.

The cDNA sequence encoding MLF2-HA was cloned into the pcDNA3.1+ vector as previously described [15] using standard PCR. WT YOD1-FLAG, YOD1-CS-FLAG, and p97-QQ constructs in pcDNA3.1+ were cloned as previously described [50]. HA-tagged and untagged LBR-1600* were cloned as previously described [28, 29]. The cDNA encoding UBXD1 was amplified from a HeLa cell cDNA library and cloned into pcDNA3.1+ using *NheI* and *XbaI* with an N-terminal FLAG tag. pENTR-AIF (AIFM1) was a gift from Huda Zoghbi (Addgene plasmid #16182; http://n2t.net/addgene:16182; RRID: Addgene_16182) and was subcloned into pcDNA3.1+ using Gibson assembly to install a C-terminal FLAG tag with the sequence DYKDDDDK. This tag was inserted without any preceding or following linker residues.

Transient plasmid transfections were performed using Lipofectamine 2000 (Invitrogen) according to the manufacturer's instructions. Constructs were allowed to express for 24 hours prior to analyses.

siRNAs, transient RNAi knockdowns, and qPCR validation

The following siRNAs [47] targeting UBXD1 were ordered from Sigma. Forward oligo 1: 5'- CCAGGUGAGAAAGGAACUU[dT][dT]-3'. Forward oligo 2: 5'- UCAGAUACCACGUUGGUCCC[dT][dT]-3'. Nontargeting and siRNAs targeting Ufd1, Npl4, p47, Hrd1, MARCH6, and gp78 were purchased from Horizon Discovery as SMARTpools.

RNAi knockdowns were performed with Lipofectamine RNAiMAX (Invitrogen) according to the manufacturer's instructions and allowed to knock targets down for 48 hours before analyses.

Knockdown efficiency was validated by quantitative PCR (qPCR) using iQ SYBR Green mix with a CFX Real-Time PCR 639 Detection System (Bio-Rad). Each knockdown was evaluated using the ΔΔCt method using the internal control transcript RPL32. Primer sequences used for qPCR were as follows: UBXD1 (FWD: TGGAGAGGCACAAGGAACAGC, REV: CCCGCTTGATCTCCTCTGCT), Ufd1 [65] (FWD: GAGGGAAGATAATTATGCCAC, REV: CTTCCAAGAGTAAGTTCTGC), Npl4 (FWD: GCTTGGCCACCTATTTGTCTCAGAA, REV: CATTGGTGACCAGGAACAGCAAGA), Hrd1 [66] (FWD: GCGAGACATGATGGCATCTG, AACCCCTGGGACAACAAGG, REV: GCGAGACATGATGGCATCTG), MARCH6 (FWD: AGCATGCTCGAAATAACAACGCT, REV: GGCGGTAAGGCTGAAAGCCA), gp78 (FWD: CGTGTGCCACTGGACCTCAG, REV: CACCAGCATGCGCTGTCTCT), p47 (FWD: AGTACCAGCTCTCCAGCCCAA, REV: CGCCGTCTGCAAGCCGAA). All primers were synthesized by Integrated DNA Technologies.

Immunofluorescence and confocal microscopy

HeLa cells were grown on coverslips prior to processing for IF. Cells were fixed onto coverslips in 4% paraformaldehyde (ThermoFisher) for 20 minutes at room temperature, then permeabilized in 0.1% Triton X-100 (Sigma-Aldrich) for 10 minutes. After blocking in 4% bovine serum albumin for 15 minutes, cells were incubated for 45 minutes with primary antibodies diluted 1:500 in blocking solution. After exhaustive washing in phosphate buffered saline (PBS), cells were incubated in fluorescent secondary antibodies diluted 1:700 in blocking solution. Prior to mounting onto slides, the cells were stained with Hoechst 33342 (Life Technologies) and adhered to slides with Fluoromount-G (Southern Biotech).

Confocal images were collected on an LSM 880 laser scanning microscope (Zeiss) with a C Plan-Apochromat 63×/1.40 oil DIC M27 objective using ZEN 2.1 software (Zeiss). Image quantification and processing was performed in Fiji [67] or CellProfiler [68] as described below.

Immunoprecipitation and immunoblot analysis

All immunoprecipitation (IP) experiments were conducted under native conditions. Cells were transfected or exposed to relevant conditions 16-24 hours prior to harvesting for IP, then lysed in NET buffer (150 mM NaCl, 50 mM Tris pH 7.4, 0.5% NP-40) supplemented with EDTA-free protease inhibitor tablet (Roche) and 5 mM NEM (Sigma-Aldrich). Equal amounts of protein were loaded onto protein A beads conjugated to 1 µg anti-p97 (Abcam, ab109240) or Anti-FLAG® M2 Affinity Gel (MilliPoreSigma, A2220). After incubating for three hours, the resin was washed extensively in NET buffer and protein was eluted in 2x SDS reducing buffer for downstream immunoblot analyses.

Cell lysates were prepared for immunoblot in NET buffer plus protease inhibitors and 5 mM NEM as described above. Immunoblotting with IP eluates or cell lysates was performed with SDS-PAGE gels (Bio-Rad) and transferred onto PVDF membranes (Bio-Rad). Membranes were blocked in 5% w/v milk in PBS + 0.1% Tween-20 (Sigma-Aldrich). Primary and HRP-conjugated secondary antibodies were diluted in blocking buffer. Blots were visualized by chemiluminescence on a ChemiDoc Gel Imaging System (Bio-Rad).

Cycloheximide chase

TorsinKO HeLa cells were plated in a 10 cm dish and transfected with HA-LBR 1600* [28], which was allowed to express for 24 hours prior to harvesting cells. After 24 hours, the cells were either trypsinized and split into two tubes for immunoblot analysis or kept within the culture dish containing coverslips for IF. Tubes for immunoblot were incubated at 37°C with gentle shaking and treated with either DMSO or 100 µg/mL CHX diluted in completed DMEM described above. Culture dishes for IF were treated with the same conditions and remained within the culturing incubator. Aliquots for immunoblot or coverslips were taken at zero, one, two, five, or seven hours post treatment. Cells were collected via centrifugation and subjected to immunoblot or fixed with 4% paraformaldehyde and processed for IF as described above.

NE enrichment

NE fractions were enriched from whole cell lysates as previously described [29]. Cells were collected by centrifugation and resuspended in buffer A (10 mM HEPES, pH 7.4, 250 mM sucrose, 2 mM $MgCl_2$) supplemented with EDTA-free protease inhibitor cocktail (Roche). Cell pellets were homogenized in 100 µL of buffer A by passing through a 25-gague needle and layered on top of 10 mL STM 0.9 buffer (50 mM Tris, pH 7.4, 0.9 M sucrose, 5 mM $MgCl_2$). The homogenates were centrifuged twice through the STM 0.9

layer at 1000 × g for 10 minutes and a white pellet was observed at the bottom. This pellet, composed of the nuclei/ER and cell debris, was resuspended in TP buffer (10 mM Tris, pH 8.0, 10 mM Na_2HPO_4, 2 mM $MgCl_2$) supplemented with heparin (2 mg/ mL), benzonase nuclease (2 µL/ mL), and protease inhibitor cocktail (Roche) and rotated overnight at 4ºC. In the morning, the nuclei were spun at 15,000 × g for 45 minutes to separate the ER/NE (pellet) from the nucleoplasm (supernatant). ER/NE enrichments were resuspended in 1% SDS and prepared for immunoblot analysis.

Image processing and statical analysis

All image quantification was performed using Fiji [67] or CellProfiler [68] software. The number of NE-associated K48-Ub foci was determined with Fiji software by defining a region of interest (ROI) around the nucleus of individual cells and quantifying the number of K48-Ub foci using the “Find Maxima” function. In line with our previous publications [15, 17, 18], the prominence or noise tolerance was set to 10. All statistical analyses for quantifying NE-associated K48-Ub foci utilized the Mann-Whitney U test, which does not assume the distributions are normal.

The intensity of K48-Ub in TorsinKO cells at 37°C and 42°C was assessed using CellProfiler software [68]. Cells were processed for IF as described above and imaged for K48-Ub using identical exposure times for each condition. For comparative analysis of K48-Ub intensity at 37°C and 42°C, the integrated intensity units of K48-Ub foci at the nuclear rim of each cell were quantified in CellProfiler. For determination of the distribution of K48-Ub at 42°C in the absence and presence of YOD1-CS-FLAG, CellProfiler was used to determine the fraction of total K48-Ub in the outer nuclear region for each cell. The populations were statistically analyzed using the Mann-Whitney U test, which does not require normal distributions.

Author contributions: Conceptualization, SMP, BSN, and CS; methodology, SMP, BSN, and CS; validation, SMP, BSN, and CS; formal analysis, SMP, BSN, and CS; investigation, SMP, BSN, and CS; resources, SMP, BSN, and CS; writing—original draft preparation, SMP.; writing—review and editing, SMP, BSN, and CS; visualization, SMP, BSN, and CS; supervision, CS; funding acquisition, SMP and CS. All authors have read and agreed to the published version of the manuscript.

Funding: This work is supported by DOD PR200788 (C.S.), NIH 5T32GM007223-44 (S.M.P.), NIH F31NS120528 (S.M.P.), and the Dystonia Medical Research Foundation (C.S.).

Data availability statement: All raw data used to generate plots and original scans of immunoblots are available upon request.

Acknowledgements: We thank members of the Schlieker lab for helpful comments regarding experimental design and manuscript preparation.

Conflicts of interest: The authors declare no conflicts of interest.

References

1. Goodchild, R.E., C.E. Kim, and W.T. Dauer, *Loss of the dystonia-associated protein torsinA selectively disrupts the neuronal nuclear envelope.* Neuron, 2005. **48**(6): p. 923-32.
2. Ozelius, L.J., et al., *The early-onset torsion dystonia gene (DYT1) encodes an ATP-binding protein.* Nat Genet, 1997. **17**(1): p. 40-8.
3. Naismith, T.V., et al., *TorsinA in the nuclear envelope.* Proc Natl Acad Sci U S A, 2004. **101**(20): p. 7612-7.
4. Zhao, C., et al., *Regulation of Torsin ATPases by LAP1 and LULL1.* Proc Natl Acad Sci U S A, 2013. **110**(17): p. E1545-54.
5. Brown, R.S., et al., *The mechanism of Torsin ATPase activation.* Proc Natl Acad Sci U S A, 2014. **111**(45): p. E4822-31.
6. Sosa, B.A., et al., *How lamina-associated polypeptide 1 (LAP1) activates Torsin.* Elife, 2014. **3**: p. e03239.

7. Goodchild, R.E. and W.T. Dauer, *The AAA+ protein torsinA interacts with a conserved domain present in LAP1 and a novel ER protein.* J Cell Biol, 2005. **168**(6): p. 855-62.

8. Demircioglu, F.E., et al., *Structures of TorsinA and its disease-mutant complexed with an activator reveal the molecular basis for primary dystonia.* Elife, 2016. **5**.

9. Rose, A.E., R.S. Brown, and C. Schlieker, *Torsins: not your typical AAA+ ATPases.* Crit Rev Biochem Mol Biol, 2015. **50**(6): p. 532-49.

10. Gonzalez-Alegre, P., *Advances in molecular and cell biology of dystonia: Focus on torsinA.* Neurobiol Dis, 2019. **127**: p. 233-241.

11. Rampello, A.J., S.M. Prophet, and C. Schlieker, *The Role of Torsin AAA+ Proteins in Preserving Nuclear Envelope Integrity and Safeguarding Against Disease.* Biomolecules, 2020. **10**(3).

12. Naismith, T.V., S. Dalal, and P.I. Hanson, *Interaction of torsinA with its major binding partners is impaired by the dystonia-associated DeltaGAG deletion.* J Biol Chem, 2009. **284**(41): p. 27866-74.

13. VanGompel, M.J., et al., *A novel function for the Caenorhabditis elegans torsin OOC-5 in nucleoporin localization and nuclear import.* Mol Biol Cell, 2015. **26**(9): p. 1752-63.

14. Pappas, S.S., et al., *TorsinA dysfunction causes persistent neuronal nuclear pore defects.* Hum Mol Genet, 2018. **27**(3): p. 407-420.

15. Rampello, A.J., et al., *Torsin ATPase deficiency leads to defects in nuclear pore biogenesis and sequestration of MLF2.* The Journal of Cell Biology, 2020. **219**(6).

16. Jacquemyn, J., et al., *Torsin and NEP1R1-CTDNEP1 phosphatase affect interphase nuclear pore complex insertion by lipid-dependent and lipid-independent mechanisms.* EMBO J, 2021. **40**(17): p. e106914.

17. Laudermilch, E., et al., *Dissecting Torsin/cofactor function at the nuclear envelope: a genetic study.* Mol Biol Cell, 2016. **27**(25): p. 3964-3971.

18. Prophet, S.M., et al., *Atypical nuclear envelope condensates linked to neurological disorders reveal nucleoporin-directed chaperone activities.* Nat Cell Biol, 2022: p. https://doi.org/10.1101/2021.10.26.465916.

19. Liang, C.C., et al., *TorsinA hypofunction causes abnormal twisting movements and sensorimotor circuit neurodegeneration.* J Clin Invest, 2014. **124**(7): p. 3080-92.

20. Lam, Y.A., et al., *A proteasomal ATPase subunit recognizes the polyubiquitin degradation signal.* Nature, 2002. **416**(6882): p. 763-7.

21. Rosenzweig, R., et al., *The Hsp70 chaperone network.* Nat Rev Mol Cell Biol, 2019. **20**(11): p. 665-680.

22. Huryn, D.M., D.J.P. Kornfilt, and P. Wipf, *p97: An Emerging Target for Cancer, Neurodegenerative Diseases, and Viral Infections.* J Med Chem, 2020. **63**(5): p. 1892-1907.

23. van den Boom, J. and H. Meyer, *VCP/p97-Mediated Unfolding as a Principle in Protein Homeostasis and Signaling.* Mol Cell, 2018. **69**(2): p. 182-194.

24. Zhou, H.J., et al., *Discovery of a First-in-Class, Potent, Selective, and Orally Bioavailable Inhibitor of the p97 AAA ATPase (CB-5083).* J Med Chem, 2015. **58**(24): p. 9480-97.

25. Anderson, D.J., et al., *Targeting the AAA ATPase p97 as an Approach to Treat Cancer through Disruption of Protein Homeostasis.* Cancer Cell, 2015. **28**(5): p. 653-665.

26. Wu, X. and T.A. Rapoport, *Mechanistic insights into ER-associated protein degradation.* Curr Opin Cell Biol, 2018. **53**: p. 22-28.

27. Ji, Z., et al., *Translocation of polyubiquitinated protein substrates by the hexameric Cdc48 ATPase.* Mol Cell, 2022. **82**(3): p. 570-584 e8.

28. Tsai, P.L., et al., *The Lamin B receptor is essential for cholesterol synthesis and perturbed by disease-causing mutations.* Elife, 2016. **5**.

29. Tsai, P.L., C. Zhao, and C. Schlieker, *Methodologies to monitor protein turnover at the inner nuclear membrane.* Methods Enzymol, 2019. **619**: p. 47-69.

30. Wu, X., et al., *Structural basis of ER-associated protein degradation mediated by the Hrd1 ubiquitin ligase complex.* Science, 2020. **368**(6489).

31. Schoebel, S., et al., *Cryo-EM structure of the protein-conducting ERAD channel Hrd1 in complex with Hrd3.* Nature, 2017. **548**(7667): p. 352-355.

32. Schmidt, C.C., V. Vasic, and A. Stein, *Doa10 is a membrane protein retrotranslocase in ER-associated protein degradation.* Elife, 2020. **9**.

33. Twomey, E.C., et al., *Substrate processing by the Cdc48 ATPase complex is initiated by ubiquitin unfolding.* Science, 2019. **365**(6452).

34. Mehrtash, A.B. and M. Hochstrasser, *Ubiquitin-dependent protein degradation at the endoplasmic reticulum and nuclear envelope.* Semin Cell Dev Biol, 2019. **93**: p. 111-124.

35. Wu, X. and T.A. Rapoport, *Translocation of Proteins through a Distorted Lipid Bilayer.* Trends Cell Biol, 2021. **31**(6): p. 473-484.

36. Ferro-Novick, S., F. Reggiori, and J.L. Brodsky, *ER-Phagy, ER Homeostasis, and ER Quality Control: Implications for Disease.* Trends Biochem Sci, 2021. **46**(8): p. 630-639.

37. Vasic, V., et al., *Hrd1 forms the retrotranslocation pore regulated by auto-ubiquitination and binding of misfolded proteins.* Nat Cell Biol, 2020. **22**(3): p. 274-281.

38. Schubert, U., et al., *Rapid degradation of a large fraction of newly synthesized proteins by proteasomes.* Nature, 2000. **404**(6779): p. 770-4.

39. Wolff, S., J.S. Weissman, and A. Dillin, *Differential scales of protein quality control.* Cell, 2014. **157**(1): p. 52-64.

40. Gloge, F., et al., *Co-translational mechanisms of protein maturation.* Curr Opin Struct Biol, 2014. **24**: p. 24-33.

41. Buchberger, A., H. Schindelin, and P. Hanzelmann, *Control of p97 function by cofactor binding.* FEBS Lett, 2015. **589**(19 Pt A): p. 2578-89.

42. Ye, Y., et al., *A Mighty "Protein Extractor" of the Cell: Structure and Function of the p97/CDC48 ATPase.* Front Mol Biosci, 2017. **4**: p. 39.

43. Ye, Y., H.H. Meyer, and T.A. Rapoport, *Function of the p97-Ufd1-Npl4 complex in retrotranslocation from the ER to the cytosol: dual recognition of nonubiquitinated polypeptide segments and polyubiquitin chains.* J Cell Biol, 2003. **162**(1): p. 71-84.

44. Kondo, H., et al., *p47 is a cofactor for p97-mediated membrane fusion.* Nature, 1997. **388**(6637): p. 75-8.

45. Haines, D.S., et al., *Protein interaction profiling of the p97 adaptor UBXD1 points to a role for the complex in modulating ERGIC-53 trafficking.* Mol Cell Proteomics, 2012. **11**(6): p. M111 016444.

46. Ritz, D., et al., *Endolysosomal sorting of ubiquitylated caveolin-1 is regulated by VCP and UBXD1 and impaired by VCP disease mutations.* Nat Cell Biol, 2011. **13**(9): p. 1116-23.

47. Papadopoulos, C., et al., *VCP/p97 cooperates with YOD1, UBXD1 and PLAA to drive clearance of ruptured lysosomes by autophagy.* EMBO J, 2017. **36**(2): p. 135-150.

48. Bento, A.C., et al., *UBXD1 is a mitochondrial recruitment factor for p97/VCP and promotes mitophagy.* Sci Rep, 2018. **8**(1): p. 12415.

49. Nagahama, M., et al., *UBXD1 is a VCP-interacting protein that is involved in ER-associated degradation.* Biochem Biophys Res Commun, 2009. **382**(2): p. 303-8.

50. Ernst, R., et al., *The otubain YOD1 is a deubiquitinating enzyme that associates with p97 to facilitate protein dislocation from the ER.* Mol Cell, 2009. **36**(1): p. 28-38.

51. Ewing, R.M., et al., *Large-scale mapping of human protein-protein interactions by mass spectrometry.* Mol Syst Biol, 2007. **3**: p. 89.

52. Liu, X., et al., *An AP-MS- and BioID-compatible MAC-tag enables comprehensive mapping of protein interactions and subcellular localizations.* Nat Commun, 2018. **9**(1): p. 1188.

53. Parag, H.A., B. Raboy, and R.G. Kulka, *Effect of heat shock on protein degradation in mammalian cells: involvement of the ubiquitin system.* EMBO J, 1987. **6**(1): p. 55-61.

54. Fujimuro, M., H. Sawada, and H. Yokosawa, *Dynamics of ubiquitin conjugation during heat-shock response revealed by using a monoclonal antibody specific to multi-ubiquitin chains.* Eur J Biochem, 1997. **249**(2): p. 427-33.

55. Maxwell, B.A., et al., *Ubiquitination is essential for recovery of cellular activities after heat shock.* Science, 2021. **372**(6549): p. eabc3593.

56. Friant, S., K.D. Meier, and H. Riezman, *Increased ubiquitin-dependent degradation can replace the essential requirement for heat shock protein induction.* EMBO J, 2003. **22**(15): p. 3783-91.

57. Kuiper, E.F., et al., *The molecular chaperone DNAJB6 provides surveillance of FG-Nups and is required for interphase nuclear pore complex biogenesis.* Nat Cell Biol, 2022.

58. Weisheit, C.E. and W.T. Dauer, *A novel conditional knock-in approach defines molecular and circuit effects of the DYT1 dystonia mutation.* Hum Mol Genet, 2015. **24**(22): p. 6459-72.

59. Li, J., et al., *TorsinB overexpression prevents abnormal twisting in DYT1 dystonia mouse models.* eLife, 2019. **9:e54285**.

60. Goodchild, R.E. and W.T. Dauer, *Mislocalization to the nuclear envelope: an effect of the dystonia-causing torsinA mutation.* Proc Natl Acad Sci U S A, 2004. **101**(3): p. 847-52.

61. Vander Heyden, A.B., et al., *Static retention of the lumenal monotopic membrane protein torsinA in the endoplasmic reticulum.* EMBO J, 2011. **30**(16): p. 3217-31.

62. Nery, F.C., et al., *TorsinA participates in endoplasmic reticulum-associated degradation.* Nat Commun, 2011. **2**: p. 393.

63. Shin, J.Y., et al., *Nuclear envelope-localized torsinA-LAP1 complex regulates hepatic VLDL secretion and steatosis.* J Clin Invest, 2019. **130**: p. 4885-4900.

64. Sasset, L., et al., *The VCP/p97 and YOD1 Proteins Have Different Substrate-dependent Activities in Endoplasmic Reticulum-associated Degradation (ERAD).* J Biol Chem, 2015. **290**(47): p. 28175-88.

65. Chen, M., G.J. Gutierrez, and Z.A. Ronai, *Ubiquitin-recognition protein Ufd1 couples the endoplasmic reticulum (ER) stress response to cell cycle control.* Proc Natl Acad Sci U S A, 2011. **108**(22): p. 9119-24.

66. Xu, Y.M., et al., *HRD1 suppresses the growth and metastasis of breast cancer cells by promoting IGF-1R degradation.* Oncotarget, 2015. **6**(40): p. 42854-67.

67. Schindelin, J., et al., *Fiji: an open-source platform for biological-image analysis.* Nat Methods, 2012. **9**(7): p. 676-82.

68. Stirling, D.R., et al., *CellProfiler 4: improvements in speed, utility and usability.* BMC Bioinformatics, 2021. **22**(1): p. 433.

Figures

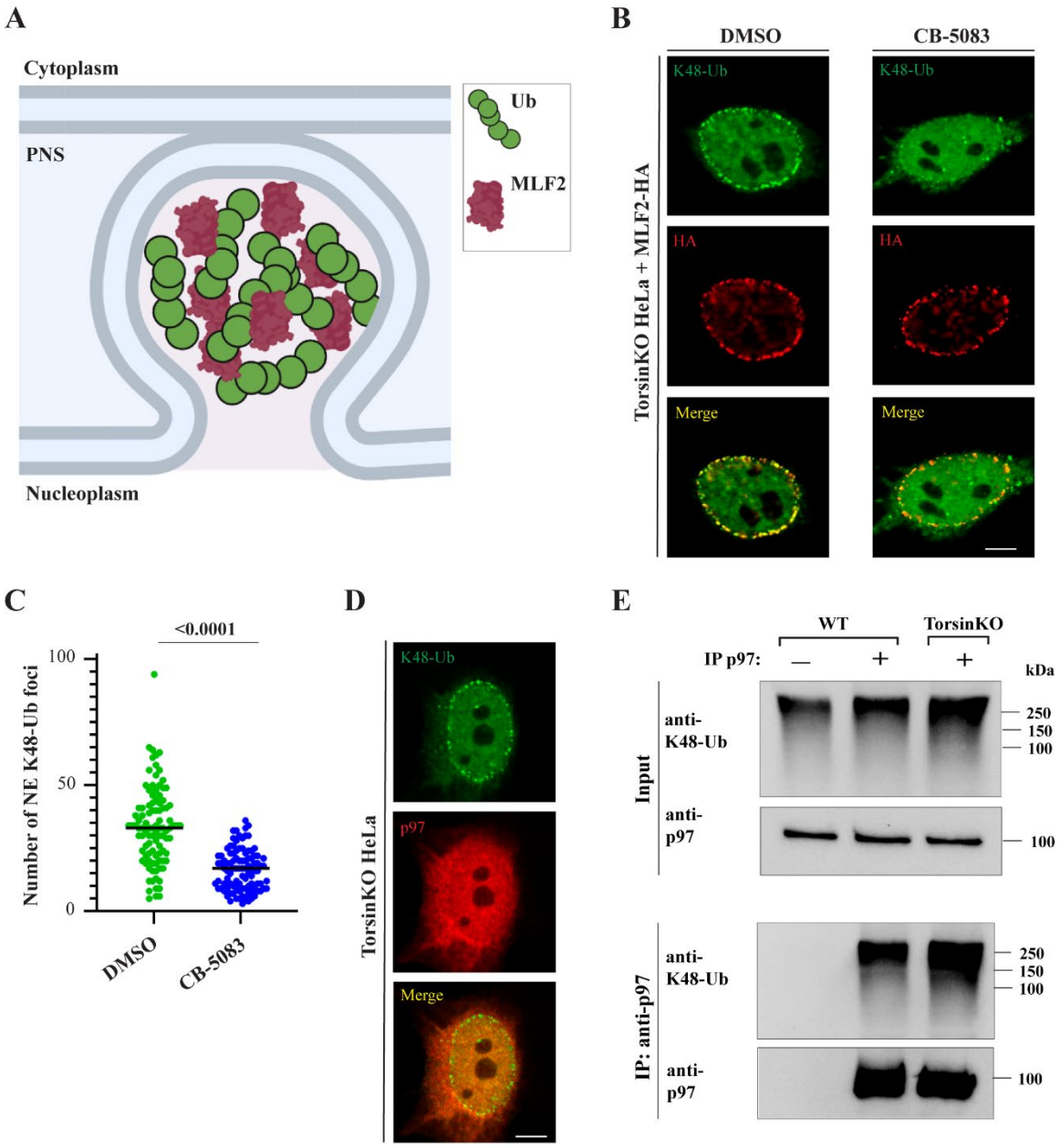

Figure 1. The K48-Ub accumulation inside NE blebs of Torsin-deficient cells requires p97 activity. (**A**) Schematic diagram of a NE bleb. PNS, perinuclear space. Ub, ubiquitin. (**B**) Representative immunofluorescence (IF) images of TorsinKO HeLa cells overexpressing MLF2-HA under vehicle (DMSO) or p97 inhibition (CB-5083) conditions. Cells were

treated with 5 μM CB-5083 for four hours before processing for IF, stained with K48-Ub and HA antibodies, and imaged by confocal microscopy. Scale bar, 5 μm. (**C**) The number of NE-associated K48-Ub foci in TorsinKO cells upon DMSO or CB-5083 treatment was quantified for 100 cells/condition. Statistical analysis was performed using a Mann-Whitney U test. (**D**) Representative IF image of p97 localization in TorsinKO cells. Cells were processed for IF and stained with p97 and K48-Ub antibodies. Scale bar, 5 μm. (**E**) An immunoprecipitation (IP) of endogenous p97 under native conditions from WT and TorsinKO cells. The IP was analyzed by immunoblot with antibodies against p97 and K48-Ub. All experiments were performed by SMP.

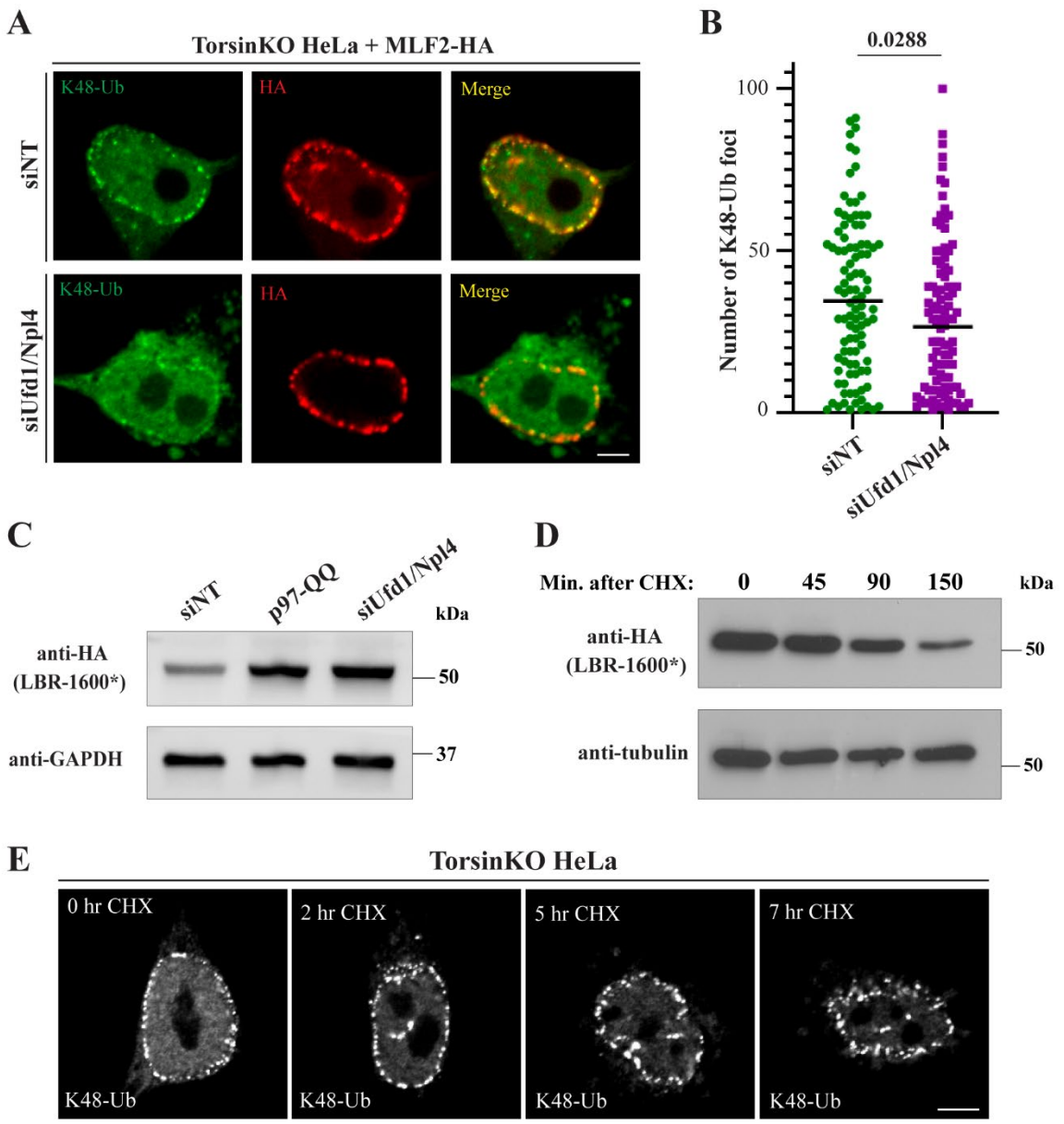

Figure 2. The K48-Ub proteins sequestered inside blebs do not result from canonical ERAD. (**A**) Representative IF images of TorsinKO cells overexpressing MLF2-HA under nontargeting (siNT) or Ufd1/Npl4 knockdown conditions. Cells were treated with 25 nM RNAi against both Ufd1 and Npl4 for 48 hours before processing for IF. Cells were stained with antibodies against K48-Ub and HA. Scale bar, 5 μm. (**B**) The number of NE-associated K48-Ub foci in TorsinKO cells under nontargeting or Ufd1/Npl4 knockdown conditions was quantified for 100 TorsinKO cells/condition. Statistical analysis was

performed using a Mann-Whitney U test. (**C**) Representative immunoblot of the ERAD substrate LBR-1600* in TorsinKO cells under siNT, siUfd1/Npl4, or p97-QQ overexpression conditions. p97-QQ is a dominant-negative mutation that inhibits endogenous p97 activity. The Ufd1/Npl4 knockdown was conducted for 48 hours while LBR-1600* and p97-QQ were expressed for 24 hours prior to immunoblotting. (**D**) TorsinKO cells expressing the short-lived HA-LBR-1600* were treated with CHX for the indicated timepoints and processed for immunoblot. Cells were allowed to express HA-LBR-1600* for 24 hours before treatment with 100 μg/mL CHX. (**E**) Representative IF images of TorsinKO cells treated with CHX for the indicated timepoints. Cells were treated with 100 μg/mL of CHX prior to processing for IF and stained with an K48-Ub antibody. Scale bar, 5 μm. All experiments were performed by SMP.

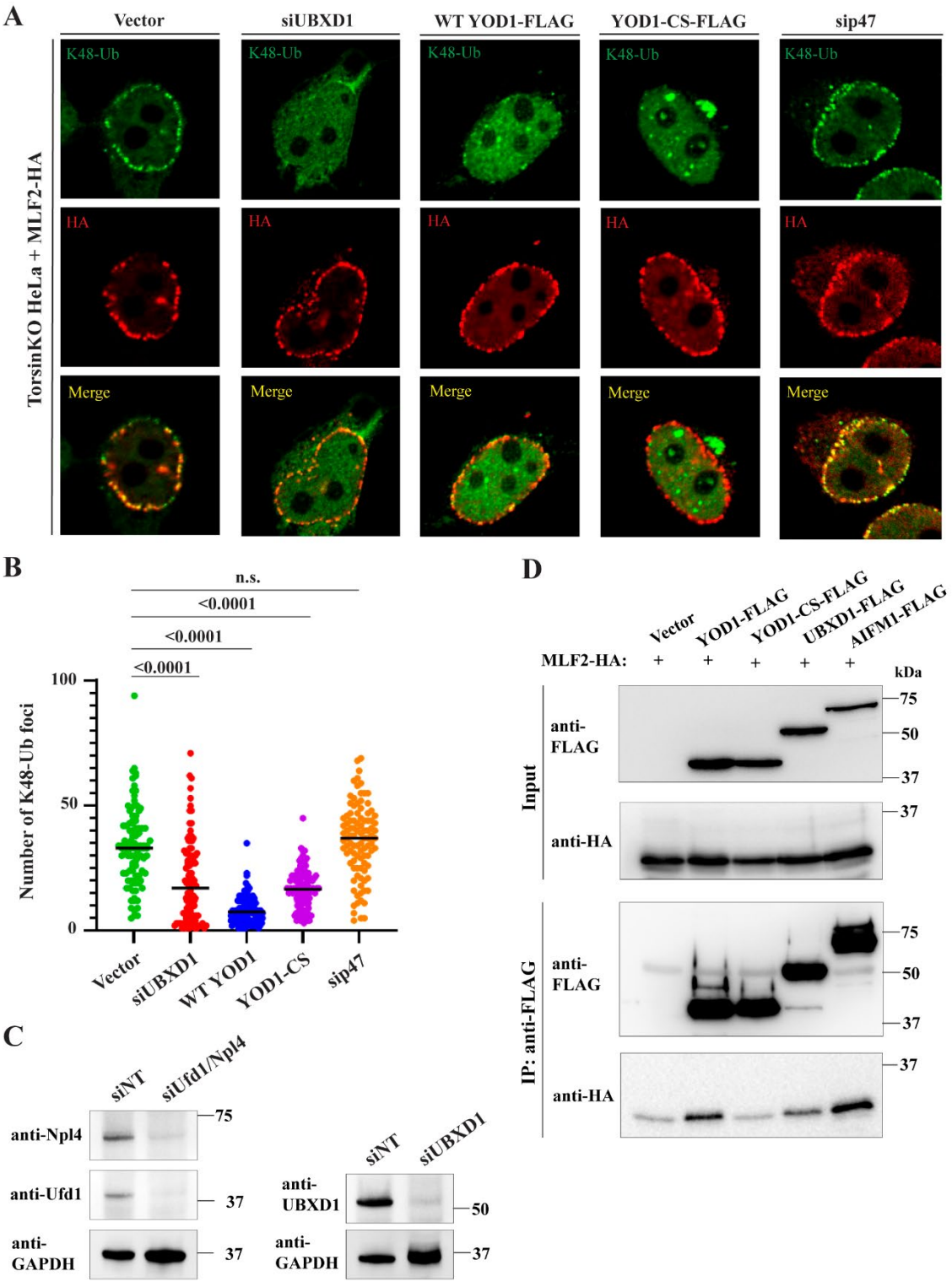

Figure 3. p97 depends on the cofactors YOD1 and UBXD1 to generate the K48-ubiquinated proteins sequestered inside blebs. (**A**) Representative IF images of TorsinKO

cells overexpressing MLF2-HA under conditions of normal or disrupted p97 activity. p97 activity was disrupted by knocking down UBXD1 or p47, or by overexpressing the dominant-negative YOD1-CS-FLAG. UBXD1 and p47 were knocked down for 48 hours and overexpressed constructs were overexpressed for 24 hours prior to processing for IF. Cells were stained with antibodies against K48-Ub and HA. Note that WT YOD1-FLAG is an active deubiquitinase (DUB) that cleaves the K48-Ub chains off clients that are normally ubiquitinated and sequestered into blebs. Scale bar, 5 μm. (**B**) The number of K48-Ub foci was quantified for 100 TorsinKO cells/condition. Statistical analysis was performed using a Mann-Whitney U test. N.s., not significant. (**C**) An immunoblot confirming the effects of siRNA targeting Ufd1, Npl4, or UBXD1 in TorsinKO cells after 48 hours of knockdown. (**D**) An IP of FLAG-tagged WT YOD1, YOD1-CS, UBXD1, or AIMF1 from TorsinKO cells expressing MLF2-HA. Cells were allowed to express the constructs for 24 hours prior to harvesting. An IP of the FLAG tag for all samples was analyzed by immunoblot against the FLAG and HA tags. MLF2-HA specifically co-immunoprecipitates with WT YOD1, UBXD1, and AIFM1. All experiments were performed by SMP.

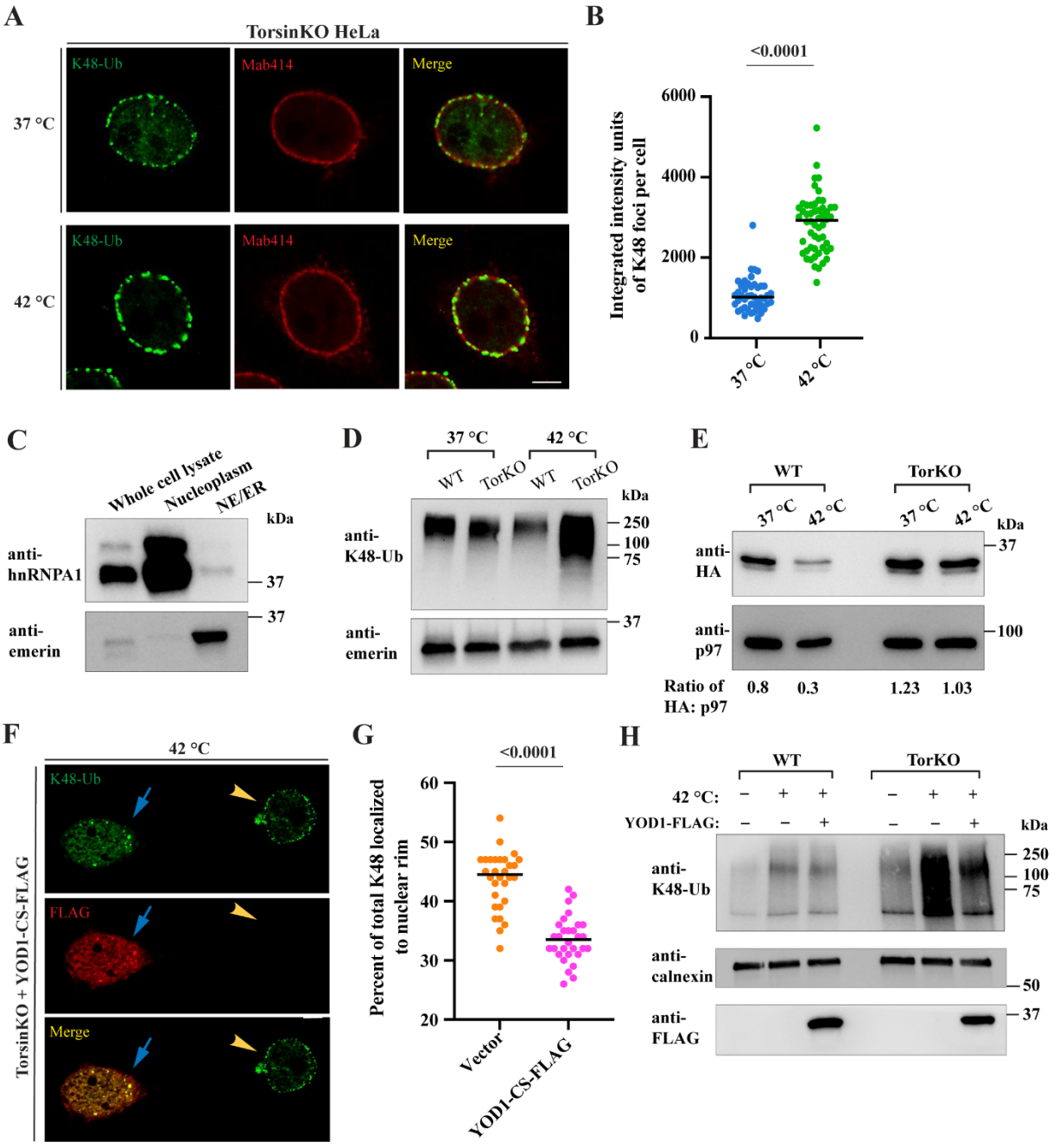

Figure 4. NE blebs in Torsin-deficient cells sequester ubiquitinated proteins that are produced by heat shock stress. (**A**) Representative IF images of NE-associated K48-Ub foci in TorsinKO cells upon heat shock. Cells were cultured at 37ºC or 42ºC for 16 hours before processing for IF. Cells were stained with an antibody against K48-Ub and Mab414,

which recognizes a subset of FG-nucleoporins. Scale bar, 5 μm. (**B**) Quantification of the average intensity of K48-Ub signal inside blebs from TorsinKO cells exposed to 37ºC or 42ºC for 16 hours. This value was quantified for 50 TorsinKO cells/condition. Statistical analysis was performed using a Mann-Whitney U test. (**C**) An immunoblot demonstrating the subcellular fractionation of TorsinKO cells. Cells were enriched for NE/ER fractions (indicated by the emerin antibody) that were free from significant nucleoplasmic contamination (indicated by the anti-hnRNPA1 antibody). (**D**) NE/ER fractions from WT or TorsinKO HeLa cells under unstressed or heat shock stress conditions were analyzed by immunoblot with antibodies against K48-Ub and emerin. Cells were exposed to a 42ºC heat shock for 16 hours before harvesting. (**E**) Unstressed or heat shocked WT and TorsinKO overexpressing MLF2-HA for 24 hours were fractionated into ER/NE enrichments. The fractions were analyzed by immunoblot using. Note that p97 controls for protein loading in this immunoblot. The ratio of HA to p97 density was calculated for each lane. (**F**) Representative IF images of TorsinKO cells expressing YOD-CS-FLAG under heat shock stress as described in panel (**A**). Cells were transfected with YOD1-CS-FLAG eight hours prior to the beginning of heat shock. Blue arrow, transfected cell. Yellow arrowhead, untransfected cell. Scale bar, 5 μm. (**G**) Quantification of the percent of total K48-Ub foci that localize to the nuclear rim in TorsinKO cells upon 42ºC heat shock with or without YOD1-CS-FLAG overexpression. This value was obtained for 30 cells/condition. Statistical analysis was performed using a Mann-Whitney U test. (**H**) WT and TorsinKO cells expressing WT YOD1-FLAG for 24 hours were subjected to heat shock stress and enriched for ER/NE fractions. These fractions were compared by immunoblot to unstressed or heat shocked cells in the absence of overexpressed YOD1-FLAG. Experiments in panels A, C-E, and H were performed by SMP. Experiments in panels B, F, and G were performed by BSN.

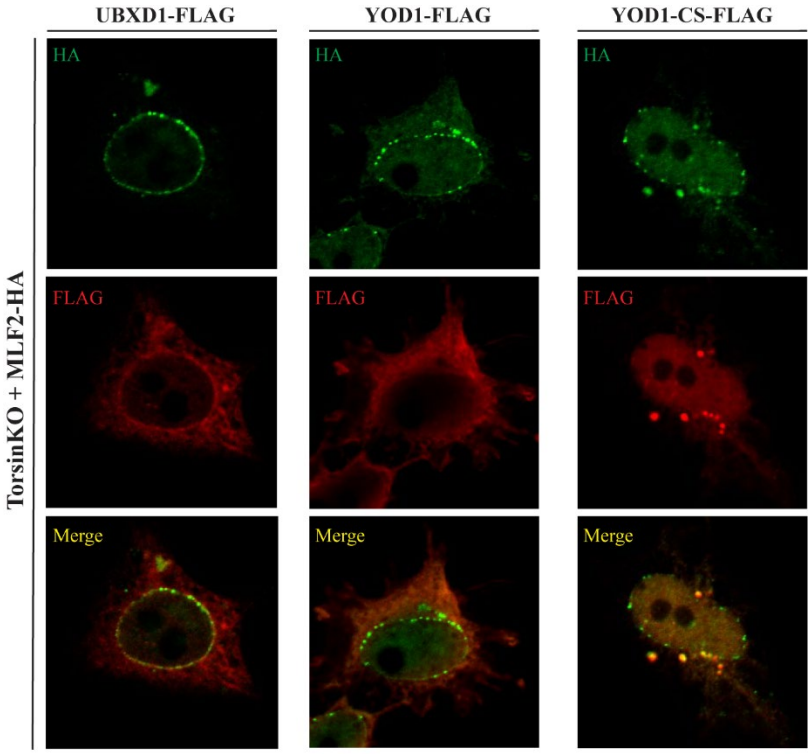

Supplemental figure 1. Localization of three p97 interaction partners in Torsin-deficient cells. Representative IF images of FLAG-tagged UBXD1, WT YOD1, or YOD1-CS co-overexpressed with MLF2-HA in TorsinKO HeLa cells for 24 hours. Cells were stained with antibodies against the FLAG and HA epitope tags. All experiments were performed by SMP.

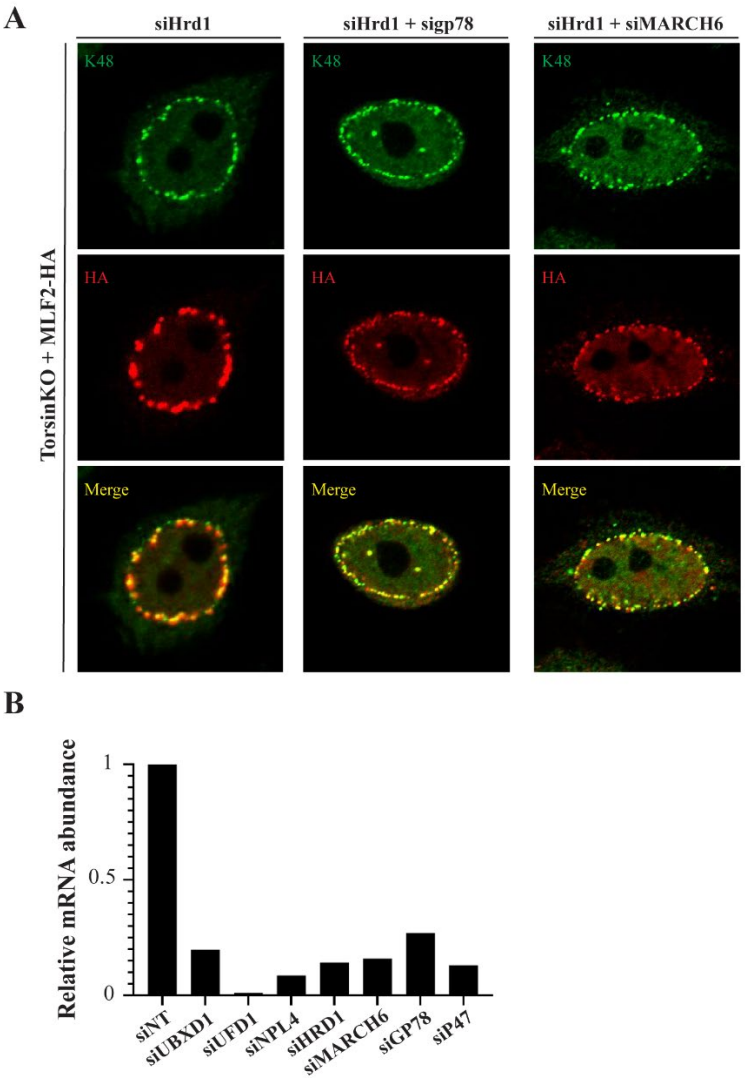

Supplemental figure 2. Effects of knocking down canonical retrotranslocons on K48-Ub bleb accumulation. (**A**) Representative IF images of the K48-Ub accumulation inside blebs and MLF2-HA localization upon knocking down the indicated retrotranslocons in TorsinKO cells. Knockdowns were achieved through targeting siRNA treatment for 48 hours. MLF2-HA was overexpressed for 48 hours prior to processing for IF. Cells were stained with antibodies against K48-Ub and the HA epitope tag. (**B**) Relative mRNA abundance assessed by qPCR for the indicated transcripts after 48 hours of knockdown. Experiments in panel A were performed by SMP. Experiments in panel B were performed by BSN.

Chapter 3: Atypical nuclear envelope condensates linked to neurological disorders reveal nucleoporin-directed chaperone activities

Sarah M Prophet[1], Anthony J Rampello[1], Robert F Niescier[1,2], Juliana E Gentile[1,2,4], Sunanda Mallik[1], Anthony J Koleske[1,2], Christian Schlieker[1,3*]

[1]Yale University, Department of Molecular Biophysics and Biochemistry, New Haven, CT, [2]Yale School of Medicine, Department of Neuroscience, New Haven, CT, [3]Yale School of Medicine, Department of Cell Biology, New Haven, CT, [4]Present address: Broad Institute of MIT and Harvard, Cambridge, MA

* Correspondence: Christian Schlieker, Department of Molecular Biophysics & Biochemistry, Yale University, 266 Whitney Avenue, P.O. Box 208114, Bass 236A, New Haven, CT 06520-8114, office phone: (203) 432-5035, office fax: (203) 432-8492, email: christian.schlieker@yale.edu

The following work was published in the journal *Nature Cell Biology*.

Abstract

DYT1 dystonia is a debilitating neurological movement disorder arising from mutation in the AAA+ ATPase TorsinA. The hallmark of Torsin dysfunction is nuclear envelope blebbing resulting from defects in nuclear pore complex biogenesis. Whether blebs actively contribute to disease manifestation is unknown. We report that FG-nucleoporins (FG-Nups) in the bleb lumen form aberrant condensates and contribute to DYT1 dystonia by provoking two proteotoxic insults. Short-lived ubiquitylated proteins that are normally rapidly degraded partition into the bleb lumen and become stabilized. Additionally, blebs selectively sequester a specific HSP40/HSP70 chaperone network that is modulated by the bleb component MLF2. MLF2 suppresses the ectopic accumulation of FG-Nups and modulates the selective properties and size of condensates *in vitro*. Our studies identify dual mechanisms of proteotoxicity in the context of condensate formation and establish FG-Nup-directed activities for a nuclear chaperone network.

Introduction

Torsin ATPases (Torsins) are the only members of the AAA+ protein superfamily that localize within the endoplasmic reticulum (ER) and nuclear envelope (NE) [1, 2]. TorsinA is essential for viability [3] and strictly requires regulatory cofactors to hydrolyze ATP [4]. A mutation in TorsinA that disrupts the interactions with its cofactors results in a loss of ATPase activity [5, 6] and is responsible for a debilitating neurological movement disorder called DYT1 dystonia [7]. Mutations in the Torsin activator LAP1 also give rise to dystonia and myopathies [8-10]. Thus, the Torsin system is critical for neurological function [9, 11].

While the molecular targets of Torsins and the mechanism of DYT1 dystonia onset are not understood, the hallmark phenotype observed across diverse animal and cell-based models of DYT1 dystonia is NE blebbing [3, 12-21]. NE blebs in the context of Torsin disruption are omega-shaped herniations of the inner nuclear membrane that are constricted at their base by a nuclear pore complex (NPC)-like structure and stem from defective NPC assembly [18, 22] (Extended Data Fig. 1a). Blebs are observed following distinct mechanisms of Torsin perturbation including dominant-negative alleles, Torsin-null alleles, siRNA, and in yeast harboring mutations of NPC-related proteins [23, 24]. As a consequence of NE blebbing, nuclear transport defects have been observed in models of compromised Torsin function including patient-derived iPSC neurons [12, 20, 21].

NPCs are composed of nucleoporins (Nups), several of which contain disordered phenylalanine-glycine (FG)-rich domains, which form a dense hydrogel and establish the permeability barrier characteristic of NPCs [25-28]. While small (<30 kDa) molecules can passively diffuse through this barrier [29], larger molecules require facilitated passage via nuclear transport receptors (NTRs) [30].

NE blebs arising from Torsin deficiency are enriched for FG-Nups but do not contain NTRs or bulk nuclear export cargo [18, 22]. Moreover, the poorly characterized protein myeloid leukemia factor 2 (MLF2) and K48-linked ubiquitin (Ub) chains are diagnostic

constituents of the bleb lumen [18, 20, 22] (Extended Data Fig. 1a). While Ub accumulation and defects in the ubiquitin/proteasome system have been implicated in many other neurological disorders including Huntington's and Parkinson's disease [31-33], it is unknown whether or how NE blebs contribute to DYT1 dystonia onset. Both the lack of suitable readouts and our incomplete understanding of the molecular composition of blebs represent major obstacles towards identifying their functional consequences.

In this study, we develop a virally-derived model substrate to define the bleb proteome and probe the significance of ubiquitin accumulation for DYT1 dystonia development. We find that normally short-lived proteins evade degradation once they are trapped inside blebs. Along with stabilized ubiquitylated proteins, blebs sequester a highly specific chaperone network composed of HSP40s and HSP70s. The FG-Nup Nup98 is required for blebs to form, and we demonstrate that blebs harbor an FG-rich condensate. We combine cellular and *in vitro* approaches to assign an FG-directed activity to MLF2 in complex with HSP70 and DNAJB6. Together, our results advance our understanding of cellular phase separation and define a link between PQC defects and disease etiology via pathological NE-associated condensates.

Results

Torsin deficiency stabilizes rapidly degraded proteins.

To develop approaches for probing the consequences of sequestering protein into NE blebs, we examined viral proteins that have been functionally tied to nuclear transport. ORF10 from Kaposi's sarcoma-associated herpesvirus (KSHV) is produced as a full length 418-residue protein and a shorter 286-residue protein (Δ133 ORF10) via an alternative translation initiation (Fig. 1a,b). The full-length protein [34] localizes diffusely within the nucleoplasm in wild type (WT) and TorsinKO HeLa cells (Fig. 1c). However, Δ133 ORF10 becomes tightly sequestered into NE foci that strictly co-localize with K48-

Ub in TorsinKO cells (Fig. 1c). Recruitment to these foci strictly depends on ubiquitylation as fusing a deubiquitylating (DUB) domain [35] to ∆133 ORF10 prevents NE sequestration (Extended Data Fig. 1b). Because ∆133 ORF10 remains diffusely nucleoplasmic in WT cells (Fig. 1c) and associates with more K48-Ub in TorsinKO compared to WT cells (Fig. 1d), we establish ∆133 ORF10 as the only known protein that localizes to blebs in a ubiquitin-dependent manner.

As ∆133 ORF10 is less abundant and associated with lower levels of K48-Ub in WT cells compared to TorsinKO cells (Fig. 1d), we hypothesized that ∆133 ORF10 is normally a short-lived protein. Indeed, we observed its half-life in WT cells to be approximately 45 minutes (Fig. 1e,f). In TorsinKO cells, ∆133 ORF10 is stabilized and exists with a half-life of four hours (Fig. 1e,f). This reveals an unexpected proteotoxic property of NE blebs.

Blebs are enriched for a specific chaperone network.

The absence of a comprehensive, bleb-specific proteome is a major limitation in understanding the molecular underpinnings of NE bleb formation. We fused the engineered ascorbate peroxidase APEX2 [36, 37] to MLF2-HA and performed a biotin-based proximity labeling reaction (Fig. 2a). To control the MLF2-APEX2-HA protein level, we placed its expression under a doxycycline (Dox)-inducible promoter (Fig. 2b). The presence of biotin conjugates within blebs after the APEX reaction was verified by immunofluorescence (IF) (Fig. 2c). The biotin-conjugating activity of APEX2 was confirmed via immunoblotting (Fig. 2d). After performing the APEX2 reaction, NE fractions were biochemically separated from WT and TorsinKO cells. Biotinylated proteins were enriched via streptavidin-coated beads and identified by mass spectrometry (LC-MS/MS) (Fig. 2e, Supplemental Table 1). In parallel, we performed an immunoprecipitation (IP) using ∆133 ORF10-HA followed by LC-MS/MS (Fig. 2e, Supplemental Table 2). This

allowed for a direct comparison of the bleb proteome from two independent approaches with our previously published dataset of immunoprecipitated K48-Ub from NE fractions [22]. From these three datasets, we considered proteins with a ≥1.5-fold enrichment of spectral counts in TorsinKO samples compared to WT (Fig. 2e).

Only three proteins were consistently enriched across all datasets in samples from TorsinKO cells—MLF2, HSPA1A, and HSC70 (Fig. 2e). HSPA1A and HSC70 are the canonical HSP70 members in mammalian cells, mediating a range of essential processes [38]. This functional diversity is achieved, at least in part, by interactions with J-domain proteins (HSP40s) [39]. Thus, we asked whether the HSP40s identified in the MLF2-APEX2 and K48-Ub datasets may also be enriched in blebs.

HSP70s and HSP40s are sequestered into NE blebs.

We performed a co-IP with Δ133 ORF10 and found it to stably interact with DNAJB6 exclusively in TorsinKO cells (Fig. 2f). Next, we determined whether HSPA1A, HSC70, DNAJB6, and DNAJB2 localized to blebs at endogenous expression levels. In TorsinKO cells, these chaperones redistributed from diffuse cytosolic/nucleoplasmic distributions to foci that decorate the nuclear rim (Fig. 3a, Extended Data Fig. 2a). By overexpressing a dominant-negative TorsinA-EQ construct, we also found that chaperones localize to blebs in the human neuroblastoma cell line SH-SY5Y (Extended Data Fig. 2b).

We additionally performed immunogold labeling and examined the ultrastructure of the NE with electron microscopy (EM) (Fig. 3b,c). While we did not detect DNAJB6 or HSPA1A at mature NPCs, DNAJB6 and HSPA1A localized within the bleb lumen (Fig. 3b,c). Thus, we conclude that multiple members of the HSP70 and HSP40 families become tightly sequestered into the bleb lumen in Torsin-deficient cells.

Neurons lacking TorsinA function sequester chaperones.

As DYT1 dystonia is a neurological disease, we investigated whether the sequestration of chaperones occurs in neurons with compromised Torsin function. In mouse models of DYT1 dystonia, ≥80% of central nervous system nuclei exhibit NE blebs in eight-day-old mice [16]. This number decreases when expression of TorsinB begins after about 14 days [16]. We therefore cultured primary murine hippocampal neurons and transfected GFP with or without the dominant-negative TorsinA-EQ construct after four days *in vitro* (DIV4). Cells were processed for IF on DIV7 to recapitulate the peak blebbing phenotype reported in conditional TorsinKO mice [16]. GFP was used to distinguish neurons from other cell types in the primary cultures.

In neurons with functional Torsins, the chaperones were diffusely localized throughout the cytosol/nucleoplasm (Fig. 3d-g). Upon expression of TorsinA-EQ, these chaperones became sequestered into blebs (Fig. 3d-g). MLF2-HA was also sequestered into blebs in Torsin-deficient neurons when overexpressed (Extended Data Fig. 2c). Thus, the sequestration of highly abundant and essential molecular chaperones into blebs is a conserved and general consequence of Torsin dysfunction.

MLF2 recruits DNAJB6 to blebs.

To understand the relationship between MLF2 and chaperones, we depleted MLF2 from TorsinKO cells. Upon MLF2 knockdown, K48-Ub and HSPA1A remained efficiently sequestered into NE foci but DNAJB6 was no longer recruited to blebs (Fig. 4a). While the recruitment of HSPA1A to blebs was independent of MLF2, the small molecule VER-155008, which approximates the ADP-bound state of HSP70 [40], strongly promoted the recruitment of K48-Ub to blebs (Extended data 3a,b).

Next, we performed a radioimmunoprecipitation of endogenous HSPA1A from WT and TorsinKO cells under non-targeting or siMLF2 conditions (Fig. 4b). Two major co-immunoprecipitating bands were highly enriched in the TorsinKO siNT condition (Fig. 4b).

The most prominent band around 28 kDa disappeared when MLF2 was knocked down, suggesting that HSPA1A interacts with significantly more MLF2 in TorsinKO cells than in WT (Fig. 4b). Another band unique to the TorsinKO siNT condition migrated at the expected molecular mass of DNAJB6 (27 kDa) and co-immunoprecipitated with HSPA1A exclusively in TorsinKO cells in an MLF2-dependent manner (Fig. 4b).

To test if this protein was DNAJB6, we performed both a DNAJB6 knockdown and a RE-IP wherein the HSPA1A co-immunoprecipitating proteins were dissociated and subjected to another IP using an antibody against DNAJB6 (Fig. 4c). When DNAJB6 was depleted by RNAi, the band migrating around 27 kDa no longer co-immunoprecipitated with HSPA1A (Fig. 4c). Unexpectedly, less MLF2 co-immunoprecipitated with HSPA1A when DNAJB6 was depleted (Fig. 4c). Upon RE-IP, a single band migrating around 27 kDa was clearly detectable from TorsinKO cells (Fig.4c). We further confirmed this interaction by traditional co-IP (Fig. 4d). The recruitment of DNAJB6 to blebs strongly depended on the S/T-rich region within DNJAB6 and not the G/F-rich region (Extended Data Fig. 3c,d). Lastly, we confirmed the identity of the 27 kDa band by mass spectrometry as DNAJB6 (Extended Data Fig. 3e). We conclude that MLF2 recruits DNAJB6 to blebs where these proteins stably interact with HSPA1A.

Sequestering chaperones may contribute to proteotoxicity.

DNAJB6 prevents the formation of toxic inclusions including polyglutamine (poly-Q) expansions [41-43]. Thus, we determined if this function is affected by sequestering DNAJB6 into blebs. In TorsinKO/MLF2 KO cells, DNAJB6 was recruited to poly-Q aggregates (Fig. 4e,f). However, upon re-introducing MLF2-HA via transient transfection, DNAJB6 was sequestered into blebs and away from the poly-Q aggregate (Fig. 4e,f). This titration of DNAJB6 out of an aggregate-prone client underscores the pronounced proteotoxic potential of NE blebs with MLF2 being a critical modulator of this property.

Sequestering protein into NE blebs requires Nup98.

While analyzing the MLF2-APEX2 MS datasets, we noticed that specific Nups including Nup98 were enriched in samples from TorsinKO cells (Fig. 5a) [44]. Since the only protein known to localize to blebs in a K48-Ub-dependent manner is KSHV ORF10 (Fig. 1), which interacts with Nup98 [34], we prioritized our analysis on Nup98.

Depleting Nup98 provoked the formation of cytosolic granules composed of K48-Ub and FG-Nups to form in TorsinKO cells (Fig. 5b, Extended Data Fig. 4a). This phenotype can be rescued by an siRNA-resistant Nup98 construct but not by Nup96, which is derived from a Nup98-96 precursor protein through proteolytic cleavage [45] (Extended Data Fig. 4b-e). We also examined whether other bleb components became incorporated into these cytosolic granules. Both MLF2-GFP and DNAJB6 also localize to these cytosolic puncta (Fig. 5c) while HSPA1A and HSC70 did not (Extended Data Fig. 4f). While we cannot rule out all possibilities of non-specific effects, knockdown of Nup98 did not significantly perturb nucleo/cytosolic transport (Extended Data Fig. 4g,h) Together, we conclude that the FG-Nup Nup98 is required for the NE bleb sequestration of granules composed of K48-Ub, MLF2, FG-Nups, and chaperones.

Overexpressing MLF2 decreases FG-Nup mislocalization.

When MLF2-GFP was overexpressed in Nup98-depleted TorsinKO cells, we noticed a significant decrease in the amount of FG-Nup incorporation into the cytosolic granule (Fig. 5d,e). We calculated the nuclear/whole cell ratio of nucleoporins in TorsinKO cells under siNT, siNup98, or siNup98 + MLF2-FLAG (Fig. 5e). When Nup98 was depleted, significant FG-Nup mislocalization occurred and the nuclear/whole cell nucleoporin ratio decreased (Fig. 5e). However, when MLF2-FLAG was overexpressed in Nup98-depleted cells, the nuclear/whole cell nucleoporin ratio significantly increased (Fig. 5e). Thus, MLF2 may possess an FG-Nup directed activity.

Blebs share properties with condensates.

The cytosolic granules that form upon siNup98 in TorsinKO cells were often spherical (Fig. 5b-d), prompting us to ask whether they may represent condensates. One strategy to probe the nature of such structures is to determine their sensitivity to 1,6-hexanediol, an alcohol that interrupts weak hydrophobic contacts and dissolves many phase separated condensates while preserving the integrity of the nuclear membrane (Extended Data Fig. 5e) [46, 47]. When exposed to 5% 1,6-hexanediol, the K48-Ub and MLF2-GFP granules typically observed in TorsinKO cells under siNup98 conditions were dissolved (Fig. 5f,g). This suggests that these cytosolic granules are indeed condensates potentially driven by FG-Nups.

The functional yeast ortholog of Nup98, Nup116, serves as “Velcro” to recruit other FG-Nups during NPC assembly [48]. We hypothesized that Nup98 may direct FG-Nups to blebs. When we treated TorsinKO cells with 1,6-hexanediol, K48-Ub and MLF2-HA were released from blebs despite the NE remaining intact (Fig. 5h,i). To rule out that blebs contain terminally aggregated protein, we overexpressed polyQ-97-GFP and found the aggregates to be resistant to 1,6-hexanediol treatment (Extended Data Fig. 5a,b). Furthermore, the K48-Ub and MLF2 sequestered inside blebs was not dissociated by 2,5-hexanediol (Extended Data Fig. 5c) [49]. We note that the NPC permeability barrier established by FG-Nups was, as expected [46], partially broken down by 1,6-hexanediol (Extended Data Fig. 5d).

MLF2 and DNAJB6b immerse into FG-rich phases *in vitro*.

MLF2 has a strikingly high methionine and arginine content (Extended Data Fig. 6a), two residues that specifically facilitate interactions with FG-domains [50]s. Thus, the recruitment of MLF2 to blebs could rely on an FG-driven condensate. To address this, we purified FG-domains from the *Homo sapiens* Nup98, *Saccharomyces cerevisiae* Nup116,

and *Tetrahymena thermophila* MacNup98A. Under denaturing conditions, these FG-domains do not phase separate [51]. However, upon dilution into buffer without denaturants, these FG-domains form condensates exhibiting selective permeability [50, 51] (Fig. 6a). We formed FG-rich phases and validated their selectivity with purified GFP derivatives 3B7C-GFP and sinGFP4a [50] (Fig. 6a). 3B7C-GFP behaves like an NTR while sinGFP4a is excluded from the phases [50] (Fig. 6a).

In Torsin-deficient cells, MLF2 localizes to FG-rich blebs where it interacts with chaperones (Fig. 4b-d). HSP70s represent the most abundant of these (Fig. 4b,c). Thus, to recapitulate the bleb lumen environment *in vitro*, we purified the MLF2:HSP70 complex from mammalian cells (Extended Data Fig. 6b,c) and tested the ability for MLF2 to immerse into FG-rich condensates (Fig. 6a). We tagged MLF2 with a C-terminal Atto488 label and found it immersed into ScNup116 and TtMacNup98A phases but remained mostly at the surface of HsNup98 condensates (Fig. 6a). To exclude the possibility that HSP70 brings MLF2:HSP70 into the phase, we purified and Atto488 tagged HSPA1A (Fig. 6b). Unlike DNAJB6b-Atto488, which we find to immerse into FG condensates, HSPA1A-Atto488 is nearly completely excluded (Fig. 6b). Thus, HSP70 is unlikely to be the major factor driving MLF2:HSP70 into Nup phases. Taken together, we conclude that MLF2 and DNAJB6b interact with phylogenetically diverse FG-domains.

Condensates have distinct properties when formed with MLF2.

FG-rich condensates formed in the presence of MLF2:HSP70 were significantly larger compared to other conditions (Fig. 6a). To quantify this effect, we performed dynamic light scattering (DLS) to obtain the distribution of apparent radii for ScNup116 condensates under different conditions. When solutions containing MLF2:HSP70, DNAJB6b, or denatured Nup116 were analyzed by DLS, small condensates (<10 nm radius) corresponding to protein monomers were detected (Fig. 6c). Diluting ScNup116 into non-

denaturing buffer caused significantly larger condensates (≥1,000 nm radius) to be detected as condensation occurred (Fig. 6d).

When ScNup116 condensates were formed in the presence of DNAJB6b or HSPA1A, we observed condensates with a similar size distribution compared to ScNup116 alone (Fig. 6d). However, when the ScNup116 condensates were formed in the presence of MLF2:HSP70, a pronounced shift towards larger condensate sizes occurred (Fig. 6d). This suggests that MLF2:HSP70 possesses an FG-Nup directed activity.

DNAJB6b and MLF2:HSP70 compete with an NTR-like molecule.

An important consequence of DNAJB6b or MLF2:HSP70 interacting with FG-rich condensates is that they prevent the full partition of 3B7C-GFP into the phase (Extended Data Fig. 6d). This is not the case when condensates are formed in the presence of HSPA1A, which is excluded from the phase (Fig. 6b, Extended Data Fig. 6d). While this may result from an excluded volume effect or from competition for binding sites in FG domains, this observation may explain why blebs are completely devoid of NTRs despite harboring FG-Nups (Supplemental Tables 1,2) [18, 22].

Chaperones preserve FG-Nup condensate integrity over time.

After three hours in solution, ScNup116 and TtMacNup98A condensates largely disassociate (Fig. 6e,g, Extended Data Fig. 7a,b). In the presence of MLF2:HSP70, however, the condensates shrink but remain intact (Fig. 6e, Extended Data Fig. 7b). When WT DNAJB6b was included with MLF2:HSP70, ScNup116 and TtMacNup98A condensates remained largely unchanged after three hours (Fig. 6e,h). In contrast, when the H31Q-DNAJB6b mutant was included, which cannot interact with HSP70, the FG-rich condensates were strongly disassociated (Fig. 6f, Extended Data Fig. 7c). This illustrates

a dominant-negative FG-directed activity for H31Q-DNAJB6b (Fig. 6e,f). While the WT DNAJB6b:HSP70 complex preserves small clusters of condensates, this was not as uniform or penetrant as the effect by the complete MLF2:HSP70:DNAJB6b complex (Fig. 6f-h, Extended Data Fig. 7c). Taken together, these data suggest that the MLF2:HSP70 complex maintains FG-rich condensates over time, an activity that is enhanced by DNAJB6b.

The MLF2:HSP70 complex reduces FG-Nup amyloid formation.

The ScNup116 FG domain is known to form cross-β amyloid-like structures [51, 52]. Initially, ScNup116 does not form amyloids as the condensates are readily reversable (Extended Data Fig. 7d). The transition to amyloids is detectable by the dye Thioflavin-T (ThT), which fluoresces upon interacting with amyloids (Extended Data Fig. 7e). We monitored ThT fluorescence of solutions containing ScNup116 plus HSPA1A, DNAJB6b, or MLF2:HSP70 (Extended Data Fig. 7f,g). While neither HSPA1A nor DNAJB6b affected ScNup116 amyloid formation, MLF2:HSP70 reduced it by approximately half in an ATP-dependent manner even at a sub-stoichiometric concentration (Extended Data Fig. 7f). We found that the DNAJB6b-HSP70 complex has a similar ATP-dependent, sub-stoichiometric ability to reduce amyloid formation (Extended Data Fig. 7g). Amyloid formation was most potently suppressed in the presence of ATP upon inclusion of MLF2, HSPA1A, and DNAJB6 (Extended Data Fig. 7g). These data reveal an additional FG-Nup directed activity of the chaperone network identified herein.

Discussion

In this study, we developed a virally-derived model substrate (Δ133 ORF10, Fig. 1) to explore the molecular composition and cellular consequences of NE herniations that arise in disease models of primary dystonia. While NE blebs are striking morphological features in dystonia model systems and found in other experimental settings [53], it has generally been unclear whether NE blebs contribute to disease development. Using Δ133 ORF10 and the APEX-derivatized MLF2 in a comparative proteomics approach, we found that blebs are highly enriched for the FG-Nup Nup98 and specific members of the HSP40 and HSP70 chaperone family (Fig. 2). In cells with perturbed Torsin function, these chaperones become tightly sequestered within the lumen of NE blebs and are titrated away from their normal subcellular localization (Fig. 3). Importantly, this sequestration also occurs in primary neurons with perturbed Torsin function (Fig. 3). This raises the question of what mechanisms are at work to cause this unusual sequestration.

We demonstrate that NE blebs contain FG-rich condensates (Fig. 5) that impose two proteotoxic challenges: an unprecedented degree of chaperone sequestration that is typically only observed upon overexpression of disease alleles, and a profound stabilization of normally short-lived proteins (Fig. 1e,f). We furthermore find that MLF2 affects FG-domain condensation (Fig. 5d,f, Fig. 6, Extended Data Fig. 7). Our observation that MLF2 expression results in a near-complete re-distribution of DNAJB6–a critical factor for suppressing proteotoxic aggregation [41, 43] – from poly-Q inclusions to NE blebs (Fig. 4e,f) establishes MLF2 as an important player in protein homeostasis. Taken together, we uncovered a direct proteotoxic contribution of blebs to DYT1 dystonia pathology and a role for MLF2, HSPA1A, and DNAJB6 in the formation and maintenance of FG-rich phases.

While NTRs function as FG-Nup-directed chaperones during postmitotic NPC assembly [54], interphase NPC biogenesis follows a distinct insertion pathway [55]. We demonstrated that MLF2 overexpression prevents the ectopic accumulation of FG-Nups

upon Nup98 depletion (Fig. 5d,e). It is therefore tempting to speculate that non-NTR chaperones like MLF2 and DNAJB6 function during interphase NPC biogenesis to prevent premature FG-Nup assembly. Indeed, Kuiper et al. have independently assigned DNAJB6 to a role in NPC biogenesis [56]. *In vitro*, we find that MLF2:HSP70 and DNAJB6 prevent the full partition of NTR-like molecules into FG-Nup phases (Extended Data Fig. 6d). While this may be explained by excluded volume effects or a competition mechanism, either scenario would result in fewer NTR-FG domain interactions, consistent with our observation that bulk nuclear transport cargo is excluded from FG-rich NE blebs [18, 22].

We previously reported that MLF2-GFP accumulates at sites of NE developing membrane curvature in Torsin-deficient cells [22]. This clustering of MLF2 juxtaposed against the curved NE may represent nucleation events of FG-Nups undergoing condensation at sites of *de novo* interphase NPC assembly. This role for MLF2 *in vivo* would reflect the activity we report *in vitro* (Fig. 6c-h, Extended Data Fig. 7).

Our proteomic experiments reveal a specific enrichment of class B HSP40s inside blebs. While future work will be required to understand whether an active exclusion of other HSP40 classes exists, we propose that DNAJB2 and DNAJB6 are recruited by the specific properties of these HSP40s. Future studies are warranted to understand whether MLF2 interacts with other HSP40 classes, and if other HSP40s can enter into condensates as exemplified here for DNAJB6 (Fig. 6b).

The observation that mutations in ER/NE-luminal Torsin ATPases give rise to an indirect proteotoxic mechanism across compartmental borders was unexpected. This feature adds a unique disease mechanism to the growing list of movement disorders with functional ties between liquid-liquid phase separation, nuclear transport machinery, and proteotoxicity [57-59]. Our finding that NE blebs exert a two-fold proteotoxicity also represents a distinct pathological mechanism from the documented

nuclear transport defects that arise in Torsin-deficient cells due to compromised NPC assembly [12, 20-22] (Extended Data Fig. 8).

We propose that this dual proteotoxicity mechanism contributes to DYT1 dystonia's unusual disease manifestation. Unlike other congenital movement disorders, DYT1 dystonia is characterized by a limited window of onset. After the age of 30, carriers of the DYT1 mutation will never develop the disease [60]. Furthermore, the disease displays a reduced penetrance as only one third of all mutation carriers develop DYT1 dystonia [11]. These features may be explained by the fact that blebs are transient structures that resolve in model organisms after TorsinB is upregulated [16, 61]. Thus, the proteotoxicity imposed by blebs is confined to a specific window in life—likely closing before the age of 30. We propose that sequestered chaperones and accumulated short-lived proteins accompany this window of vulnerability and generate a high but potentially manageable degree of proteotoxic stress. Further insult on the PQC machinery that may normally be inconsequential could cause severe problems in these pre-sensitized cells. This model describes a stochastic and previously underappreciated influence on disease manifestation (Extended Data Fig. 8). While additional studies will be required to test these ideas, our data provide a strong motivation to investigate pharmacological modulators of the cellular PQC system for DYT1 dystonia prevention and management.

Acknowledgements

This work was supported by NIH R01GM114401 (CS), DOD PR200788 (CS), NIH 5T32GM007223-44 (SMP), NIH F31NS120528 (SMP), NIH R56MH122449 (AJK), NIH R01MH115939 (AJK), NIH NS105640 (AJK), NIH F31MH116571 (JEG) and the Dystonia Medical Research Foundation (CS and AJR). The mass spectrometers and accompanying biotechnology tools at the Keck MS & Proteomics Resource at Yale University were funded in part by the Yale School of Medicine and by the Office of the Director, National Institutes of Health (S10OD02365101A1, S10OD019967, and S10OD018034). We thank Dirk Görlich and members of his laboratory for sharing reagents. We thank the Yale Keck Biophysical Resource Center, Morven Graham, and the Yale Center for Cellular and Molecular Imaging. We also thank the MS & Proteomics Resource at Yale University for providing the necessary mass spectrometers and the accompany biotechnology tools funded in part by the Yale School of Medicine and by the Office of The Director, National Institutes of Health. The funders had no role in study design, data collection and analysis, decision to publish, or preparation of the manuscript.

Author contributions

SMP, AJR, JEG, RFN, SM, AJK, and CS conceptualized and designed experiments. SMP, AJR, JEG, RFN, and SM performed experiments. SMP, AJR, JEG, RFN, SM, AJK, and CS analyzed and interpreted data. SMP and CS wrote the original manuscript. SMP, AJR, JEG, RFN, AJK, and CS edited the manuscript.

Competing interests statement

The authors declare no competing interests.

Methods

This research complies with all relevant ethical regulations. All experiments using animal models were approved by the Yale University School of Medicine Institutional Animal Care and Use Committee as described in protocol 2022-07912.

Cell culture and cell lines

HeLa, SH-SY5Y, and HEK293T cells were maintained in Dulbecco's modified Eagle's medium (DMEM) supplemented with 10% v/v FBS (Thermo Fisher Scientific) and 100 U/mL of penicillin-streptomycin (Thermo Fisher Scientific). Cells were routinely checked for mycoplasma and determined to be free of contamination through the absence of extranuclear Hoechst 33342 (Life Technologies) staining.

Expi293 suspension cells were cultured at 37ºC in flat-bottom shaking flasks in preformulated Expi293 Expression Media (Gibco, A1435102) in an 8% CO_2 atmosphere.

To generate stable HeLa cell lines expressing MLF2-APEX2-HA, 6 µg of MLF2-APEX-HA within the pcDNA3.1 backbone was transiently transfected into HEK293T cells along with 2 µg of a plasmid encoding MMLV gag/pol and 1 µg of a plasmid encoding the viral envelope protein VSV-G. After 72 hours of expression, the supernatant was collected and filtered through a 0.45 µm filter before storage at -80°C. HeLa cells were seeded in 6-well plates and transduced with 100 µL viral supernatant plus 4 µg/mL polybrene reagent (Sigma-Aldrich). After 24 hours, the medium was switched to contain 1 µg/mL of puromycin (Sigma-Aldrich). Antibiotic selection was performed for 7 days before the dox-inducible MLF2-APEX2-HA expression was verified.

Plasmids, transient RNAi knockdowns, and transient transfections

KSHV ORF10-HA was synthesized by Genscript into the pcDNA3.1 vector. ∆133 ORF10-HA was cloned from the full length cDNA into pcDNA3.1. Plasmids encoding the deubiquitylating enzyme M48 [35] were a gift from Hidde L. Ploegh (Whitehead Institute for Biomedical Research, Cambridge, MA). MLF2-HA and MLF2-GFP were cloned into pcDNA3.1 or pEGFP-N1 using standard molecular cloning techniques. polyQ-72-GFP and polyQ-97-GFP were a gift from Susan Lindquist (Addgene plasmid # 1179; http://n2t.net/addgene:1179; RRID:Addgene_1179, Addgene plasmid # 1180; http://n2t.net/addgene:1180; RRID:Addgene_1180) [62]. These polyQ constructs were subcloned into pcDNA3.1 using standard cloning techniques.

MLF2-APEX2-HA was cloned into the pRetroX-Tight-Pur vector from pcDNA3.1 using standard cloning techniques. mito-V5-APEX2 was a gift from Alice Ting (Addgene plasmid # 72480; http://n2t.net/addgene:72480; RRID:Addgene_72480) [36].

DNAJB6b-ΔG/F-HA and DNAJB6b-ΔG/F-S/T-HA were synthesized by Genscript into the pcDNA3.1 vector. The G/F-rich region was defined as G72-G131 and the S/T-rich region as S132-T195. All phenylalanine residues within these regions were mutated to alanine to generate the DNAJB6b mutants.

pCMV-PV-NES-GFP was a gift from Anton Bennett (Addgene plasmid # 17301; http://n2t.net/addgene:17301; RRID:Addgene_17301) [63].

The plasmids encoding His-tagged 3B7C-GFP, sinGFP4a, HsNup98, TtMacNup98A, and ScNup116 FG domains were gifts from Dirk Görlich (Max Planck Institute for Biophysical Chemistry, Göttingen, Germany) [50, 51].

MLF2-LPEXTG-Tev-MBP-His-FLAG, DNAJB6b-LPETG-His and HSPA1A-LPETG-His were synthesized by Genscript into pcDNA3.1 (for the MLF2 construct) or pET11a (DNAJB6b and HSPA1A constructs). The LPETG motif was included as a sortase enzyme recognition motif for tagging with the Atto488 dye.

Nontargeting RNAi and RNAi targeting MLF2, DNAJB6, and Nup98 were performed with SMARTpool oligos from Horizon Discovery. Knockdown efficiency was validated by quantitative PCR (qPCR) using iQ SYBR Green mix with a CFX Real-Time PCR 639 Detection System (Bio-Rad). For each knockdown, we employed the comparative Ct method using the internal control transcript RPL32 [22]. All primers were synthesized by Integrated DNA Technologies.

All plasmid transfections were performed with Lipofectamine 2000 (Invitrogen) according to the manufacturer's instructions and allowed to express for 24 hours prior to analyses. All RNAi knockdowns were performed with Lipofectamine RNAiMAX (Invitrogen) according to manufacturer's instructions and allowed to incubate for 48 hours before analyses.

CRISPR/Cas9 generation of MLF2 knockout

To generate MLF2 KO HeLa cells, we employed the CRISPR/Cas9 system [64] as previously implemented [65]. Briefly, a guide RNA targeting MLF2 was cloned into the px459 vector and transfected into HeLa cells. pSpCas9(BB)-2A-Puro (px459) V2.0 was a gift from Feng Zhang (Addgene plasmid # 62988; http://n2t.net/addgene:62988; RRID:Addgene_62988) [66]. The transfected cells underwent antibiotic selection for 48 hours via treatment with 0.4 μg/mL puromycin (Thermo Fisher Scientific). After selection, cells were seeded at a low density such that single-cell colonies could be isolated after 10

days in culture. These colonies were expanded and screened for MLF2 knockout by genotyping PCR [65].

Hippocampal cultures, transfection, and immunofluorescence

Hippocampal cells were cultured from seven mixed sex BALB/c P0 pups in accordance with IACUC protocol number 2022-07912 (Yale University School of Medicine IACUC). Hypothermia was induced in pups, followed by decapitation and hippocampal dissection. Hippocampi were dissociated using 200 units Papain (Worthington LS003124, 200 U) and were plated on 14 mm poly-D-lysine coated coverslips in a 24 well dish at a density of 150,000 cells/well. Neurons were transfected at DIV 4 with 1 µL per reaction of Lipofectamine 2000 (Thermo Fisher Scientific) at a concentration of 0.6 µg per plasmid, for a total of 1.8 µg of DNA. Neurons were fixed at DIV 7 with 4% v/v paraformaldehyde (PFA) in PBS at room temperature for 15 minutes, permeabilized with 0.1% v/v Triton-X for 15 minutes, blocked with 1% w/v BSA for one hour, and stained with primary antibodies in blocking buffer overnight at 4°C (1:1000 rat HA, 1:200 rabbit TorsinA). Following the primary stain, coverslips were washed with PBST three times for 5 minutes, followed by a secondary antibody stain in blocking buffer for 1 hour at room temperature (1:1000 rat Alexa 568 and rabbit 633). Coverslips were washed with PBST three times for 5 minutes, stained with DAPI for 10 minutes at room temperature, washed with PBST three times for 5 minutes, and mounted in Aqua-Mount (Lerner Laboratories).

Immunofluorescence and confocal microscopy

HeLa and SH-SY5Y cells were grown on coverslips and prepared for IF by fixing in 4% v/v PFA (Thermo Fisher Scientific), permeabilized in 0.1% v/v Triton X-100 (Sigma-Aldrich) for 10 minutes, then blocked in 4% w/v bovine serum albumin (BSA). Primary

antibodies were diluted into 4% w/v BSA and incubated with coverslips for 45 minutes at RT. After extensive washing with PBS, fluorescent secondary antibodies were diluted in 4% w/v BSA and incubated with coverslips for 45 minutes. Cells were stained with Hoechst 33342 (Life Technologies) before mounting onto slides with Fluoromount-G (Southern Biotech).

For hexanediol experiments, cells were incubated for five minutes with complete DMEM containing 5% w/v hexanediol (Millipore) before fixing in 4% v/v PFA and processing for IF as described above. VER-155008 was dissolved in DMSO at a stock concentration of 10 mM and used at a final concentration of 20 μM for 24 hours prior to fixation for IF.

Phase separated condensates were imaged by spotting a 10 μL volume of the indicated conditions onto a glass bottom dish (WillCo Wells). To visualize effects of protein on Nups after three hours, FG phases were formed in supplemented TBS (50 mM Tris (pH 7.5), 150 mM NaCl, 2 mM DTT, 10 mM $Mg(CH_3COO)_2$, 10 mM $K(CH_3COO)_2$, 4 mM creatine phosphate, 0.25 μL creatine kinase, 2 mM ATP). Where indicated, ATP was omitted from the supplemented TBS (the ATP regenerating system remained). Incubation took place at 30ºC.

All images were collected on an LSM 880 laser scanning confocal microscope (Zeiss) with a C Plan-Apochromat 63×/1.40 oil DIC M27 objective using ZEN v2.1 & v3.4 software (Zeiss).

Spectroscopic measurements of Nup solutions

Turbidity of Nup solutions was measured at an excitation and emission wavelength of 550 nm (Synergy Mx, BioTek Instruments, Inc).

To monitor ScNup116 amyloid formation, Nups were diluted into TBS supplemented with the indicated proteins. Solutions were brought to 2 μM ThT. Bottom reads of ThT fluorescence (excitation 440 nm, emission 480 nm) were captured every two minutes at 30ºC for 24 hours (Synergy Mx, BioTek Instruments, Inc).

Cycloheximide chase

WT and TorsinKO cells were plated in a 10 cm dish and transfected with ∆133 ORF10-HA. After 24 hours of expression, each cell line was trypsinized and split into two tubes. Tubes were incubated at 37°C with gentle shaking and treated with 1.1 ug/mL of DMSO with or without 100 μg/mL CHX and aliquots were taken at 0, 1, 2, 3, or 4 hours post treatment. Cells were collected via centrifugation and subjected to immunoblot for analyses.

Immunoprecipitation, mass spectrometry preparation, and immunoblot analysis

For native IP experiments, cells were transfected with the indicated constructs 24 hours before harvesting. Cells were lysed in NET buffer (150 mM NaCl, 50 mM Tris pH 7.4, 0.5% v/v NP-40) supplemented with EDTA-free protease inhibitor cocktail (Roche) and 5 mM NEM (Sigma-Aldrich). Immunoprecipitation was conducted with pre-cleared lysates on anti-HA affinity matrix (Roche), magnetic beads conjugated to streptavidin, or magnetic protein G beads (Pierce) non-covalently coupled to anti-HSPA1A. Stable interactions were eluted for immunoblot analyses in 30 μL of 2x SDS reducing buffer and heated at 70°C for five minutes. For mass spectrometry applications, protein complexes were briefly run into SDS-PAGE gels, stained with SimplyBlue Safe Stain (Thermo Fisher Scientific) before bands of 2-4 mm were extracted. Gel bands were submitted to the MS & Proteomics Resource at the Yale University Keck Biotechnology Laboratory.

Radioimmunoprecipitations were carried out as described previously [4, 67]. Briefly, metabolically labeled cells were grown in complete DMEM containing 150 µCi/mL ^{35}S-Cys/Met labeling mix (PerkinElmer) for 16 hours prior to lysis in NET buffer. Co-eluting protein were detected by autoradiography and imaged on a Typhoon laser-scanning platform (Cytiva).

Immunoblotting was carried out with IP eluates or cell lysates in supplemented NET buffer. Equal micrograms of protein were resolved in SDS-PAGE gels (Bio-Rad) and transferred onto PVDF membranes (Bio-Rad). Membranes were blocked in 5% w/v milk in PBS + 0.1% v/v Tween-20 (Sigma-Aldrich). Primary and HRP-conjugated secondary antibodies were diluted in blocking buffer. Blots were visualized by chemiluminescence on a ChemiDoc Gel Imaging System (Bio-Rad).

APEX2 reaction and NE enrichment

To induce the expression of MLF2-APEX2-HA, cells were treated with 500 µg/mL dox for 24 hours. After 24 hours, cells were incubated for 30 minutes with complete DMEM containing 500 µM biotin phenol. For the APEX2 reaction, cells were treated with 1 mM H_2O_2 for one minute before quenching by washing the plates three times with quenching buffer (PBS, pH 7.4, 0.5 mM $MgCl_2$, 1 mM $CaCl_2$, 5 mM Trolox, 10 mM sodium ascorbate, 10 mM sodium azide). Cells were collected and enriched for NE fractions as described previously [22, 68]. Briefly, cells were gently pelleted in buffer containing 250 mM sucrose and homogenized via trituration through a 25-guage needle. The homogenates were layered onto a 0.9 M sucrose buffer and spun down. The pellets (membrane fractions and nuclei) were solubilized overnight in buffer without sucrose containing benzonase, heparin, NEM, and protease inhibitors. The solubilized nuclei were spun at 15,000 x g for

45 minutes and the supernatant was collected as the nucleoplasm and pellet as the NE/ER enriched fraction. The ER/NE fraction was solubilized in 8 M urea and equal amounts of protein were loaded onto streptavidin beads for capture of biotinylated proteins, which were analyzed by immunoblot or mass spectrometry.

Transmission electron microscopy and immunogold labeling

Electron microscopy (EM) and immunogold labeling was performed as previously described [18, 22] at the Yale School of Medicine's Center for Cellular and Molecular Imaging. Briefly, cells were fixed by high-pressure freezing (Leica EM HPM100) and freeze substitution (Leica AFS) was carried out at 2,000 pounds/square inch in 0.1% w/v uranyl acetate/acetone. Samples were infiltrated into Lowicryl HM20 resin (Electron Microscopy Science) and sectioned onto Formvar/carbon-coated nickel grids for immunolabeling.

Samples were blocked in 1% w/v fish skin gelatin, then incubated with primary antibodies diluted 1:50 in blocking buffer. 10 nm protein A-gold particles (Utrecht Medical Center) were used to detect the primary antibodies and grids were stained with 2% w/v uranyl acetate and lead citrate.

Images were captured with an FEI Tecnai Biotwin TEM at 80Kv equipped with a Morada CCD and iTEM (Olympus) software.

Recombinant protein expression and purification

HsNup98, TtMacNup98A, and ScNup116 [50, 51] were purified from BL21(DE3) *E. coli* strains under denaturing conditions by virtue of an N-terminal His_{18} tag. Cell pellets containing the FG domains were resuspended in denaturing lysis buffer (8 M urea, 150

mM NaCl, 50 mM Tris (pH 8), 20 mM imidazole, 10 mM β-ME, 2 mM PMSF). Solubilized His-tagged Nups were complexed with Ni-NTA agarose (Qiagen) at 4ºC for 16 hours before the columns were extensively washed at room temperature (6 M urea, 150 mM NaCl, 50 mM Tris (pH 8), 25 mM imidazole, 10 mM β-ME). Protein was eluted in room temperature elution buffer (6 M urea, 150 mM NaCl, 50 mM Tris (pH 8), 400 mM imidazole, 10 mM β-ME) and dialyzed overnight at 4°C into UTS buffer (2 M urea, 150 mM NaCl, 50 mM Tris (pH 7.4)). Finally, the dialyzed Nup was concentrated to 500 μM using a Macrosep 10,000 MWCO centrifugation unit (Pall Corporation).

Phase separated condensates were formed by diluting 500 μM Nup stock solutions in denaturing UTS buffer into tris-buffered saline (TBS; 50 mM Tris (pH 7.4), 150 mM NaCl) to a final concentration of 10 μM [51].

His-tagged GFP variants were purified as previously described [50]. BL21(DE3) [50, 69] cell pellets containing His-*Brachypodium distachyon* (bd)-SUMO-sinGFP4a or His-bdSUMO-3B7C-GFP[50, 69] were resuspended in resuspension buffer (50 mM Tris (pH 7.5), 150 mM NaCl, 10 mM β-ME, 20 mM imidazole, 1 mM PMSF) and passed through the French Press. His-tagged proteins were bound to Ni-NTA agarose (Qiagen) for 1 hour at 4°C before washing in resuspension buffer. GFP constructs were eluted in resuspension buffer containing 400 mM imidazole, then concentrated with a Macrosep 10,000 MWCO centrifugation unit (Pall Corporation). Final concentrates were buffer-exchanged into TBS.

DNAJB6b-LPETG-His_{10} was purified as previously described [70]. BL21(DE3) cell pellets were resuspended in resuspension buffer (100 mM Tris (pH 8), 150 mM KCl, 10 mM β-Me, 1 mM PMSF) and were passed through the French Press. DNAJB6b-LPETG-His_{10}

was solubilized from inclusion bodies in pellet buffer (100 mM Tris (pH 8), 8 M urea, 150 mM KCl, 20 mM imidazole, 10 mM β-Me, 1 mM PMSF). DNAJB6b-LPETG-His_{10} was allowed to bind Ni-NTA agarose (Qiagen) for 1 hour at 4°C. The matrix was washed (100 mM Tris (pH 8), 8 M urea, 150 mM KCl, 20 mM imidazole, 10 mM β-Me) and DNAJB6-LPETG-His_{10} was eluted in elution buffer (100 mM Tris (pH 8), 150 mM KCl, 10 mM β-Me, 350 mM imidazole). The protein was dialyzed overnight into final buffer (50 mM Tris (pH 7.5), 150 mM KCl) and concentrated with a Macrosep 10,000 MWCO centrifugation unit (Pall Corporation).

HSPA1A-LPETG-His_{10}-FLAG was purified from BL21(DE3) cells resuspended in resuspension buffer (100 mM HEPES (pH 8), 500 mM NaCl, 10% v/v glycerol, 10 mM β-Me, 20 mM imidazole, 1 mM PMSF) and passed through the French Press The supernatant was applied to Ni-NTA agarose (Qiagen) for 1 hour at 4ºC. The matrix was washed (30 mM HEPES (pH 7.4), 500 mM NaCl, 10% v/v glycerol, 20 mM imidazole, 10 mM β-Me) and protein was eluted in wash buffer with 400 mM imidazole. Protein was dialyzed overnight into TBS and concentrated as described above.

The MLF2-LPETG-TEV-MBP-His-FLAG:HSP70 complex was purified from a mammalian Expi293 suspension system. Cells were harvested after 72 hours of expression and pellets were lysed in ice cold lysis buffer (50 mM Tris (pH 7.5), 150 mM NaCl, 1% w/v DDM, 10% v/v glycerol, protease inhibitor tablet (Roche)). Clarified supernatant was applied to anti-FLAG M2 Affinity Gel (Sigma-Aldrich) and allowed to bind overnight at 4°C. The matrix was washed (50 mM Tris (pH 7.5), 150 mM NaCl, 0.05% w/v DDM), then washed with buffer minus detergent. Protein was eluted in final buffer (50 mM Tris (pH 7.5), 150 mM NaCl, 0.3 mg/mL FLAG peptide) for 1 hour at 4°C. TEV enzyme (New England BioLabs)

was added to the elution and the mixture was dialyzed overnight into TBS. The resulting MLF2:HSP70 complex was concentrated as described above.

Atto-tagging via the sortase reaction

To produce Atto488-tagged MLF2, DNAJB6b, and HSPA1A, constructs were purified with an LPETG sortase recognition sequence between the C-terminal end and the downstream purification tag. This motif is recognized by the transpeptidase sortase, which catalyzes a reaction wherein a molecule harboring a poly-glycine label is attached to the LPETG sequence [71]. Reactions were carried out using purified MLF2-LPETG, DNAJB6b-LPETG, or HSPA1A-LPETG and the Sortag-IT™ ATTO 488 Labeling Kit (Active Motif) according to the manufacturer's instructions. After the sortase reaction, free dye was removed from the Atto-tagged proteins by washing extensively with TBS in Amicon Ultra-0.5 mL Centrifugal Filters (MilliporeSigma), then running through a PD MiniTrap desalting column (Cytiva).

Dynamic light scattering

DLS was used to assess the size distribution of FG-rich condensates forming in the presence or absence of MLF2:HSP70. Measurements were taken on a DynaPro Titan DLS instrument (Wyatt Technologies) at 25°C and data were analyzed using DYNAMICS software (Wyatt Technologies). 10 µL reactions of 10 µM ScNup116 in TBS containing no additional protein, 5 µM MLF2:HSP70, 5 µM HSPA1A, or 5 µM DNAJB6b were allowed to form for one minute before diluting 1:10 in TBS. 30 µL of this dilution was transferred to a quartz cuvette and datasets of 100 measurements of five-second acquisition times were collected.

Image processing

The number of immunogold beads against HSPA1A or DNAJB6 was manually counted for 400 μm^2 centered around the NE from WT or TorsinKO cells (Fig. 3c). The number of immunogold beads was quantified for a square of 2 µm by 2 µm with the NE in the middle. This value was obtained for 100 2x2 µm squares centered around the NE and involved approximately 10 distinct cells per condition.

The ratio of DNAJB6 within polyQ aggregates compared to the whole cell was calculated using Fiji Software [72] (Fig. 4f). The DNAJB6 antibody signal intensity was obtained by defining a region of interest (ROI) within the polyQ aggregate (Q), then of the whole cell (W). The Q/W ratio was calculated for at least eight cells/condition.

The rescue effect of MLF2 on FG-Nup mislocalization (Fig. 5e) was determined for 94 cells/condition. The nucleoporin (Mab414 antibody) signal intensity in the whole cell and the nucleus was quantified using Fiji by selecting these as ROIs. From these values, the ratio of nuclear Mab414 intensity to whole cell intensity was calculated.

The presence of cytosolic granules under siNup98 conditions (Fig. 5g, Extended Data Fig. 4c) was determined by visualizing the presence or absence of cytosolic K48-Ub deposits for 300 cells/condition.

To quantify the number of NE-associated K48-Ub foci in TorsinKO cells treated with 1,6-hexanediol (Fig. 5i), the nucleus was selected in Fiji as the region of interest (ROI) and the number of foci was quantified as previously performed [18, 22]. The “Find Maxima” function was employed with a noise tolerance of 10. Foci were quantified for 100 cells/condition.

The nuclear to cytoplasmic (N/C) ratio of the Ran GTPase under siNT or siNup98 was quantified using CellProfiler software [73] (Extended Data Fig. 4h). Briefly, the Ran IF signal was quantified within cell regions co-localizing or not co-localizing with DAPI stain to define the nuclear and cytoplasmic regions, respectively. These values were used to calculate the N/C ratio for 85 cells/condition.

The 3B7C-GFP signal intensity was determined in Fiji using the measure function (Extended Data Fig. 6d). The center of Nup condensates was selected as an ROI, then the average GFP signal intensity was measured for 100 condensates/condition.

Statistics and reproducibility

All data were considered representative by repeating experiments at least three times with similar results or using three independent samples for analysis. Datasets were tested for normality using the Shapiro-Wilk test. If found to be normally distributed, datasets were analyzed using a two-tailed unpaired *t*-test. Datasets not normally distributed were analyzed with a two-tailed unpaired Mann-Whitney test. GraphPad Prism 9.4.0 was used for all statistical analyses. *P* values <0.05 were considered significant. Data are displayed with the mean value indicated and error bars showing the standard deviation (SD). No statistical method was used to predetermine sample size. No data were excluded from the analyses. The Investigators were not blinded to allocation during experiments and outcome assessment. The experiments were not randomized.

Data availability statement

Mass spectrometry datasets are uploaded to the massIVE database (Supplemental Table 1 accession MSV000090177. Supplemental Table 2 accession number MSV000090186.

Supplemental Table 3 accession number MSV000090187. Supplemental Table 4 accession number MSV000090188). The mass spectrometry proteomics data have been deposited to the ProteomeXchange Consortium via the PRIDE partner repository with the following accession numbers: Supplemental Table 1, PXD036262. Supplemental Table 2, PXD036264. Supplemental Table 3, PXD036266. Supplemental Table 4, PXD036267. All other data supporting the findings of this study are available from the corresponding author on reasonable request.

Figures

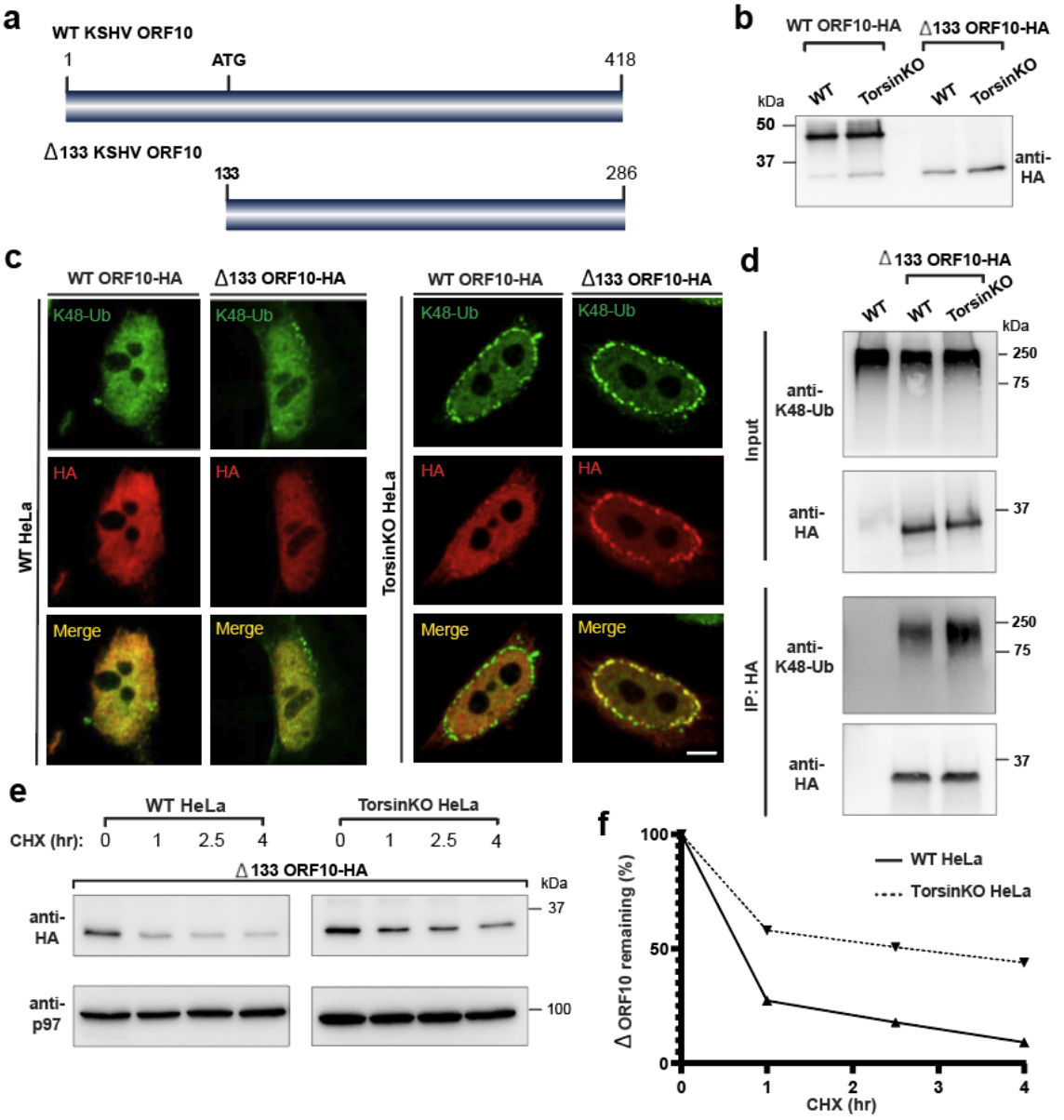

Figure 1. **NE herniations arising from Torsin ATPase deficiency sequester and stabilize short-lived protein. a**, Schematic model of the ORF10 protein from KSHV. KSHV ORF10 contains an internal start codon at residue 133 that produces Δ133 ORF10. **b**, Immunoblot demonstrating expression of Δ133 ORF10-HA in WT and TorsinKO HeLa cells 24 hours post transfection. Note that ORF10-HA is produced as a major full-length protein a lower abundance Δ133 product. **c**, Representative IF images

of full length and ∆133 ORF10-HA in WT and TorsinKO cells. Scale bar, 5 μm. **d**, Anti-HA immunoprecipitation (IP) from WT or TorsinKO cells expressing ∆133 ORF10-HA. The IP was probed with antibodies against K48-Ub and HA. Note that ∆133 ORF10-HA is associated with more K48-Ub in TorsinKO than WT cells. **e**, A cycloheximide (CHX) chase over four hours in WT and TorsinKO cells expressing ∆133 ORF10-HA. Cells were treated with 100 μg/mL of CHX at 37°C for the indicated timepoints. p97 serves as a loading control. **f**, Relative percentage of ∆133 ORF10-HA obtained in (**e**) was determined via densitometry by comparing to the abundance at time = 0. All data were standardized to p97 levels. Source numerical data and unprocessed blots are available in source data. All experiments were performed by SMP.

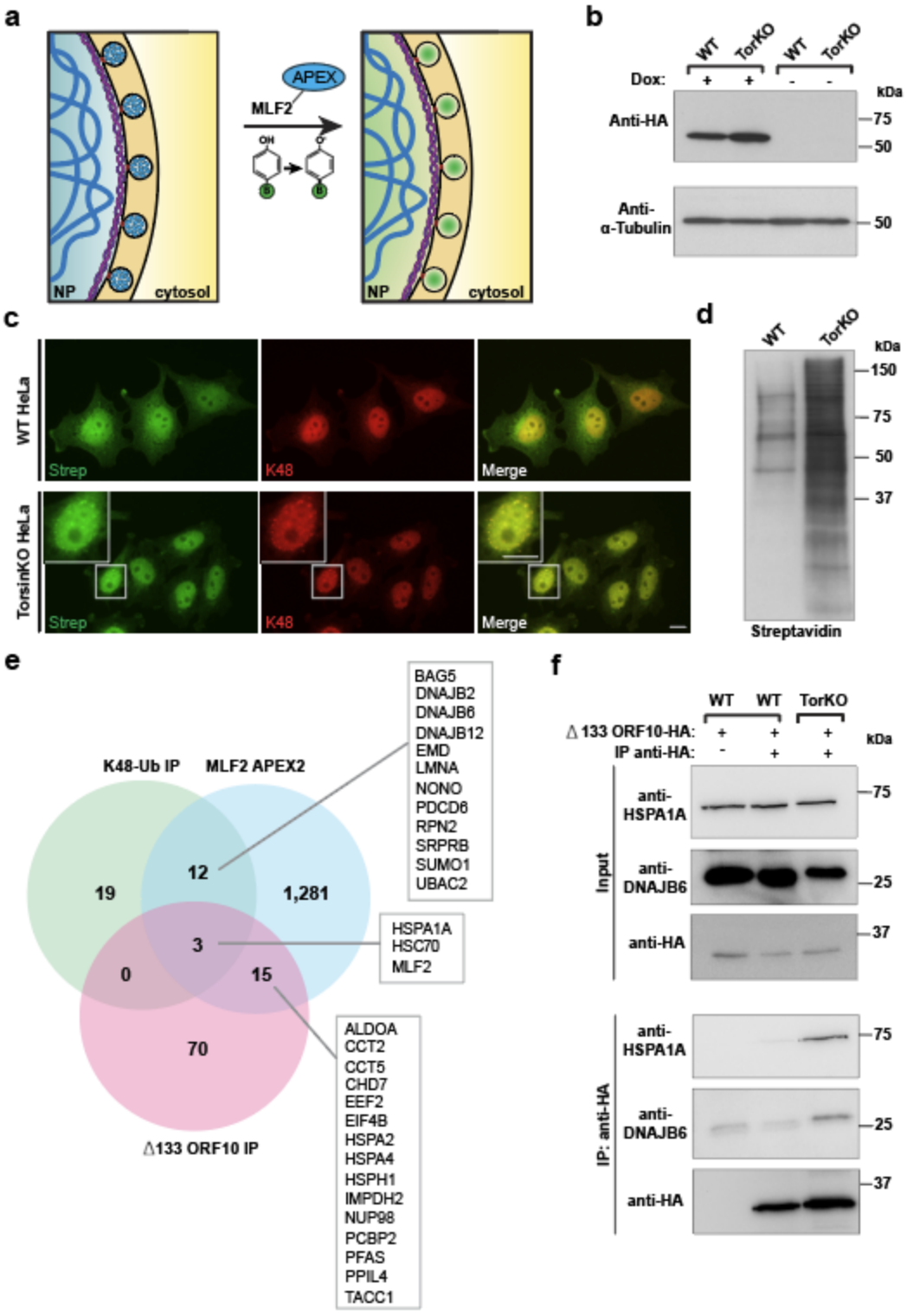

Figure 2. A comparative proteomics approach reveals NE blebs in Torsin-deficient cells are enriched for a highly specific chaperone network. a, A schematic

illustration of the APEX2 reaction strategy to identify bleb protein contents. Left panel, the MLF2- APEX2-HA fusion protein (blue) localizes within the bleb lumen. Right panel, after incubation with 500 μM of biotin-phenol, cells were treated with 1 mM H_2O_2. Upon exposure to H_2O_2, APEX2 oxidizes biotin phenol to form highly reactive biotin radicals that covalently label protein within a ~20 nm radius (ref. [74]) (green cloud). NP, nucleoplasm. **b**, The expression of MLF2-APEX2-HA was engineered in WT and TorsinKO cells to be under doxycycline (Dox) induction. Cells were treated with Dox for 24 hours before immunoblotting. **c**, Representative IF images of WT and TorsinKO cells after the APEX2 reaction. Note the enrichment of biotin conjugates in blebs of TorsinKO cells compared to the diffuse nuclear signal in WT cells. Strep (green) indicates fluorescently conjugated streptavidin signal and K48-Ub (red) indicate NE blebs. Scale bar, 10 μm. **d**, Immunoblot of biochemically enriched NE fractions from WT and TorsinKO cells after the MLF2- APEX2 reaction as described in (**c**). **e**, Candidate proteins potentially enriched in blebs were identified by mass spectrometry (MS). These were defined as proteins with spectral counts ≥1.5-fold enriched in APEX2 reactions carried out in TorsinKO cells compared to WT. The number of candidates identified for each of the three MS datasets are displayed as numbers within the Venn diagram. Hits overlapping between datasets are listed in alphabetical order. See Supplemental Tables 1,2 for complete datasets. **f**, To validate MS findings, the stable interaction between Δ133 ORF10-HA and HSPA1A or DNAJB6 was interrogated by co-IP. These interactions are unique to TorsinKO cells, consistent with the findings by comparative MS in panel (**e**). Unprocessed blots are available in source data. Experiments in panels a-d were performed by AJR. Experiments in panel e were performed by AJR and SMP. Experiments in panel f were performed by SMP.

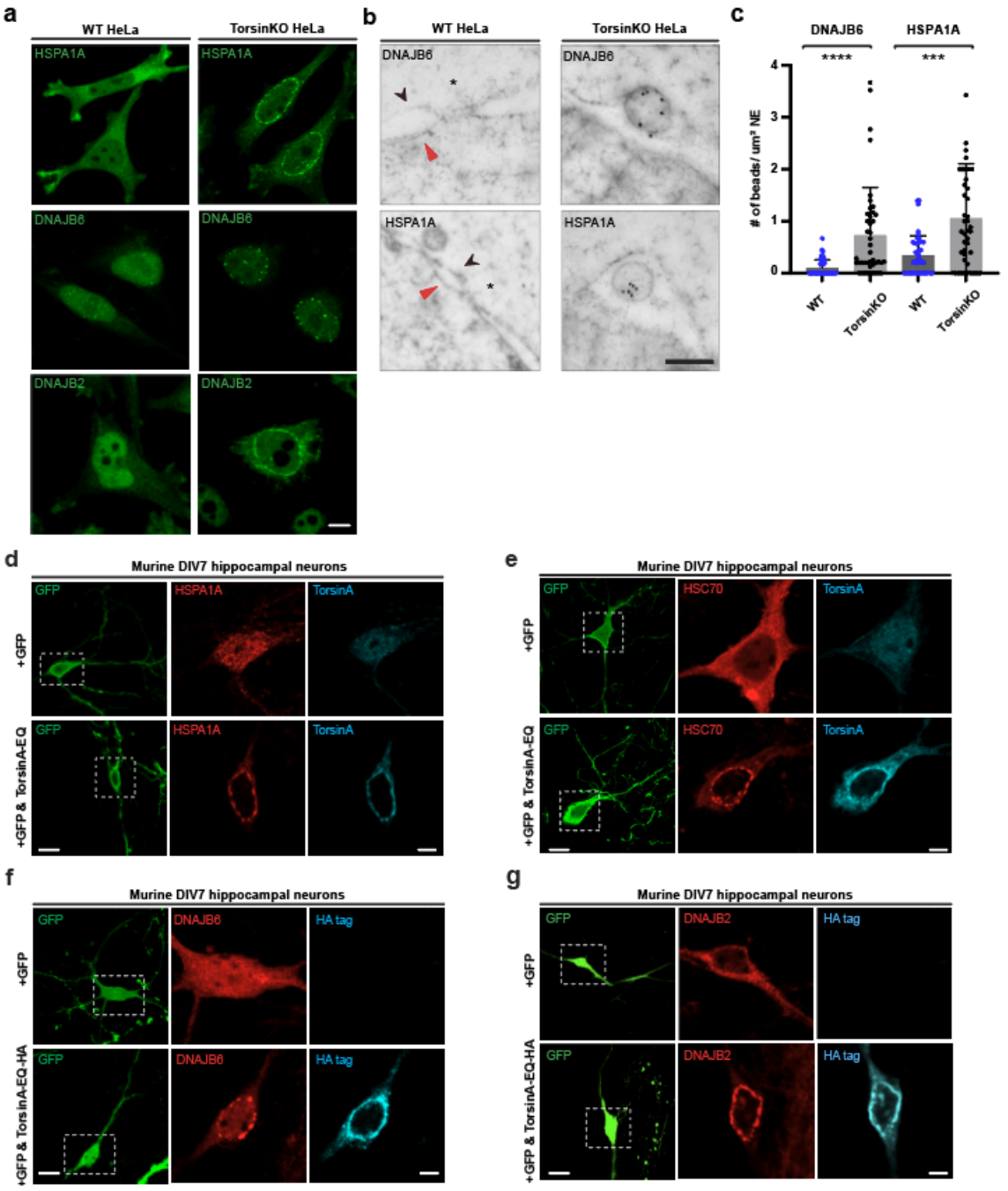

Figure 3. Highly abundant molecular chaperones are sequestered into NE blebs of tissue culture cells and primary mouse neurons with compromised TorsinA function. a, Antibodies against endogenous HSPA1A, DNAJB6, and DNAJB2 (green) reveal that chaperones from the HSP70 and HSP40 families become tightly sequestered into NE blebs upon Torsin deficiency. Scale bar, 5 μm. **b**, EM ultrastructure of the NE

from WT or TorsinKO cells labeled with immunogold beads conjugated to anti-DNAJB6 (top) or anti-HSPA1A (bottom). Black arrowhead, outer nuclear membrane. Red arrowhead, inner nuclear membrane. Asterisk, NPC. Scale bar, 250 nm. **c**, The number of DNAJB6 or HSPA1A immunogold beads per μm^2 centered around the NE (DNAJB6, WT n=50 micrographs, TorsinKO n=43 micrographs. HSPA1A, WT n=45 micrographs, TorsinKO n=43 micrographs. 400 μm^2 of NE was quantified/condition). Error bars, SD. Statistical analyses were performed using a two-tailed unpaired Mann-Whitney test where **** indicates $p < 0.0001$ and *** $p = 0.0002$. **d-g**, Murine DIV4 hippocampal neurons were transfected with GFP and empty vector (top row of all panels) or a dominant-negative TorsinA-EQ construct (bottom row of all panels). Constructs were allowed to express for 72 hours before processing the DIV7 cultures for IF. GFP expression was used to distinguish neurons from other cell types in the heterogeneous primary cell culture. Localization of the chaperones shown in panels (**d-g**) was probed using antibodies against the indicated endogenous chaperone (red). Untagged TorsinA-EQ was transfected in panels (**d**) and (**e**) and detected with a TorsinA antibody (cyan). TorsinA-EQ-HA was transfected in panels (**f**) and (**g**) and detected with an anti-HA antibody (cyan). Scale bar, 20 μm for unmagnified images, 5 μm for magnified images. Source numerical data are available in source data. Experiments in panel a-c were performed by SMP. Experiments in panels d-g were performed by RFN, JSG, and SMP.

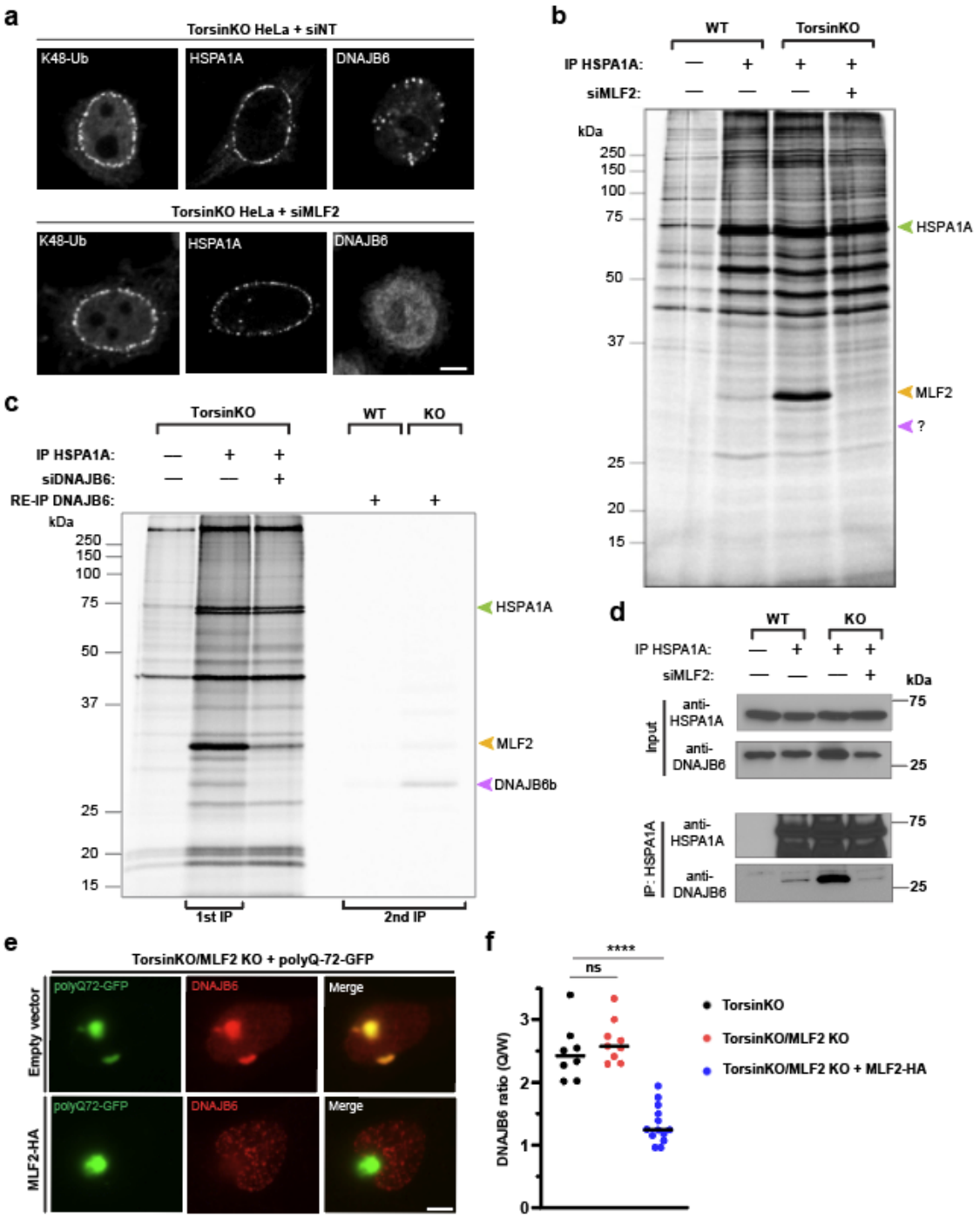

Figure 4. MLF2 is required for DNAJB6 to localize to NE blebs in Torsin-deficient cells. a, Representative IF images of chaperone localization upon knocking down MLF2 for 48 hours. Scale bar, 5 μm. **b**, WT and TorsinKO cells were metabolically labeled overnight with 150 μCi/mL ^{35}S-Cys/Met and treated with a nontargeting or MLF2-

targetting siRNA for 48 hours. HSPA1A was immunoprecipitated and stably associated proteins were detected by autoradiography. Green arrowhead, HSPA1A. Yellow arrowhead, MLF2. Purple arrowhead, unknown protein. **c**, Lanes 1-3, metabolically labeled TorsinKO cells were treated with a nontargeting or siRNA targeting DNAJB6 for 48 hours. HSPA1A was immunoprecipitated and co-eluting proteins were visualized by autoradiography. Lanes 4-5, metabolically labeled WT or TorsinKO cells under nontargeting siRNA were subjected to an HSPA1A IP, then disassociated and subjected to a second IP against DNAJB6 (RE-IP). **d**, HSPA1A was immunoprecipitated from TorsinKO and WT HeLa cells under siNT or siMLF2 conditions. **e**, A “tug of war” IF experiment showing that overexpression of MLF2-HA in TorsinKO/MLF2 KO cells titrates DNAJB6 out of polyQ72-GFP aggregates and into blebs. Representative IF images of TorsinKO/MLF2KO cells transfected with polyQ72-GFP alone (left column) or in combination with MLF2-HA (right column). Note that the HA channel is not shown. Scale bar, 5 μm. **f**, The ratio of DNAJB6 fluorescence signal inside polyQ72-GFP foci (Q) compared to whole cell (W) was calculated for at least eight cells/condition. Bars over datapoints indicate the mean ratio. Statistical analysis was performed using a two-tailed unpaired Mann-Whitney test where **** indicates $p < 0.0001$. ns, not significant. Source numerical data and unprocessed blots are available in source data. Experiments in panels a-d were performed by SMP. Experiments in panel e-f were performed by AJR.

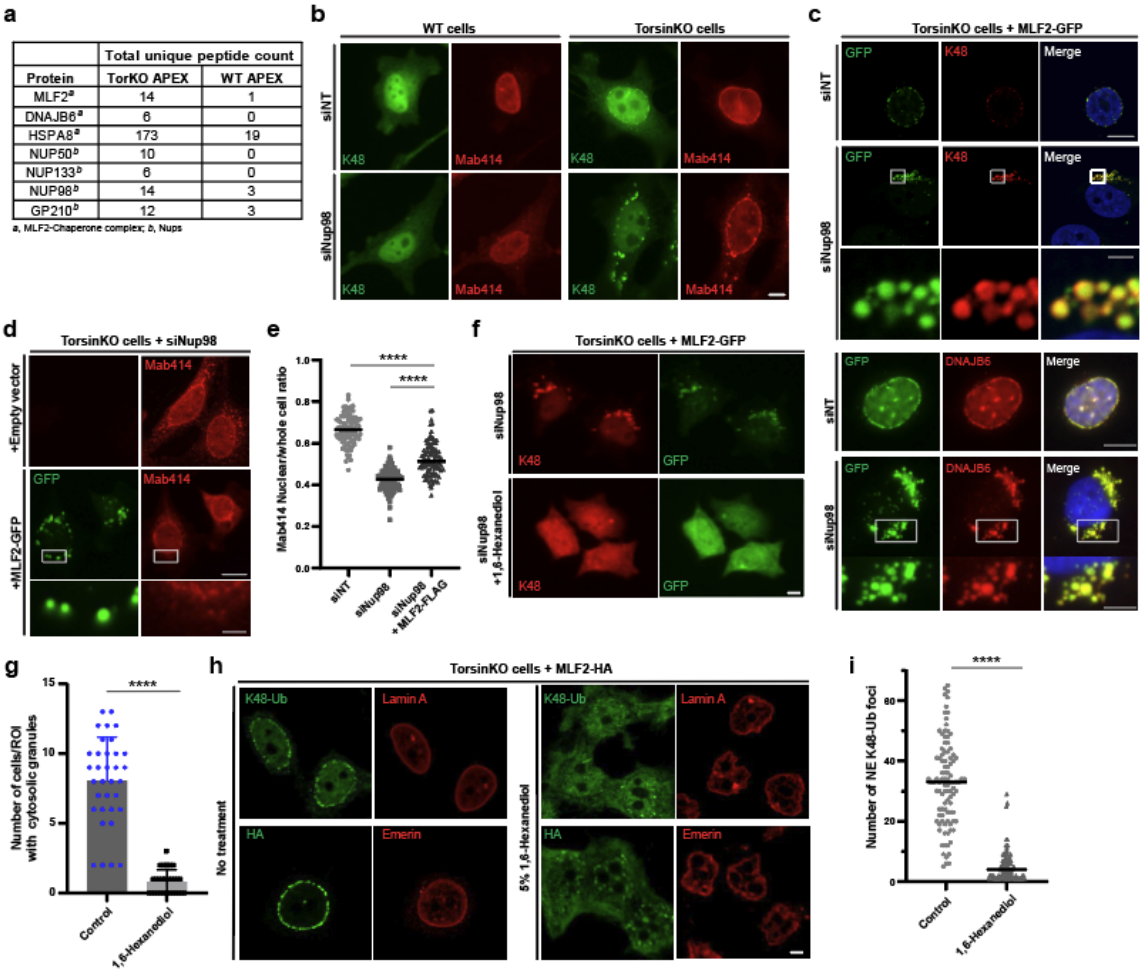

Figure 5. Nup98 is required for the sequestration into NE blebs harboring condensates composed of K48-Ub, FG-nucleoporins, MLF2, and chaperones. a, The APEX2 MS strategy described in (figure **2a**) reveals an enrichment of chaperones and nucleoporins interacting with MLF2 in TorsinKO cells. **b**, Representative IF images of WT and TorsinKO cells under siNup98 conditions. In TorsinKO cells, cytosolic granules enriched for K48-Ub and FG-Nups (Mab414, red) form upon siNup98. Note the normal NE accumulation of K48-Ub in TorsinKO cells is abolished under siNup98. Scale bar, 5 μm. **c**, Representative IF images of TorsinKO cells expressing MLF2-GFP under siNup98 conditions. MLF2-GFP (top panels) localizes to the cytosolic granules containing K48-Ub that arise upon Nup98 depletion in TorsinKO cells. DNAJB6 (bottom

panels) is also recruited to the cytosolic granules. 1x images scale bar, 10 μm. 8x magnification scale bar, 1.25 μm. **d**, Representative IF images of the effect on the FG-Nup accumulation in cytosolic granules upon overexpression of MLF2-GFP under siNup98 conditions. 1x images scale bar, 10 μm. 8x magnification scale bar, 1.25 μm. **e**, The ratio of nuclear to whole cell nucleoporin (Mab414) signal was determined for 94 cells/condition. Bars over datapoints indicate the mean ratio. Expressing MLF2-FLAG significantly decreases the amount of cytosolic FG-Nup mislocalization upon siNup98. **f**, Representative IF images of TorsinKO cells expressing MLF2-GFP under siNup98 conditions in the absence or presence of 5% 1,6-hexanediol for five minutes. Scale bar, 5 μm. **g**, The presence of cytosolic K48-Ub granules upon Nup98 depletion was assessed for 300 cells/condition (≥35 regions of interest (ROI) quantified/condition). Error bar, SD. **h**, Representative IF images of TorsinKO cells expressing MLF2-HA in the absence (left columns) or presence (right columns) of 5% 1,6-hexanediol for five minutes. The intact NE is indicated by lamin A (top panels) and emerin (bottom panels). Scale bar, 5 μm. **i**, The number of K48-Ub foci around the NE rim was determined for 100 cells/condition. Bars over datapoints indicate the mean number of K48-Ub foci. For all panels, statistical analyses were performed using a two-tailed unpaired Mann-Whitney test. **** indicates $p < 0.0001$. Source numerical data are available in source data. Experiments in panels a-g were performed by AJR. Experiments in panels h and i were performed by SMP.

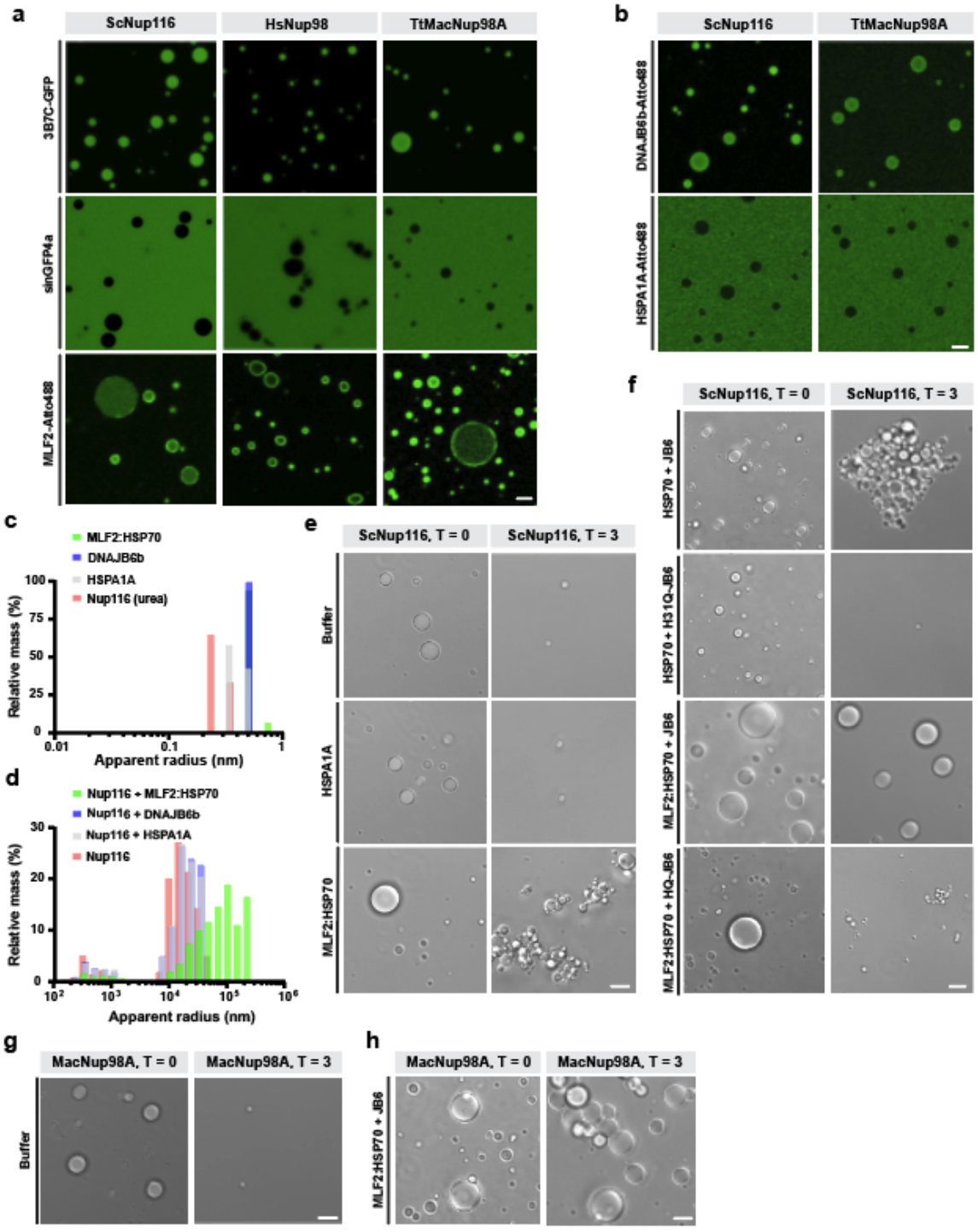

Figure 6. MLF2 interacts with FG-rich phases and preserves condensate integrity over time with HSP70 and DNAJB6. a, Atto488-tagged MLF2 interacts with phylogenetically diverse FG-Nups. Purified, label-free ScNup116, HsNup98, or

TtMacNup98A FG-domains were diluted from 500 μM stocks in 2 M urea to 10 μM in tris-buffered saline (TBS) to form condensates. Condensates were formed at room temperature in TBS containing 5 μM 3B7C-GFP, sinGFP4a, or MLF2-Atto488. **b**, HSPA1A-Atto488 is excluded from ScNup116 and TtMacNup98A condensates while DNAJB6b-Atto488 readily immerses into FG-rich phases. **c**, Solutions of 5 μM MLF2:HSP70, DNAJB6b, HSPA1A, or urea-denatured ScNup116 were analyzed by dynamic light scattering (DLS). Datasets of 100 reads with five-second acquisition times were collected for each condition. **d**, Solutions of 10 μM ScNup116 were formed in TBS with no additional protein (pink), 5 μM DNAJB6b (blue), 5 μM HSPA1A (grey), or 5 μM MLF2:HSP70 (green). Condensate size distributions were analyzed by DLS as described above. **e**, Phase contrast images of 10 μM ScNup116 condensates formed in the presence of 5 μM HSPA1A or 5 μM MLF2:HSP70. Images were taken immediately after condensates formation (T = 0) or after three hours of incubation at 30ºC (T = 3) in the presence of ATP. Note that the buffer condition is also shown in Extended Data Fig. 7a. **f**, Phase contrast images of 10 μM ScNup116 condensates formed in the presence of 5 μM HSPA1A or 5 μM of MLF2:HSP70 and 2.5 μM DNAJB6b constructs. Note the H31Q-DNAJB6b mutant cannot interact with HSP70. Images were taken at timepoints described in panel (**e**). **g**, Phase contrast images of 10 μM ThMacNup98A condensates immediately following formation or after three hours of incubation as described above. Note that the buffer condition is also shown in Extended Data Fig. 7b. **h**, Images of 10 μM ThMacNup98A condensates formed in the presence of 5 μM MLF2:HSP70 and 2.5 μM DNAJB6b at the zero timepoint or after three hours of incubation. Note that this condition is also shown in Extended Data Fig. 7c. Scale bar, 5 μm for all panels. Source numerical data are available in source data. All experiments were performed by SMP and SM.

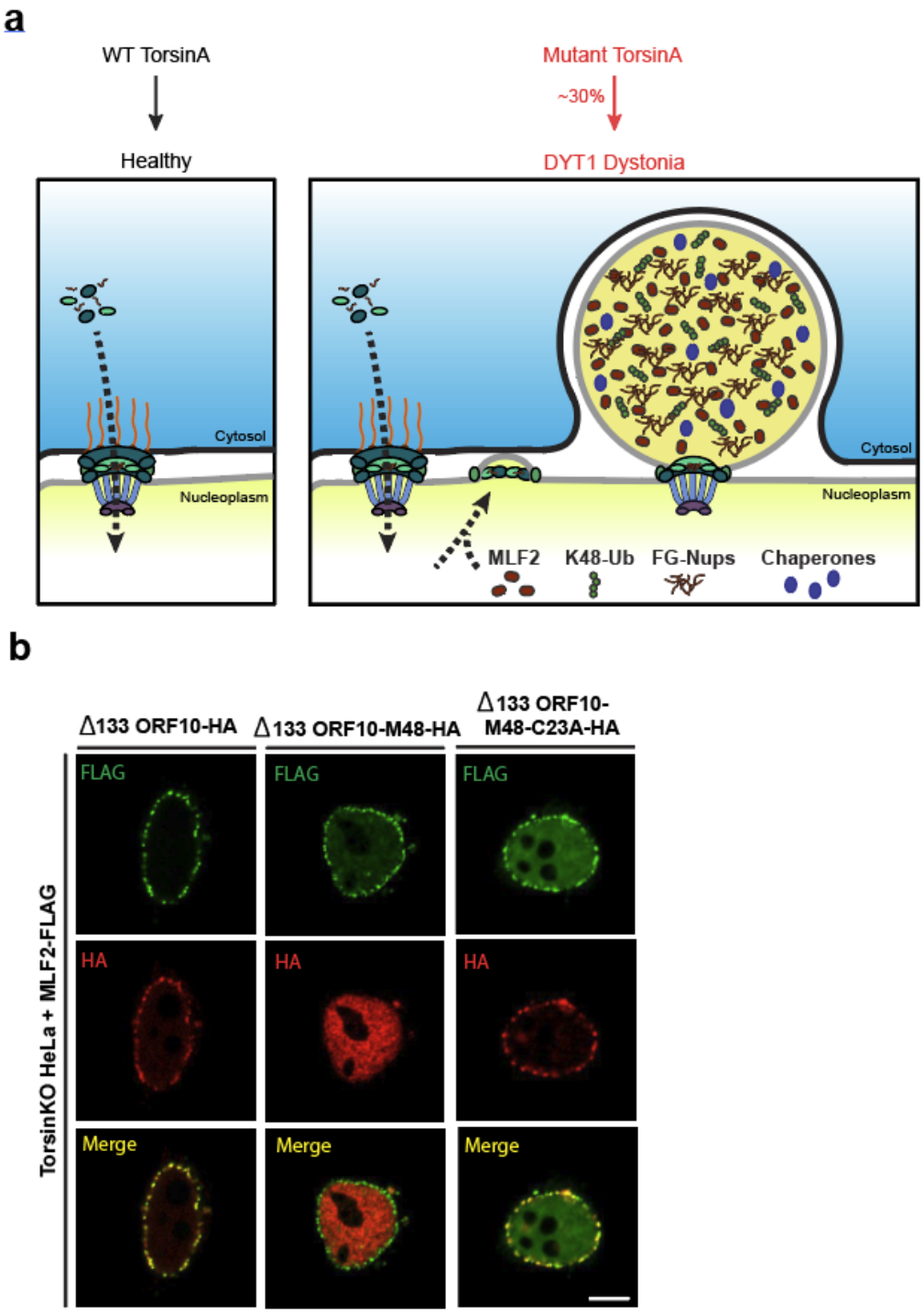

Extended data 1. NE blebs recruit Δ133 ORF10 in a ubiquitin-dependent manner. a, Schematic illustration of the NE blebs that form upon Torsin deficiency. In cells with mutant TorsinA, NPC biogenesis is compromised and a subset of nascent NPCs are arrested (ref. [22]). These arrested NPCs form blebs that are enriched for K48-linked

ubiquitin (K48-Ub), FG-nucleoporins (FG-Nups), myeloid leukemia factor 2 (MLF2), and a specific chaperone network. The inner nuclear membrane (INM) is depicted in gray, outer nuclear membrane in black. **b**, Representative IF images of TorsinKO cells expressing MLF2-FLAG and ∆133 ORF10-HA fusion constructs. ∆133 ORF10 was fused to the cytomegalovirus deubiquitinase (DUB) domain, M48 (ref. [75]). M48 is a highly active DUB domain that efficiently removes ubiquitin conjugates (ref. [22, 35]). A C23A mutation renders the DUB domain catalytically inactive (ref. [75]). Scale bar, 5 μm. Panel a was created by AJR. Experiments in panel b were performed by SMP.

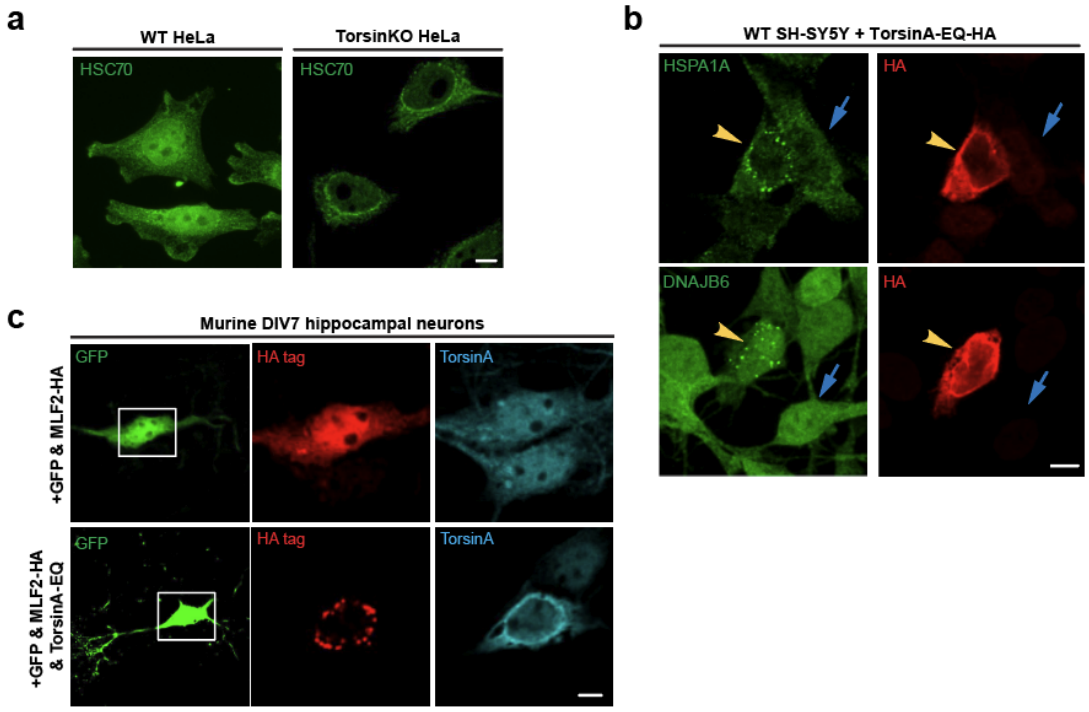

Extended data 2. Additional abundant molecular chaperones are sequestered into NE blebs of tissue culture cells and primary mouse neurons. a, Representative image of endogenous HSC70 in WT and TorsinKO HeLa cells. Note that HSC70 re-localizes from diffusely throughout the cell to nuclear rim foci in TorsinKO cells. **b**, SH-SY5Y cells expressing a dominant-negative TorsinA construct, TorsinA-EQ-HA, sequester HSPA1A and DNAJB6 into NE blebs. Yellow arrowhead, transfected cell. Blue arrow, untransfected cell. Endogenous chaperones (green) form foci around the nuclear rim upon TorsinA-EQ-HA (red) expression. **c**, Murine DIV4 hippocampal neurons were transfected with GFP and either MLF2-HA alone or in combination with a dominant-negative TorsinA-EQ construct. Constructs were allowed to express for 72 hours before processing the DIV7 cultures for IF. Note that GFP expression was used to distinguish neurons from other cell types in the heterogeneous primary cell culture. Scale bar, 5 μm. Experiments in panels a and b were performed by SMP. Experiments in panel c were performed by RFN and SMP.

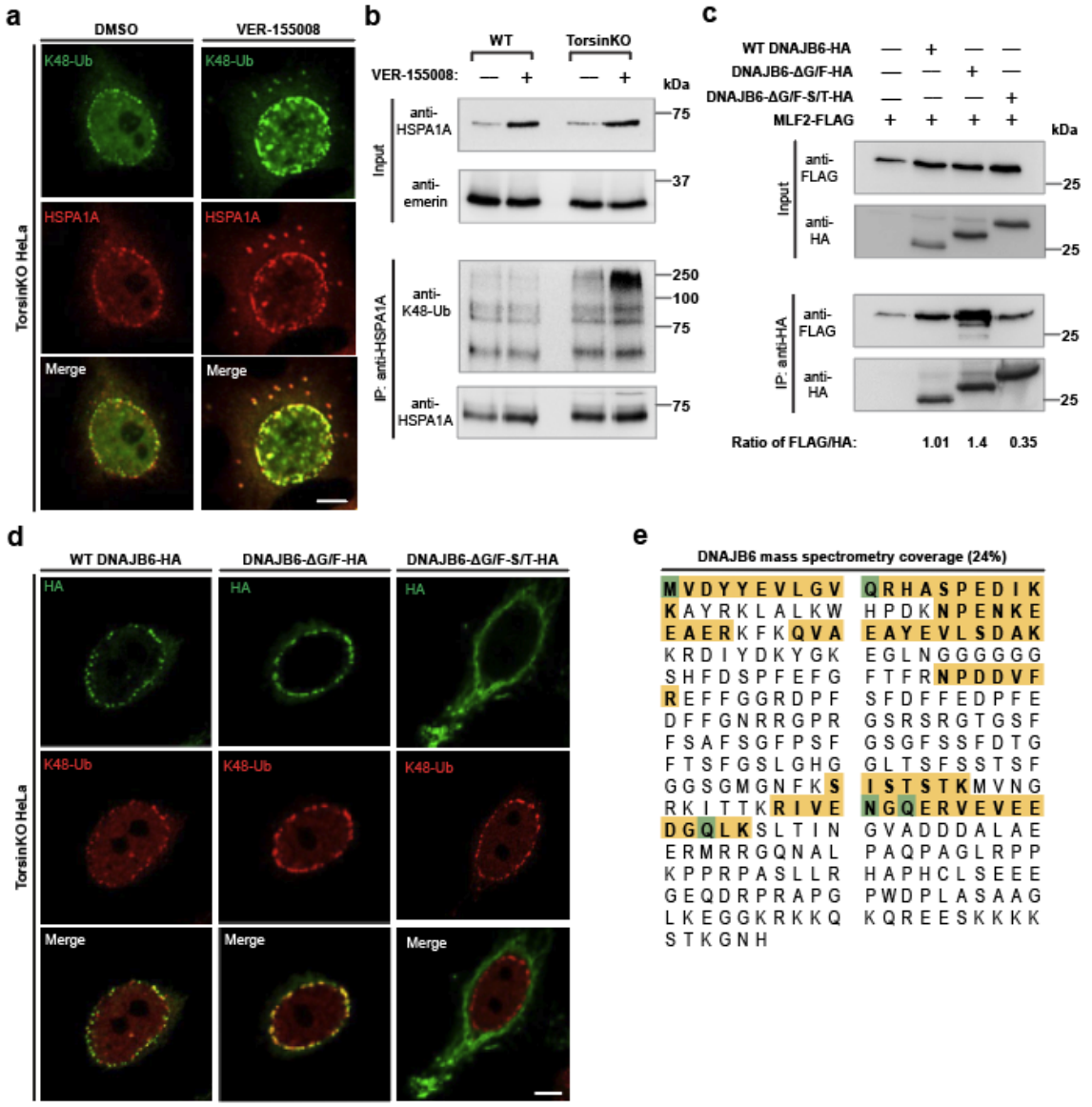

Extended data 3. Chaperones are recruited to blebs by different mechanisms. a, Representative IF images of TorsinKO cells treated with DMSO or VER-155008 for 24 hours. VER-155008 is a small molecule inhibitor of HSP70 ATPase activity, which targets the HSP70 ATP binding pocket and approximates an ADP-bound state (ref. [40]). This compound causes elevated HSPA1A expression and more K48-Ub to accumulate in blebs. Scale bar, 5 μm. **b**, An IP of HSPA1A from biochemically enriched ER/NE fractions from WT or TorsinKO cells treated with DMSO or VER-155008. **c**, A co-IP of MLF2-FLAG with HA-tagged DNAJB6 constructs lacking functional G/F-rich or S/T-rich

regions in TorsinKO cells. ΔG/F indicates all phenylalanine residues have been mutated to alanine within the G/F-rich region, and ΔG/F-S/T indicates the mutation of the phenylalanine residues within the G/F- and S/T-rich regions. Note that DNAJB6-ΔG/F-S/T-HA retrieves significantly less MLF2-FLAG, suggesting that the S/T-rich region strongly promotes its interaction with MLF2 and recruitment to blebs. **d**, Representative IF images of the DNAJB6 constructs described in panel (**c**) in TorsinKO cells. Note that interfering with the S/T-rich region, but not the G/F-rich region, prevents DNAJB6 from reaching the bleb. Scale bar, 5 μm. **e**, DNAJB6 peptides identified by mass spectrometry from an IP of HSPA1A from TorsinKO cells (see figure 4b-d). Peptides identified by mass spectrometry are highlighted in yellow and post-translationally modified residues are rendered in green. While an IP of HSPA1A from TorsinKO cells identified DNAJB6 with 24% coverage, no DNAJB6 peptides were identified in the HSPA1A IP from WT HeLa cells. See Supplemental Table 3 for complete dataset. Unprocessed blots are available in source data. All experiments were performed by SMP.

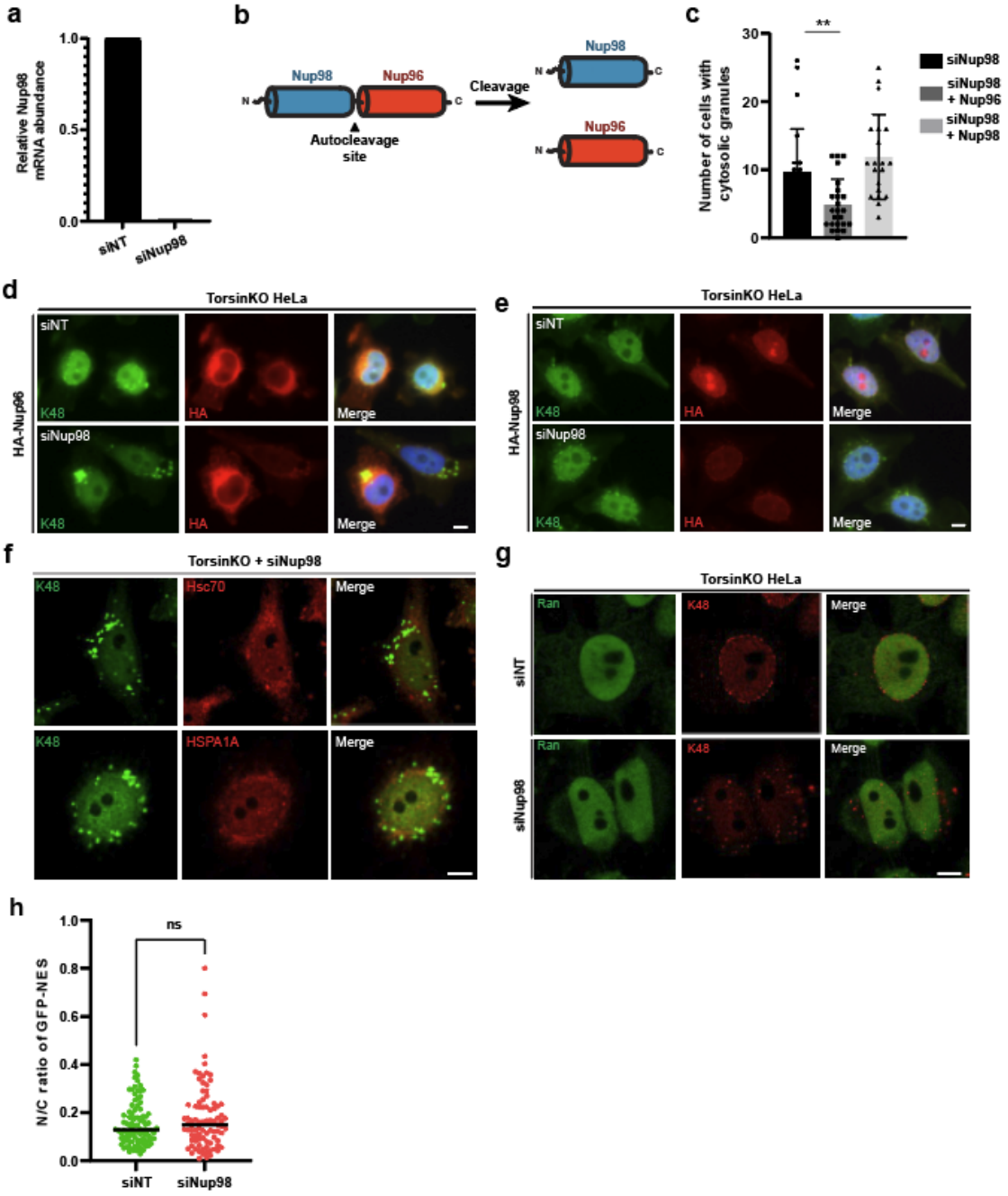

Extended data 4. Validation of Nup98 knockdown and effect on nuclear transport.

a, qPCR validation of Nup98 depletion upon 48 hours of 50 nM siRNA treatment. Relative Nup98 transcript levels are normalized to RPL32. **b**, Nup98 and Nup96 are translated as a single precursor protein that undergoes an autocleavage event to produce the two individual proteins (ref. [45]). Thus, RNAi knockdown of Nup98 results

in the simultaneous depletion of Nup96. **c-e**, To distinguish which protein knockdown produces the cytosolic granules in TorsinKO cells, HA-tagged Nup98 or Nup96 was assessed for the ability to rescue the phenotype under knockdown conditions. **c**, Quantification of the rescue affect when HA-Nup96 or HA-Nup98 are expressed. The presence of cytosolic inclusions was assessed for 300 cells/condition in ≥20 ROIs. Error bar, SD. Statistical analysis was performed using a two-tailed unpaired Mann-Whitney test. ** indicates $p = 0.0013$. **d**, Representative IF images of TorsinKO cells expressing HA-Nup96 or HA-Nup98 (**e**) under nontargeting or siNup98-96 conditions. Results are quantified in panel (**c**). **f**, Representative IF images of endogenous Hsc70 and HSPA1A in TorsinKO cells upon Nup98 depletion. Note that these HSP70 members are not recruited to the cytosolic granules. **g**, Representative IF images of the Ran GTPase in TorsinKO cells under 48 hours of siNT or siNup98 conditions. **h**, The nuclear to cytoplasmic ratio was calculated for GFP-NES in TorsinKO cells under siNT (n = 94) or siNup98 (n = 87) conditions. The ratio was calculated using CellProfiler software (ref. [73]). Statistical analysis was performed using a two-tailed unpaired Mann-Whitney test. Ns, not significant. Scale bar, 5 μm for all panels. Source numerical data are available in source data. Experiments in panels a-e were performed by AJR. Experiments in panel f-h were performed by SMP.

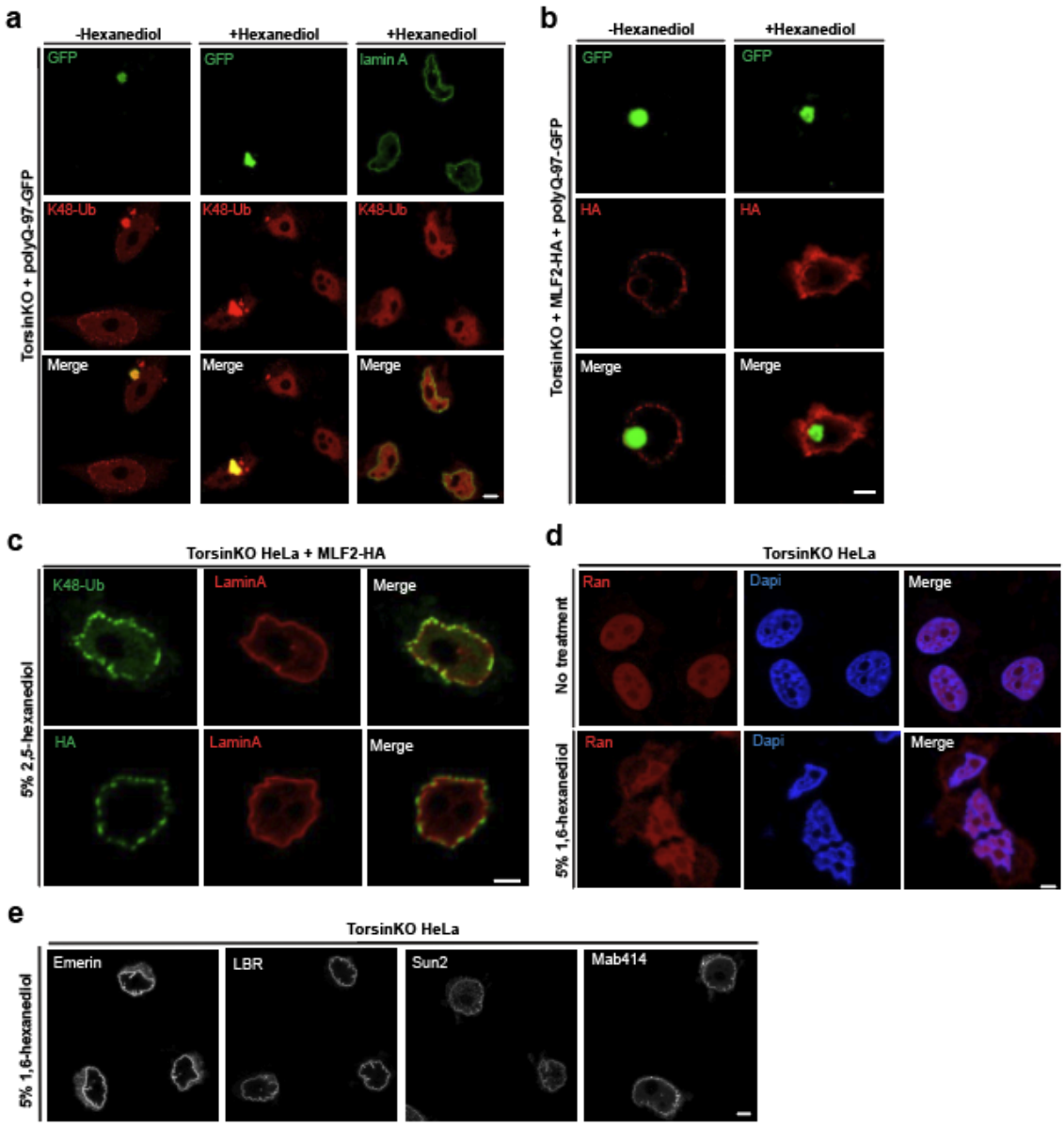

Extended data 5. The effects of 5% 1,6-hexanediol on NE integrity and bleb sensitivity to 2,5-hexanediol. **a**, Representative IF images of TorsinKO cells expressing polyQ-97-GFP under normal IF conditions or exposed to 5% 1,6-hexanediol for five minutes prior to fixation. Note that the K48-Ub inside polyQ aggregates is not dissolved by 1,6-hexanediol but the K48-Ub inside blebs is sensitive to this alcohol. Lamin A staining demonstrates this 5% 1,6-hexanediol treatment does not break down NE membranes (see also panel (**e**)). **b**, Representative IF images of TorsinKO cells

expressing polyQ-97-GFP and MLF2-HA treated with 5% 1,6-hexanediol for five minutes. A five-minute treatment with 5% 1,6-hexanediol does not dissolve polyQ aggregates but can selectively dissolve the contents of blebs. **c**, Treatment with the related alcohol 5% w/v 2,5-hexanediol for five minutes does not dissolve the K48-Ub or MLF2-HA sequestered inside blebs. **d**, Representative IF images of Ran in TorsinKO cells under normal IF conditions or after treatment with 5% 1,6-hexanediol for five minutes. Although the NE membranes are not disassembled by a 5% 1,6-hexanediol, the permeability barrier established by NPCs is lost. 1,6-hexanediol is known to disrupt the hydrophobic contacts required for the cohesion of FG-Nups within the central channel of the NPC (ref. [51]). **e**, Representative IF images of TorsinKO cells treated with 5% w/v 1,6-hexanediol for five minutes prior to fixation. This treatment does not compromise the integrity of the NE as determined by staining for multiple inner nuclear membrane proteins. Scale bar, 5 μm for all panels. All experiments were performed by SMP.

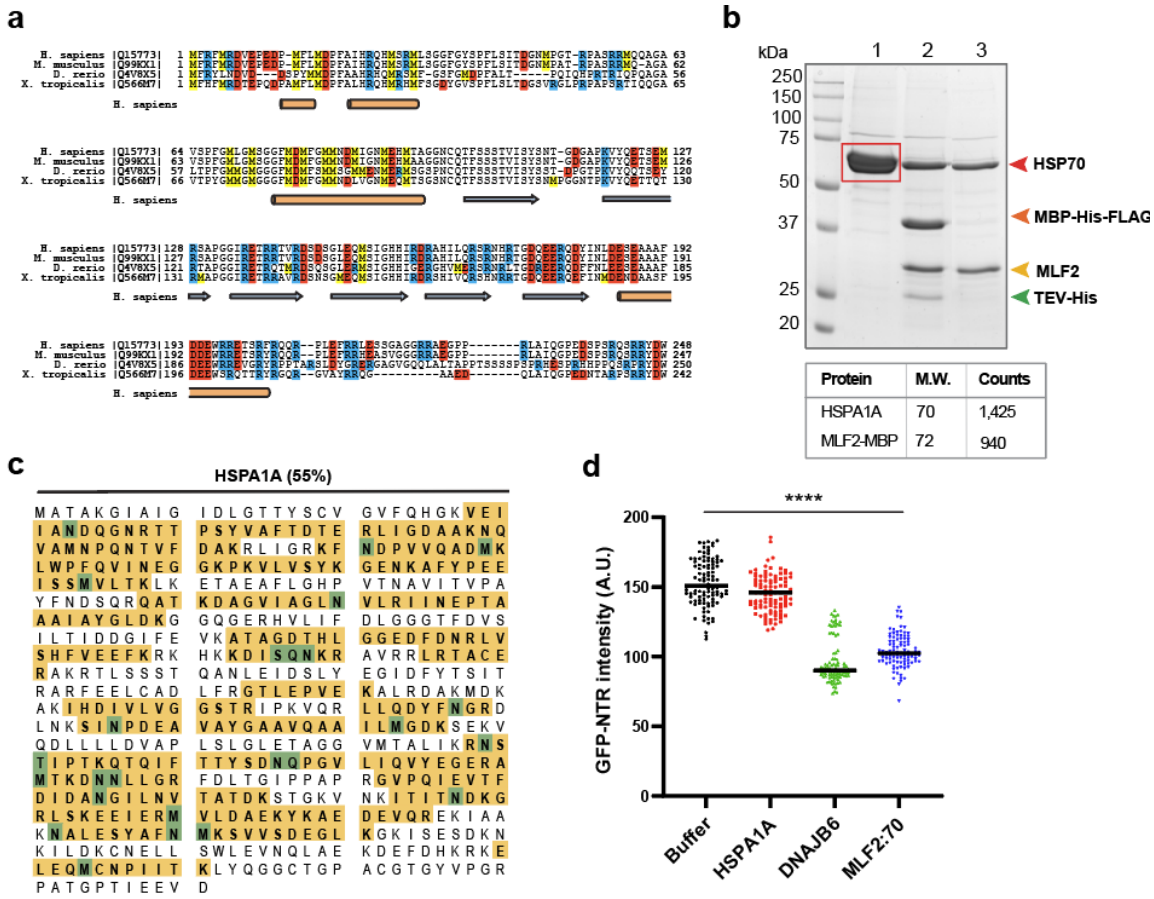

Extended data 6. MLF2 is a methionine/arginine rich protein and associates with HSPA1A. a, Multiple sequence alignment of MLF2 homologs from *Xenopus tropicalis*, *Danio rerio*, *Mus musculus*, and *Homo sapiens*. MLF2 is a methionine- and arginine-rich protein with a high degree of conservation. Methionine residues are highlighted in yellow boxes, arginine in blue, and positively charged residues in red. Orange cylinders indicate alpha helices predicted by AlphaFold [76] and blue arrows represent predicted beta sheets. **b**, MLF2 purified from Expi293F cells associates with HSPA1A. MLF2 was expressed as a maltose binding protein (MBP) fusion and affinity purified by virtue of FLAG- and His-tags. Lane 1, anti-FLAG resin elution composed of MLF2-Tev-MBP-His-FLAG and associating protein. Red box, gel section analyzed by mass spectrometry. Lane 2, incubation with Tev-His cleaved MBP-His from MLF2. Lane 3, Ni-NTA flowthrough in which MBP-His and Tev-His are removed. Mass spectrometry of the gel

segment indicated in lane 1 confirmed the identity of the associating protein as HSPA1A. **c**, Mass spectrometry analysis of the co-purifying protein from panel (**b**) revealed 55% coverage of HSPA1A. Identified peptides mapping to HSPA1A are in yellow, post-translationally modified residues in green. See Supplemental Table 4 for complete dataset. **d**, 10 μM TtMacNup98A condensates were formed in the presence of 5 μM 3B7C-GFP plus 10 μM HSPA1A, DNAJB6Bb, or MLF2:HSP70. 3B7C-GFP signal intensity was measured in the center of 100 condensates/condition. Bars over datapoints indicate the mean intensity value. Statistical analysis was performed using a two-tailed unpaired Mann-Whitney test comparing buffer or HSPA1A conditions to DNAJB6b or MLF2:HSP70. **** indicates $p < 0.0001$. Source numerical data and unprocessed blots are available in source data. Panel a was prepared by AJR. Experiments in panels b-d were performed by SMP.

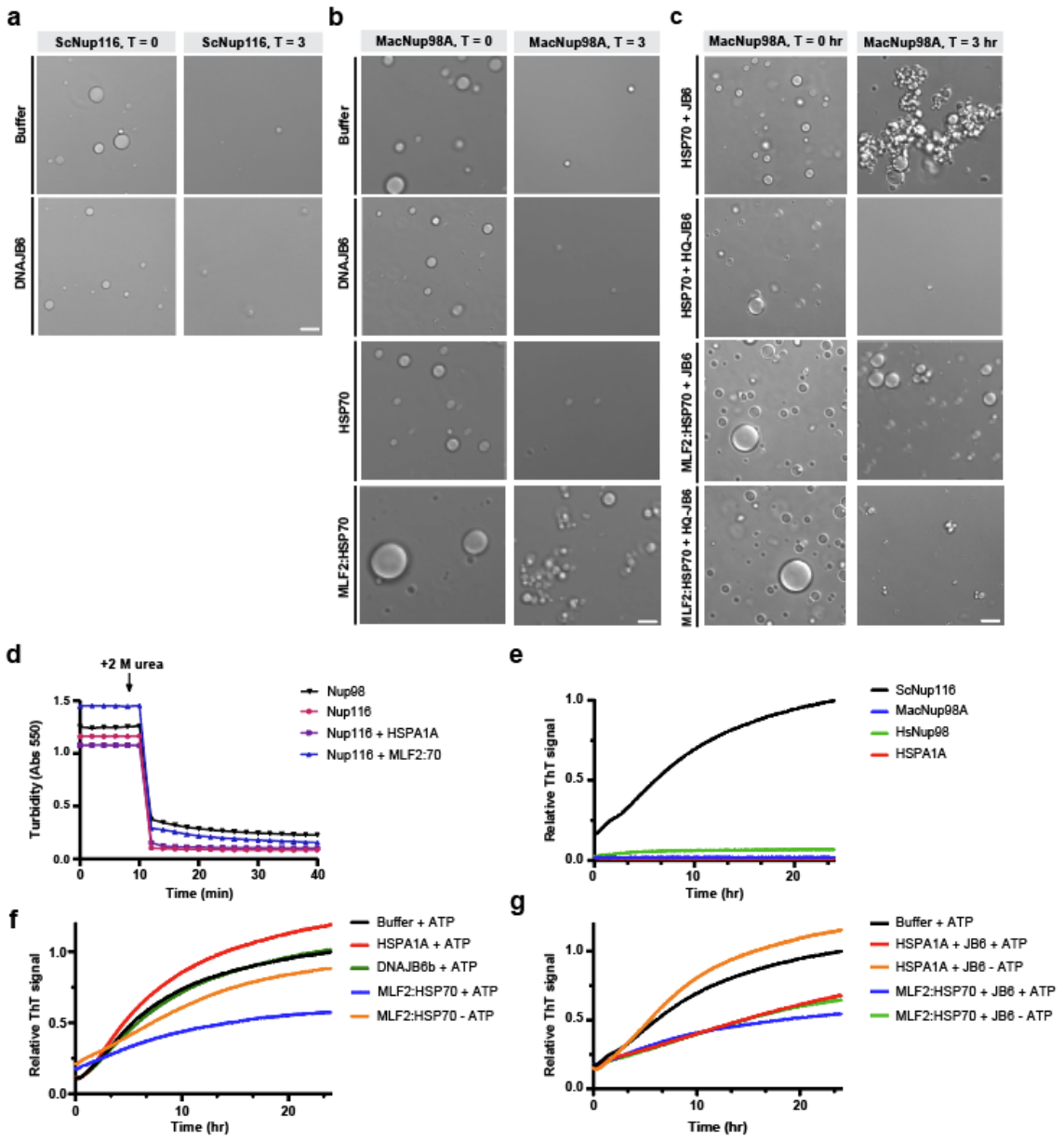

Extended data 7. MLF2 in complex with HSP70 and DNAJB6 preserves FG-rich condensate integrity over time. a, Phase contrast images of 10 μM ScNup116 condensates formed in the presence of 2.5 μM DNAJB6b. Images were taken immediately after condensate formation (T = 0) or after three hours of incubation at 30ºC (T = 3) in the presence of ATP. Note the buffer condition is also shown in Fig. 6e. **b**, Phase contrast images of 10 μM TtMacNup98A condensates formed in the presence of 2.5 μM DNAJB6b, 5 μM HSPA1A, or 5 μM MLF2:HSP70. Images were taken at the

timepoints described in panel (**a**). **c**, Images of 10 μM TtMacNup98A condensates formed in the presence of 5 μM HSPA1A plus 2.5 μM of the indicated DNAJB6b construct or 5 μM of the MLF2:HSP70 complex with 2.5 μM H31Q-DNAJB6b. Images were taken at the timepoints described in panel (**a**). Note the buffer condition is also shown in Fig. 6g. **d**, The turbidity of 10 μM ScNup116 or HsNup98 solutions in the absence or presence of 5 μM HSPA1A or the MLF2:HSP70 complex. Upon addition of 2 M urea, the condensates fully reverse and the solution loses turbidity as assessed by monitoring absorbance at 550 nm. **e**, 10 μM of ScNup116, TtMacNup98A, HsNup98, or 5 μM HSPA1A was incubated with 5 μM Thioflavin T (ThT) for 24 hours at 30ºC. ThT fluorescence (excitation 440 nm, emission 480 nm) was monitored to detect amyloid formation. All reactions contained 2 mM ATP and an ATP regenerating system. ThT signals for all conditions were normalized to the ScNup116 maximum value. **f**, 10 μM of ScNup116 was monitored for amyloid formation as described above in buffer containing 5 μM HSPA1A, 2.5 μM DNAJB6b, or 5 μM of the MLF2:HSP70 complex. Where indicated, 2 mM ATP was included or omitted. **g**, ScNup116 amyloid formation was observed under conditions with 5 μM HSP70 or the MLF2:HSP70 complex plus 2.5 μM DNAJB6b. Where indicated, 2 mM ATP was included or omitted. ThT conditions were as described for panel (**e**). Scale bar 5 μM for all panels. Source numerical data are available in source data. All experiments were performed by SMP and SM.

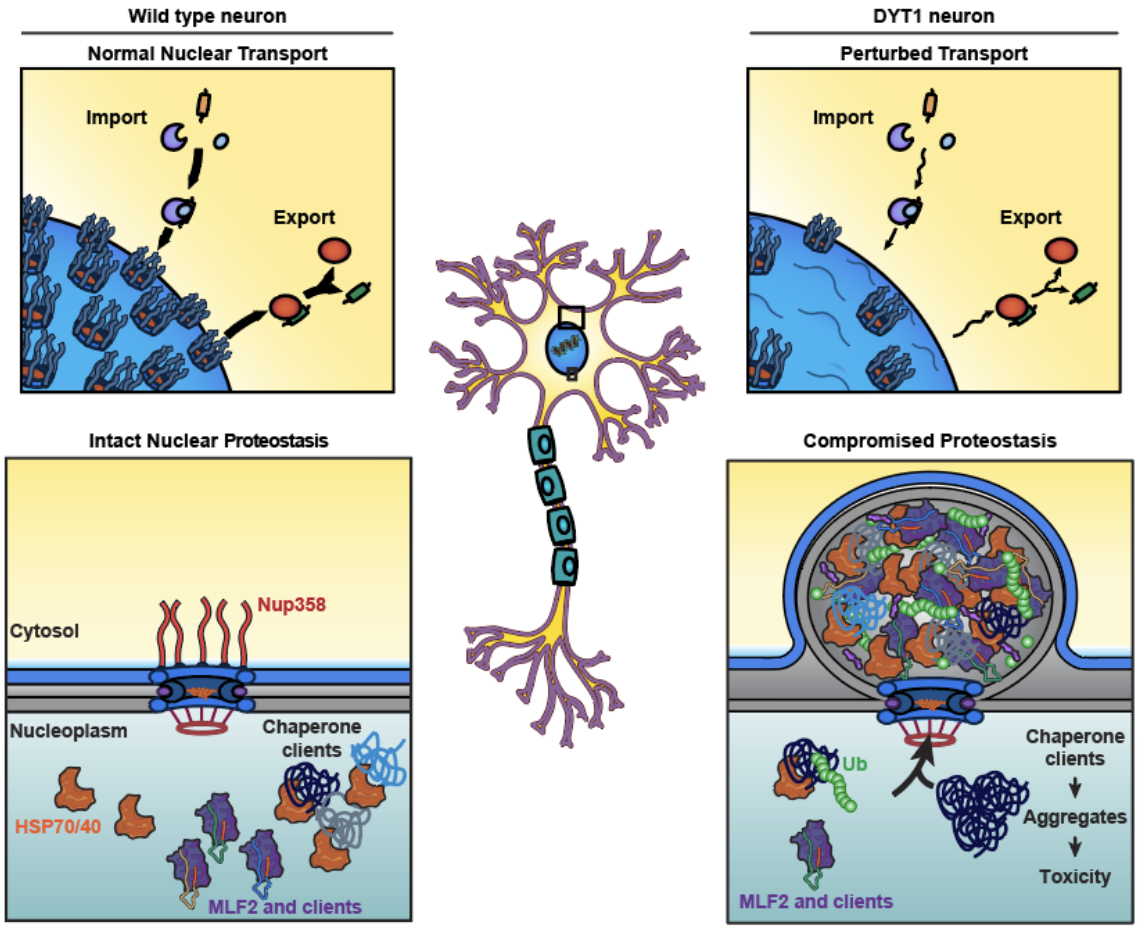

Extended data 8. A dual proteotoxicity mechanism contributes to DYT1 Dystonia onset. Schematic model for how proteotoxicity may accumulate in Torsin-deficient cells. In wild type neurons, NPC biogenesis is unperturbed and chaperones are free to interact with clients. In DYT1 dystonia neurons, nuclear transport is perturbed due to defective NPC biogenesis. As FG-Nup containing blebs form instead of mature NPCs, they sequester proteins normally destined for degradation, chaperones, and MLF2. When essential chaperones are sequestered away from clients in Torsin-deficient cells, proteotoxic species may be allowed to form and persist to a greater extent than in cells with normal chaperone availability, sensitizing cellular proteostasis towards additional insults. This figure was created by AJR.

References

1. Khan, Y.A., K.I. White, and A.T. Brunger, *The AAA+ superfamily: a review of the structural and mechanistic principles of these molecular machines.* Crit Rev Biochem Mol Biol, 2021: p. 1-32.

2. Rose, A.E., R.S. Brown, and C. Schlieker, *Torsins: not your typical AAA+ ATPases.* Crit Rev Biochem Mol Biol, 2015. **50**(6): p. 532-49.

3. Goodchild, R.E., C.E. Kim, and W.T. Dauer, *Loss of the dystonia-associated protein torsinA selectively disrupts the neuronal nuclear envelope.* Neuron, 2005. **48**(6): p. 923-32.

4. Zhao, C., et al., *Regulation of Torsin ATPases by LAP1 and LULL1.* Proc Natl Acad Sci U S A, 2013. **110**(17): p. E1545-54.

5. Demircioglu, F.E., et al., *Structures of TorsinA and its disease-mutant complexed with an activator reveal the molecular basis for primary dystonia.* Elife, 2016. **5**.

6. Brown, R.S., et al., *The mechanism of Torsin ATPase activation.* Proc Natl Acad Sci U S A, 2014. **111**(45): p. E4822-31.

7. Ozelius, L.J., et al., *The early-onset torsion dystonia gene (DYT1) encodes an ATP-binding protein.* Nat Genet, 1997. **17**(1): p. 40-8.

8. Fichtman, B., et al., *Combined loss of LAP1B and LAP1C results in an early onset multisystemic nuclear envelopathy.* Nat Commun, 2019. **10**(1): p. 605.

9. Rampello, A.J., S.M. Prophet, and C. Schlieker, *The Role of Torsin AAA+ Proteins in Preserving Nuclear Envelope Integrity and Safeguarding Against Disease.* Biomolecules, 2020. **10**(3).

10. Shin, J.Y. and H.J. Worman, *Molecular Pathology of Laminopathies.* Annu Rev Pathol, 2021.

11. Gonzalez-Alegre, P., *Advances in molecular and cell biology of dystonia: Focus on torsinA.* Neurobiol Dis, 2019. **127**: p. 233-241.

12. VanGompel, M.J., et al., *A novel function for the Caenorhabditis elegans torsin OOC-5 in nucleoporin localization and nuclear import.* Mol Biol Cell, 2015. **26**(9): p. 1752-63.

13. Jokhi, V., et al., *Torsin mediates primary envelopment of large ribonucleoprotein granules at the nuclear envelope.* Cell Rep, 2013. **3**(4): p. 988-95.

14. Kim, C.E., et al., *A molecular mechanism underlying the neural-specific defect in torsinA mutant mice.* Proc Natl Acad Sci U S A, 2010. **107**(21): p. 9861-6.

15. Liang, C.C., et al., *TorsinA hypofunction causes abnormal twisting movements and sensorimotor circuit neurodegeneration.* J Clin Invest, 2014. **124**(7): p. 3080-92.

16. Tanabe, L.M., C.C. Liang, and W.T. Dauer, *Neuronal Nuclear Membrane Budding Occurs during a Developmental Window Modulated by Torsin Paralogs.* Cell Rep, 2016. **16**(12): p. 3322-3333.

17. Naismith, T.V., et al., *TorsinA in the nuclear envelope.* Proc Natl Acad Sci U S A, 2004. **101**(20): p. 7612-7.

18. Laudermilch, E., et al., *Dissecting Torsin/cofactor function at the nuclear envelope: a genetic study.* Mol Biol Cell, 2016. **27**(25): p. 3964-3971.

19. Jacquemyn, J., et al., *Torsin and NEP1R1-CTDNEP1 phosphatase affect interphase nuclear pore complex insertion by lipid-dependent and lipid-independent mechanisms.* EMBO J, 2021. **40**(17): p. e106914.

20. Pappas, S.S., et al., *TorsinA dysfunction causes persistent neuronal nuclear pore defects.* Hum Mol Genet, 2018. **27**(3): p. 407-420.

21. Ding, B., et al., *Disease Modeling with Human Neurons Reveals LMNB1 Dysregulation Underlying DYT1 Dystonia.* J Neurosci, 2021. **41**(9): p. 2024-2038.

22. Rampello, A.J., et al., *Torsin ATPase deficiency leads to defects in nuclear pore biogenesis and sequestration of MLF2.* The Journal of Cell Biology, 2020. **219**(6).

23. Wente, S.R. and G. Blobel, *A temperature-sensitive NUP116 null mutant forms a nuclear envelope seal over the yeast nuclear pore complex thereby blocking nucleocytoplasmic traffic.* J Cell Biol, 1993. **123**(2): p. 275-84.

24. Zhang, W., et al., *Brr6 and Brl1 locate to nuclear pore complex assembly sites to promote their biogenesis.* J Cell Biol, 2018. **217**(3): p. 877-894.

25. Ribbeck, K. and D. Gorlich, *Kinetic analysis of translocation through nuclear pore complexes.* EMBO J, 2001. **20**(6): p. 1320-30.

26. Frey, S. and D. Gorlich, *A saturated FG-repeat hydrogel can reproduce the permeability properties of nuclear pore complexes.* Cell, 2007. **130**(3): p. 512-23.

27. Hulsmann, B.B., A.A. Labokha, and D. Gorlich, *The permeability of reconstituted nuclear pores provides direct evidence for the selective phase model.* Cell, 2012. **150**(4): p. 738-51.

28. Schmidt, H.B. and D. Gorlich, *Transport Selectivity of Nuclear Pores, Phase Separation, and Membraneless Organelles.* Trends Biochem Sci, 2016. **41**(1): p. 46-61.

29. Bonner, W.M., *Protein migration into nuclei. I. Frog oocyte nuclei in vivo accumulate microinjected histones, allow entry to small proteins, and exclude large proteins.* J Cell Biol, 1975. **64**(2): p. 421-30.

30. Gorlich, D. and U. Kutay, *Transport between the cell nucleus and the cytoplasm.* Annu Rev Cell Dev Biol, 1999. **15**: p. 607-60.

31. Labbadia, J. and R.I. Morimoto, *The biology of proteostasis in aging and disease.* Annu Rev Biochem, 2015. **84**: p. 435-64.

32. Sweeney, P., et al., *Protein misfolding in neurodegenerative diseases: implications and strategies.* Transl Neurodegener, 2017. **6**: p. 6.

33. Le Guerroue, F. and R.J. Youle, *Ubiquitin signaling in neurodegenerative diseases: an autophagy and proteasome perspective.* Cell Death Differ, 2021. **28**(2): p. 439-454.

34. Gong, D., et al., *A Herpesvirus Protein Selectively Inhibits Cellular mRNA Nuclear Export.* Cell Host Microbe, 2016. **20**(5): p. 642-653.

35. Schlieker, C., et al., *Structure of a herpesvirus-encoded cysteine protease reveals a unique class of deubiquitinating enzymes.* Mol Cell, 2007. **25**(5): p. 677-87.

36. Lam, S.S., et al., *Directed evolution of APEX2 for electron microscopy and proximity labeling.* Nat Methods, 2015. **12**(1): p. 51-4.

37. Hung, V., et al., *Spatially resolved proteomic mapping in living cells with the engineered peroxidase APEX2.* Nat Protoc, 2016. **11**(3): p. 456-75.

38. Rosenzweig, R., et al., *The Hsp70 chaperone network.* Nat Rev Mol Cell Biol, 2019. **20**(11): p. 665-680.

39. Dekker, S.L., H.H. Kampinga, and S. Bergink, *DNAJs: more than substrate delivery to HSPA.* Front Mol Biosci, 2015. **2**: p. 35.

40. Li, X., et al., *Targeting Allosteric Control Mechanisms in Heat Shock Protein 70 (Hsp70).* Curr Top Med Chem, 2016. **16**(25): p. 2729-40.

41. Thiruvalluvan, A., et al., *DNAJB6, a Key Factor in Neuronal Sensitivity to Amyloidogenesis.* Mol Cell, 2020. **78**(2): p. 346-358 e9.

42. Kakkar, V., et al., *Versatile members of the DNAJ family show Hsp70 dependent anti-aggregation activity on RING1 mutant parkin C289G.* Sci Rep, 2016. **6**: p. 34830.

43. Hageman, J., et al., *A DNAJB chaperone subfamily with HDAC-dependent activities suppresses toxic protein aggregation.* Mol Cell, 2010. **37**(3): p. 355-69.

44. Lin, D.H. and A. Hoelz, *The Structure of the Nuclear Pore Complex (An Update).* Annu Rev Biochem, 2019. **88**: p. 725-783.

45. Fontoura, B.M., G. Blobel, and M.J. Matunis, *A conserved biogenesis pathway for nucleoporins: proteolytic processing of a 186-kilodalton precursor generates Nup98 and the novel nucleoporin, Nup96.* J Cell Biol, 1999. **144**(6): p. 1097-112.

46. Ribbeck, K. and D. Gorlich, *The permeability barrier of nuclear pore complexes appears to operate via hydrophobic exclusion.* EMBO J, 2002. **21**(11): p. 2664-71.

47. Shulga, N. and D.S. Goldfarb, *Binding dynamics of structural nucleoporins govern nuclear pore complex permeability and may mediate channel gating.* Mol Cell Biol, 2003. **23**(2): p. 534-42.

48. Onischenko, E., et al., *Natively Unfolded FG Repeats Stabilize the Structure of the Nuclear Pore Complex.* Cell, 2017. **171**(4): p. 904-917 e19.

49. Lin, Y., et al., *Toxic PR Poly-Dipeptides Encoded by the C9orf72 Repeat Expansion Target LC Domain Polymers.* Cell, 2016. **167**(3): p. 789-802 e12.

50. Frey, S., et al., *Surface Properties Determining Passage Rates of Proteins through Nuclear Pores.* Cell, 2018. **174**(1): p. 202-217 e9.

51. Schmidt, H.B. and D. Gorlich, *Nup98 FG domains from diverse species spontaneously phase-separate into particles with nuclear pore-like permselectivity.* Elife, 2015. **4**.

52. Ng, S.C., T. Guttler, and D. Gorlich, *Recapitulation of selective nuclear import and export with a perfectly repeated 12mer GLFG peptide.* Nat Commun, 2021. **12**(1): p. 4047.

53. Thaller, D.J. and C. Patrick Lusk, *Fantastic nuclear envelope herniations and where to find them.* Biochem Soc Trans, 2018. **46**(4): p. 877-889.

54. Walther, T.C., et al., *RanGTP mediates nuclear pore complex assembly.* Nature, 2003. **424**(6949): p. 689-94.

55. Otsuka, S., et al., *Nuclear pore assembly proceeds by an inside-out extrusion of the nuclear envelope.* Elife, 2016. **5**.

56. Kuiper, E.F., et al., *The molecular chaperone DNAJB6 provides surveillance of FG-Nups and is required for interphase nuclear pore complex biogenesis.* Nat Cell Biol, 2022.

57. Alberti, S. and D. Dormann, *Liquid-Liquid Phase Separation in Disease.* Annu Rev Genet, 2019. **53**: p. 171-194.

58. Hofweber, M., et al., *Phase Separation of FUS Is Suppressed by Its Nuclear Import Receptor and Arginine Methylation.* Cell, 2018. **173**(3): p. 706-719 e13.

59. Guo, L., et al., *Nuclear-Import Receptors Reverse Aberrant Phase Transitions of RNA-Binding Proteins with Prion-like Domains.* Cell, 2018. **173**(3): p. 677-692 e20.

60. Tanabe, L.M., et al., *Primary dystonia: molecules and mechanisms.* Nat Rev Neurol, 2009. **5**(11): p. 598-609.

61. Li, J., et al., *TorsinB overexpression prevents abnormal twisting in DYT1 dystonia mouse models.* eLife, 2019. **9:e54285**.

62. Krobitsch, S. and S. Lindquist, *Aggregation of huntingtin in yeast varies with the length of the polyglutamine expansion and the expression of chaperone proteins.* Proc Natl Acad Sci U S A, 2000. **97**(4): p. 1589-94.

63. Pusl, T., et al., *Epidermal growth factor-mediated activation of the ETS domain transcription factor Elk-1 requires nuclear calcium.* J Biol Chem, 2002. **277**(30): p. 27517-27.

64. Ran, F.A., et al., *Genome engineering using the CRISPR-Cas9 system.* Nat. Protocols, 2013. **8**(11): p. 2281-2308.

65. Turner, E.M., et al., *The Torsin Activator LULL1 Is Required for Efficient Growth of Herpes Simplex Virus 1.* J Virol, 2015. **89**(16): p. 8444-52.

66. Ran, F.A., et al., *Genome engineering using the CRISPR-Cas9 system.* Nat Protoc, 2013. **8**(11): p. 2281-2308.

67. Zhao, C., et al., *Site-specific Proteolysis Mobilizes TorsinA from the Membrane of the Endoplasmic Reticulum (ER) in Response to ER Stress and B Cell Stimulation.* J Biol Chem, 2016. **291**(18): p. 9469-81.

68. Tsai, P.L., C. Zhao, and C. Schlieker, *Methodologies to monitor protein turnover at the inner nuclear membrane.* Methods Enzymol, 2019. **619**: p. 47-69.

69. Frey, S. and D. Gorlich, *A new set of highly efficient, tag-cleaving proteases for purifying recombinant proteins.* J Chromatogr A, 2014. **1337**: p. 95-105.

70. Mansson, C., et al., *DNAJB6 is a peptide-binding chaperone which can suppress amyloid fibrillation of polyglutamine peptides at substoichiometric molar ratios.* Cell Stress Chaperones, 2014. **19**(2): p. 227-39.

71. Pishesha, N., J.R. Ingram, and H.L. Ploegh, *Sortase A: A Model for Transpeptidation and Its Biological Applications.* Annu Rev Cell Dev Biol, 2018. **34**: p. 163-188.

72. Schindelin, J., et al., *Fiji: an open-source platform for biological-image analysis.* Nat Methods, 2012. **9**(7): p. 676-82.

73. Stirling, D.R., et al., *CellProfiler 4: improvements in speed, utility and usability.* BMC Bioinformatics, 2021. **22**(1): p. 433.

74. Rhee, H.W., et al., *Proteomic mapping of mitochondria in living cells via spatially restricted enzymatic tagging.* Science, 2013. **339**(6125): p. 1328-1331.

75. Schlieker, C., et al., *A deubiquitinating activity is conserved in the large tegument protein of the herpesviridae.* J Virol, 2005. **79**(24): p. 15582-5.

76. Varadi, M., et al., *AlphaFold Protein Structure Database: massively expanding the structural coverage of protein-sequence space with high-accuracy models.* Nucleic Acids Res, 2022. **50**(D1): p. D439-D444.

Chapter 4: Conclusions and future directions

The past decade has witnessed an incredible expansion of knowledge about the once-enigmatic NE. This complex double membrane system is perfectly poised to influence a wide range of cellular activities beyond its most prominent role of establishing compartmentalization. While more than ever we understand the NE to be a metabolically active site for lipid synthesis and protein degradation, questions continue to be generated with every step forward. How does the NE bend and fuse during NPC biogenesis? Why do ubiquitylated protein become sequestered into stalled NPC intermediates? How can an ER-localized ATPase affect processes exclusive to the cytosol and nucleoplasm? Answering these questions along with numerous others will begin to unravel poorly understood concepts with both basic and translational scientific relevance.

Like a skyscraper that can withstand wind force, the NE must be flexible enough to move with its environment. Cytoskeletal connections that pull the nucleus along during cell migration are achieved via LINC complexes, but recent work demonstrates that other forms of NE flexibility are perhaps equally important. One such form is of the phospholipid bilayer, which must be flexible enough to allow for extreme bending during NPC biogenesis and NE blebbing during stress. It cannot be overstated how unusual and energetically unfavorable it is to impose such an extreme degree of membrane bending. If this bending was to go wrong, it could cause a catastrophic loss of spatial separation between transcription and translation—a defining feature for eukaryotic cells. Thus, it is of critical importance that cells control the bending event and respond to errors when they inevitably arise. Evidence of NE resealing mechanisms were first described in mammalian cells [1, 2] and certainly exist in yeast as well [3, 4].

Because terminally differentiated cells within mature animals are postmitotic, it is almost certain that they possess mechanisms of NE resealing or otherwise responding to

defective NE bending/fusion. While the potential mechanism for NE resealing in higher eukaryotes may be related to that in yeast, these organisms have strikingly different ER/NE structures and could require separate repairs pathways. One major difference is that yeast NE do not have a lamina component, nor do they have a postmitotic NPC insertion pathway. Other differences in protein composition certainly exist as well; Torsin ATPases are exclusively encoded by metazoan genomes. Likely resealing or surveillance of NE membrane fusion in metazoan cells will differ from the process in yeast and could involve some of the many uncharacterized NE proteins. Indeed, proteomic datasets suggest that close to 100 proteins concentrate at the INM, many of which have unknown functions [5, 6]. Characterization of these proteins at the INM will likely identify the fusogenic and resealing machinery.

Another immerging aspect of the ER/NE is its role in communicating messages across compartments. Transmembrane complexes associated with ERAD are essential for normal PQC and provide a physical connection between the ER lumen and cytoplasm. However, canonical ERAD is not the only PQC pathway that requires a connection between these two compartments. Work described within this thesis demonstrates that a molecular defect within the ER lumen can cause perturbations to proteasome flux in a seemingly ERAD-independent mechanism. Loss of the Torsin ATPase from within the ER/NE membrane system causes not only the stabilization of protein that is otherwise degraded, but their nuclear accumulation [7, 8]. Depleting cells of canonical ERAD components does not significantly affect this [7] and there is no data to suggest that the stabilized protein originate from the ER. There is furthermore little to no ER stress found in cells without functional Torsin [9]. Thus, a line of communication exists between the ER lumen and cytosol that mediates a PQC pathway distinct from ERAD. This pathway requires the AAA+ ATPase p97 and its adaptor UBXD1 [7]. How is the status of Torsin activity communicated to cytosolic p97? While Torsins interact with the transmembrane

ER protein LULL1, there is no evidence that this would mediate an interaction with p97. More likely is the possibility that loss of Torsin function interferes with the biogenesis of a cytosolic or nuclear factor normally responsible for efficient proteasome-mediated degradation. Future work is required to identify precisely how Torsins communicate with the cytosol and whether this could be a therapeutic target for DYT1 dystonia.

The Torsin-regulated PQC pathway at the center of this thesis is clearly involved in balancing the amount of K48-Ub conjugates within cells. That loss of Torsins results in the accumulation of K48-Ub could mean more K48-Ub is produced or less is degraded. While these scenarios are not mutually exclusive, it is not trivial to unambiguously distinguish between these two options. One piece of evidence to support the claim that Torsin loss of function causes less K48-Ub to be degraded comes from interfering with the HSP70 ATPase cycle. When HSP70 is bound to ATP, it has a relatively low affinity for clients compared to the ADP-bound form. Ubiquitylated clients bound to HSP70 are rapidly degraded by the proteasome and trapping HSP70 in an ADP-bound conformation expedites degradation for these clients [10]. HSP70 can be trapped in a structural conformation that mimics the ADP-bound form via the small molecule VER-155008. In wild type (WT) HeLa cells treated with VER-155008, the overall steady state amount of K48-Ub is reduced compared to untreated cells due to this facilitated turnover [8]. However, in cells devoid of functional Torsin, VER-155008 causes a drastic increase in the amount of steady state K48-Ub [8]. This suggests that ubiquitylated clients of HSP70 that are normally degraded are unable to reach the proteasome and fail to be turned over. Treating Torsin knockout (KO) HeLa cells with VER-155008 causes a substantial increase in the amount of K48-Ub inside blebs, thus, the clients that cannot be degraded are shuttled to the NE [8]. In addition to this piece of evidence supporting a failure to efficiently degrade protein, a rapidly turned over viral protein is greatly stabilized in TorsinKO cells [8]. Taken together, evidence points to a loss of Torsin function causing a degradation

problem rather than generating more K48-Ub. Future work aimed at clearing the stabilized protein could lead to the discovery of targeted therapies for DYT1 dystonia.

While the accumulation of K48-Ub protein in NE herniations has been reported for every model of DYT1 dystonia, the ubiquitylated protein have not been identified. Despite multiple attempts and techniques to enrich for ubiquitin, not a single ubiquitylated protein as been found to be specifically enriched inside blebs. Neither MLF2 nor the chaperones are directly conjugated to ubiquitin; in fact, MLF2 is an unusually lysine-poor protein. With only one such residue in the entire protein, this property likely allows MLF2 to function as a co-chaperone within the HSP70 system and avoid degradation.

Because no directly ubiquitylated protein has been found to be significantly enriched inside blebs, there are many explanations for what the ubiquitin signal could be. First, it is possible that the K48-Ub chains are unconjugated. While perhaps unlikely, this is potentially supported by the unpublished observation that inhibiting the proteasome *decreases* the amount of K48-Ub inside blebs. How could proteasome activity be required for ubiquitin to accumulate in Torsin-deficient cells? Prior to degrading a ubiquitylated protein, the proteasome clips off the conjugated ubiquitin chain. In this way, proteasome activity generates free ubiquitin chains that are recycled. It is possible that these unconjugated chains become sequestered into blebs in Torsin-deficient cells, however, treatment of isolated NE with the isopeptidase IsoT does not change the amount of associated ubiquitin (unpublished observations). IsoT is capable of degrading unanchored ubiquitin chains, and its activity would likely decrease the amount of ubiquitin inside blebs if these were free K48-Ub conjugates. Thus, it seems unlikely that blebs harbor unconjugated ubiquitin chains but the requirement for proteasome activity remains unexplained.

A second possibility for the accumulation is that membrane itself becomes ubiquitylated. Phospholipids are ubiquitylated in both yeast and mammalian cells [11], and

this would be consistent with a lack of enriched ubiquitylated protein. While it has not been exhaustively explored, the possibility of NE ubiquitylation appears at face value somewhat unlikely but warrants further research.

Perhaps the most likely explanation for the lack of enriched K48-Ub inside blebs is invoked by Occam's razor; there is simply not a specific enrichment of ubiquitylated protein. Instead, random ubiquitylated cargo that varies from cell to cell gets trapped inside blebs, and efforts to identify the protein to which ubiquitin is conjugated will never reveal any specific enrichment. This model would speak to how general and severe the PQC defect that arises in DYT1 dystonia may be. In line with this model is the observation described in this thesis that heat shock greatly increases the amount of K48-Ub inside blebs [7]. Future research directed at understanding why K48-Ub conjugates are stabilized in Torsin-deficient cells and how they are directed to blebs will further our understanding of cellular trafficking and proteasome dynamics.

A novel intersection that recent data has uncovered exists between NPC biogenesis and molecular chaperones. Work described within this thesis identifies a role for HSP70s and HSP40s in maintaining the phase separation driven by FG-Nups [8]. This is in concert with the little-studied protein MLF2, which was found to have FG-Nup-directed chaperone activity *in vitro*. In independent work, the HSP40 member DNAJB6 was found to be required for normal NPC biogenesis [12]. Like MLF2, DNAJ6B can immerse into FG-Nup phases [8]. MLF2 in complex with HSP70 prevents the terminal aggregation of FG-Nups, promotes the formation of large FG-Nup condensates, and maintains the phase integrity over time. These *in vitro* activities may be recapitulated *in vivo* where the overexpression of MLF2 decreases the amount of mis-localized FG-Nups. MLF2 has also been observed to concentrate at the INM, perhaps nucleating with FG-Nups to facilitate membrane deformation [13]. Future work directed at understanding the activity of MLF2 during NPC

biogenesis will further our understanding of basic NE biology and membrane fusion processes.

Within the past few years, connections between PQC systems, NE dynamics, and neurological diseases have come to light. As our population lives longer, unraveling these complex systems becomes more critical than ever. Given that many neurological diseases correlate with age and are characterized by a collapse of PQC systems, the basic biology underlying these conditions must be well understood to develop targeted therapeutics. Currently, there are no medications that effectively treat diseases such as frontotemporal dementia. With continuing efforts to understand PQC mechanisms, this currently bleak reality will become something of the past.

References

1. Vietri, M., et al., *Spastin and ESCRT-III coordinate mitotic spindle disassembly and nuclear envelope sealing.* Nature, 2015. **522**(7555): p. 231-5.

2. Olmos, Y., et al., *ESCRT-III controls nuclear envelope reformation.* Nature, 2015. **522**(7555): p. 236-9.

3. Webster, B.M., et al., *Surveillance of nuclear pore complex assembly by ESCRT-III/Vps4.* Cell, 2014. **159**(2): p. 388-401.

4. Thaller, D.J., et al., *An ESCRT-LEM protein surveillance system is poised to directly monitor the nuclear envelope and nuclear transport system.* Elife, 2019. **8**: e45284.

5. Cheng, L.C., et al., *Identification of new transmembrane proteins concentrated at the nuclear envelope using organellar proteomics of mesenchymal cells.* Nucleus, 2019. **10**(1): p. 126-143.

6. Cheng, L.C., et al., *Shared and Distinctive Neighborhoods of Emerin and Lamin B Receptor Revealed by Proximity Labeling and Quantitative Proteomics.* J Proteome Res, 2022. **21**(9): p. 2197-2210.

7. Prophet, S.M., B.S. Naughton, and C. Schlieker, *p97/UBXD1 Generate Ubiquitylated Proteins That Are Sequestered into Nuclear Envelope Herniations in Torsin-Deficient Cells.* Int J Mol Sci, 2022. **23**(9): 4627.

8. Prophet, S.M., et al., *Atypical nuclear envelope condensates linked to neurological disorders reveal nucleoporin-directed chaperone activities.* Nat Cell Biol, 2022. In press.

9. Laudermilch, E., et al., *Dissecting Torsin/cofactor function at the nuclear envelope: a genetic study.* Mol Biol Cell, 2016. **27**(25): p. 3964-3971.

10. Massey, A.J., et al., *A novel, small molecule inhibitor of Hsc70/Hsp70 potentiates Hsp90 inhibitor induced apoptosis in HCT116 colon carcinoma cells.* Cancer Chemother Pharmacol, 2010. **66**(3): p. 535-45.

11. Sakamaki, J.I., et al., *Ubiquitination of phosphatidylethanolamine in organellar membranes.* Mol Cell, 2022. https://doi.org/10.1016/j.molcel.2022.08.008.

12. Kuiper, E.F., et al., *The molecular chaperone DNAJB6 provides surveillance of FG-Nups and is required for interphase nuclear pore complex biogenesis.* Nat Cell Biol, 2022. In press.

13. Rampello, A.J., et al., *Torsin ATPase deficiency leads to defects in nuclear pore biogenesis and sequestration of MLF2.* The Journal of Cell Biology, 2020. **219**(6): e201910185.